RMA RESOURCE MANAGEMENT ASSOCIATES
WATER RESOURCES ENGINEERING

Numerical Modeling in Support of Reclamation Delta Smelt Summer/Fall Habitat Analysis

Technical Memorandum

May 14, 2021

Prepared For:
United States Bureau of Reclamation

Prepared By:
Resource Management Associates
1756 Picasso Avenue, Suite G
Davis, CA 95618
Contact: Stacie Grinbergs
530-564-7043

EXECUTIVE SUMMARY

The Delta Smelt Summer-Fall Habitat Action aims to improve the recruitment, growth and survival of Delta Smelt by implementing distinct management actions designed to increase the quantity and quality of Delta Smelt abiotic habitat and food supply, contributing to the growth and survival of Delta Smelt. Environmental conditions that contribute to Delta Smelt abiotic habitat suitability include salinity, turbidity, temperature and current speed.

Management scenarios included seven different combinations of the following three management actions in addition to the No Action scenario for each of four water year types.

1. Suisun Marsh Salinity Control Gate Action (SMSCG): a two-month period of additional SMSCG gate operation period during June through October of Below Normal, Above Normal and Wet years to improve abiotic habitat by reducing salinity in Suisun Marsh;

2. The North Delta Flow Action (NDFA): a food enhancement action to redirect 500 cfs of flow from Colusa Basin agricultural drainage or the Sacramento River through the Yolo Bypass Toe Drain from August 29 to September 21 in order to increase food web productivity and export of food to downstream regions; and

3. The Sacramento Deepwater Ship Channel Action (DWSC): a food enhancement action in July during which 700 cfs of water is diverted from the Sacramento River to stimulate primary and secondary production and/or transport of production in the shipping channel to other portions of the North Delta.

Four water year types were simulated: Dry, Below Normal, Above Normal and Wet. Note that the SMSCG action does not occur in Dry years so that combination of action and water year type was not simulated. For these water year types, scenarios used inflows generated with CalSim II by Reclamation. During above normal and wet years, an X2 action (X2 at 80 km) was included in flow estimates from the CalSim II model for all management scenarios. For each scenario, current speed, salinity, and temperature were simulated for summer and fall conditions. Turbidity was estimated from observations while turbidity modeling is in progress. The model results were analyzed to provide monthly maps of variables and habitat suitability metrics.

Historical conditions, some of which included Delta Smelt Summer-Fall Habitat Actions were also simulated. The simulation of these recent historical periods

allowed for habitat evaluation as well as validation of models and associated model input data. Historical conditions and scenarios were simulated with two models, the RMA2/11 Bay-Delta model and depth-averaged modeling tools and the three-dimensional RMA UnTRIM San Francisco Estuary model (RMA UnTRIM). RMA2/11 was applied to all scenarios while RMA UnTRIM was applied to a subset of the scenarios. Analysis of three-dimensional model results allowed identification of locations where management actions may influence processes not represented by the depth-averaged modeling tools, such as temperature stratification. Partially redundant modeling was also useful to identify and implement improvements to individual models.

The full set of simulated changes to abiotic fields and associated habitat suitability for No Action scenarios and differences resulting from management actions can be viewed at https://dshm.rmanet.app/overview/. Due to the limited temporal and spatial extent of actions, the differences indicated on the maps are usually local and often small. The largest change was a dramatic reduction in Suisun Marsh salinity from Suisun Marsh Salinity Control Gate operation, consistent with historical effects reported in Sommer et al. (2020). This salinity decrease resulted in habitat improvement through a large portion of Suisun Marsh. Some changes to the current speed metric were noted which also generally increased the estimated habitat metric in Suisun Marsh when the action occurred in August and September. In contrast, the food enhancement actions had smaller abiotic effects, the most notable being shifts in temperature distribution in the Sacramento Deepwater Ship Channel during flow augmentation in July. The North Delta Flow Action had negligible effects to relevant abiotic metrics.

The work described herein has been funded by the U.S. Bureau of Reclamation through contract number GS00F010CA/140R8118F0322 with ICF Jones & Stokes, where Resource Management Associates, Inc., is working as a subcontractor under ICF Basic Ordering Agreement 19KCBO0097, Task Order 01.

CONTENTS

TABLE OF FIGURES

LIST OF TABLES

INTRODUCTION

Background

Delta Smelt (*Hypomesus transpacificus*) is protected under the California and federal Endangered Species Act. During the summer and fall, Delta Smelt life stages include post-larvae and juveniles and transition to sub-adults late in the fall (Moyle 2016). They rear in freshwater and low salinity habitats (Feyrer et al. 2007). Sommer and Mejia (2013) report that the habitat conditions typically associated with Delta Smelt are salinity less than 6 psu (practical salinity units), turbidity > 12 NTU (nephelometric turbidity unit) and temperatures from 7°C to 25°C. Bever et al. (2016) developed a specific habitat suitability relationship described below using salinity, turbidity and current speed as inputs.

Objectives of Study

The work is intended to provide a decision support tool to aid managers in understanding the effects of management actions on Delta Smelt habitat. This report focuses on abiotic habitat analysis. An analysis of potential changes to copepod availability to Delta Smelt will be reported separately. Because management effects are likely to vary by water year type, the study includes four water year types: Dry, Below Normal, Above Normal and Wet, as defined by the Sacramento Valley Index. For each month from June through October, metrics associated with abiotic habitat properties are calculated at a 10-meter spacing through the model domain from model results. These metrics are then combined to estimate a Habitat Suitability Index (HSI). The results are available as a large set of monthly maps for online viewing by decision makers.

Overview of Approach

Two types of simulations were performed:

1. Historical periods were simulated to quantify the historical conditions associated with the water year types of interest and to validate the ability of the selected models to represent effects associated with proposed management actions.
2. Scenarios of proposed management actions were simulated using flow inputs generated by CalSim II.

For the historical period simulations, extensive comparisons were made between model predictions and observations. Detailed model calibration reports are available through the Shiny App

(https://dshm.rmanet.app/overview/rma_calibration_reports/calReport_2018_RMA_2D-1D_CalibrationReport.pdf and https://dshm.rmanet.app/overview/rma_calibration_reports/calReport_2019_RMA_2D-1D_CalibrationReport.pdf). In addition to providing confidence in the models, this calibration/validation process allowed for vetting of model input data such as atmospheric data driving the temperature modeling.

The second set of scenarios used a mix of CalSim II and DSM2 inputs for flow, diversions and operations and historical data from the same water year type for other inputs. Specifically, the wind velocity, air temperature, solar radiation and cloudiness from historic conditions were used in the scenario simulations for the equivalent water year type. Salinity and water temperature boundary conditions were also taken from historical data except for Vernalis salinity, which was specified using DSM2 inputs. These results were then analyzed to calculate monthly metrics of current speed, salinity and temperature conditions. Historical observations from the same water year type were used to define Secchi depth. This abiotic information was combined to calculate two habitat suitability metrics defined below.

In addition to the full set of scenario results from the depth-averaged RMA2/11 modeling platform, a limited set of three-dimensional results are available from the UnTRIM model. Those results include Below Normal and Wet water year types and both a No Action scenario and a scenario with all 3 management actions simulated (4 scenario simulations total).

Limited turbidity modeling of historical conditions and scenarios is in progress. For HSI calculations presented here, we monthly-averaged historical observations of turbidity and spatially interpolated them to form maps used in the HSI calculations (see Turbidity – Secchi Depth section).

Prey (copepod) abundance estimates will be reported separately. While these are unlikely to be incorporated into HSI metrics, they may be used in Delta Smelt bioenergetic calculations.

Management Actions

The following management action alternatives were simulated:

1. No Action alternative
2. North Delta Flow Action (NDFA)
3. Operation of the Suisun Marsh Salinity Control Gates (SMSCG)

4. Sacramento Deepwater Ship Channel (DWSC)
5. North Delta Flow Action and operation of the Suisun Marsh Salinity Control Gates (NDFA+SMSCG)
6. Operation of the Suisun Marsh Salinity Control Gates and Sacramento Deepwater Ship Channel (SMSCG+DWSC)
7. North Delta Flow Action and Sacramento Deepwater Ship Channel (NDFA+DWSC)
8. North Delta Flow Action, operation of the Suisun Marsh Salinity Control Gates, and Sacramento Deepwater Ship Channel (NDFA+SMSCG+DWSC)

Evaluation of management scenarios will be based on four different water years covering the water year types selected from the CalSim II results. One exception is the SMSCG scenario was not simulated for Dry years because that action is not expected to occur in Dry years (Table 2). Observed data from similar historical years will be used to characterize boundary conditions for parameter types not available from CalSim II, such as turbidity, wind and other meteorological data.

The study addresses four water year types: Dry, Below Normal, Above Normal, and Wet, as defined by the Sacramento Valley Index. For the historical simulations, recent years were chosen with good data availability for model input and calibration. The most recent above normal year was 2005. The years selected for each water year type are described in Table 1. Only recent years had adequate spatial coverage of turbidity data, so 2018 (Below Normal) data was used for both Dry and Below Normal water years and 2019 (Wet) was used for both Above Normal and Wet water years.

Table 1 Historical and CalSim II (CS) years selected for each water year type

Water Year Type	Historical Year	CalSim II (CS) Year	Turbidity Year	X2 at 80 km
Dry	2009	1930	2018	No
Below Normal	2018	1979	2018	No
Above Normal	2005	1940	2019	Yes
Wet	2019	1986	2019	Yes

CalSim II results specifically representing the No Action alternative (1) and the Suisun Marsh Salinity Control Gates Operation (3) management actions spanning the relevant water year types was provided by Reclamation. These CalSim II results correspond to a contemporary regulatory environment (as of December 27, 2017) and a project year 2030 level of development (LTO EIS). The simulations are

performed using precipitation from water year 1922 through 2003. Table 1 provides the historical and CalSim II (CS) years selected for each water year type. Above Normal and Wet water years included an action to maintain an X2 of 80 km in September and October. Boundary conditions for the remaining management action scenarios were developed by adding the appropriate flow actions. Management action timing, water year types and associated flows and volumes are provided in Table 2.

Table 2 Management action timing, water year types and associated flows and volumes

Action	Start Date	End Date	Average Flow (cfs)	Water Year Types	Volume (ac-ft)
X2 at 80	Sep 1	Oct 31	--	Above Normal, Wet	--
NDFA	Aug 28	Sep 23	500 cfs	All	28,000
SMSCG	Jul 1	Aug 31	--	Above Normal, Wet	~255,000*
SMSCG	Aug 1	Sep 30	--	Below Normal	~255,000*
DWSC	Jul 1	Jul 28	700 cfs	All	39,000

*Additional volume through Montezuma Slough during SMSCG management action period

Some of these actions were present in historical conditions. 2018 (Below Normal) included both a Suisun Marsh Salinity Control Gate (SMSCG) operation during October (Sommer et al. 2020) and implementation of a North Delta Flow Action (NDFA) action from late August to late September (Frantzich et al. in progress). A Fall X2 outflow action was implemented in 2019 (Wet) (https://www.usbr.gov/mp/nepa/includes/documentShow.php?Doc_ID=40623).

For the scenario simulations, Yolo Bypass Toe Drain flows from the similar historical year were applied, as they were not available from CalSim II. For the Below Normal (1979 CS) No Action simulation, the historical NDFA flows were removed from the 2018 (Below Normal) Toe Drain flows. For the NDFA simulation a synthetic NDFA constant 500 cfs flow was added to the No Action Toe Drain flows from August 28 through September 23. The historical, No Action and NDFA Toe Drain flows are plotted in Figure 1. For all other scenario years, the 500 cfs NDFA flow was applied directly to the historical Toe Drain flows with no other modifications needed. To represent the diversion from the Sacramento River, which occurs upstream of the model boundary, the Sacramento River inflows were reduced by 500 cfs during the same period for the NDFA simulations.

For the DWSC flow action, flow was diverted from the Sacramento River to the DWSC at a constant rate of 700 cfs from July 1 through July 28. Diversion and inflow locations are shown in Figure 2.

A timeline of all management actions applied in the scenario simulations is shown in Figure 3.

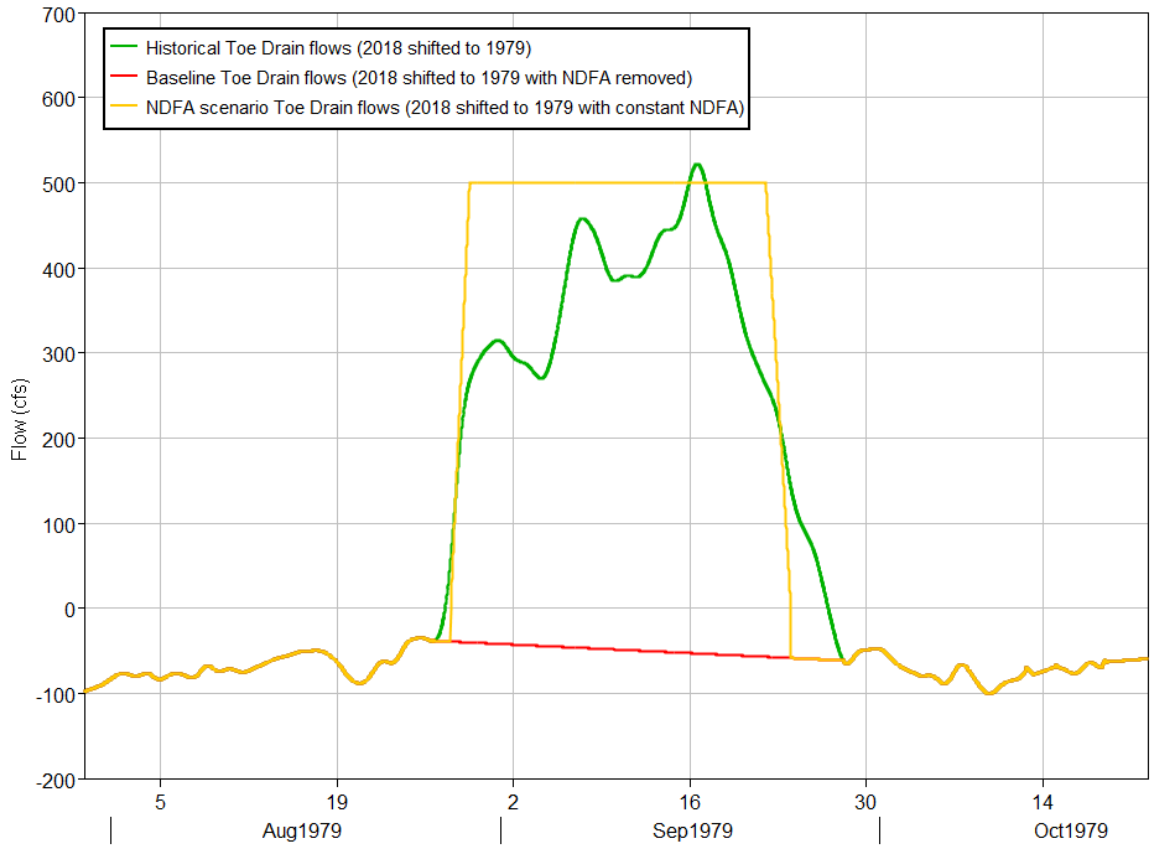

Figure 1 Historical, No Action and NDFA Toe Drain flows for the Below Normal (1979 CS) scenario simulations

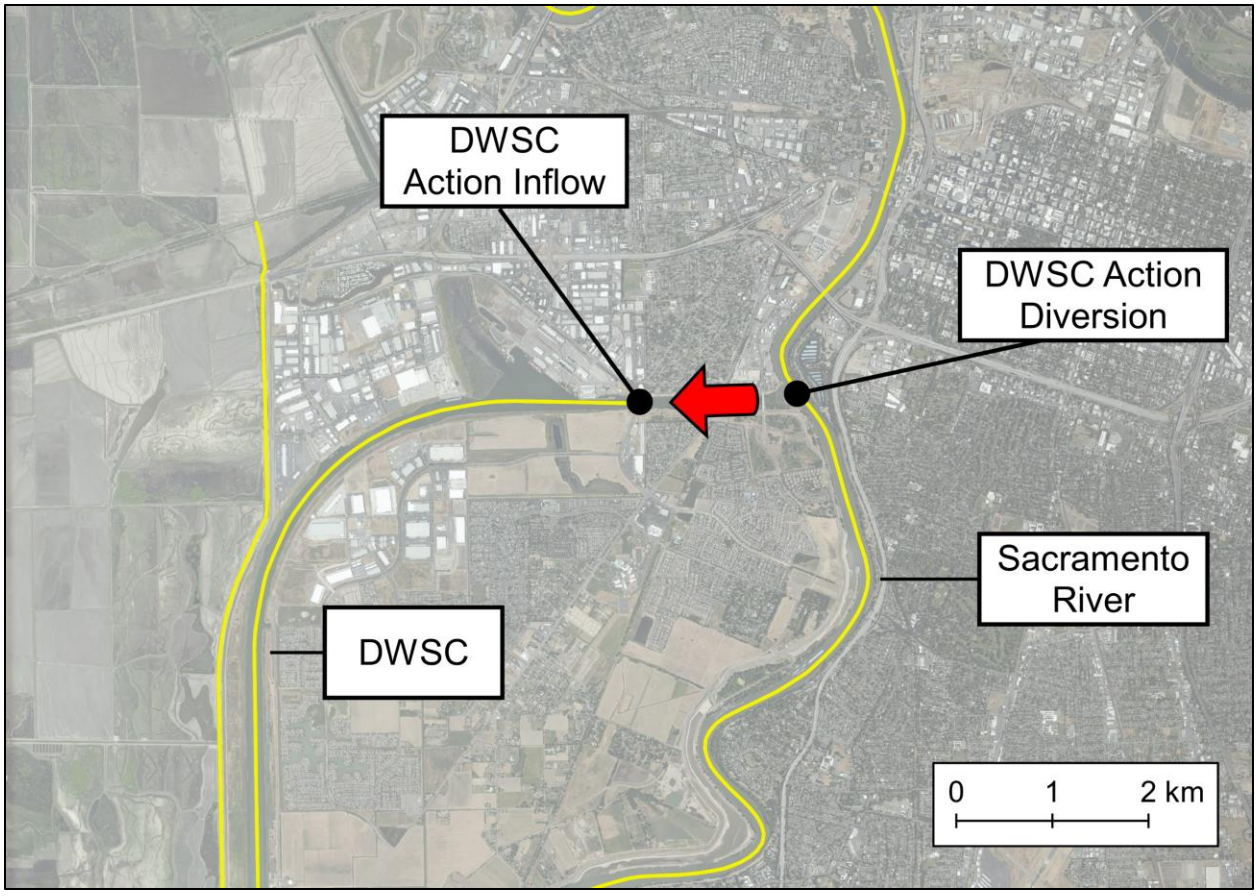

Figure 2 DWSC action diversion and inflow locations

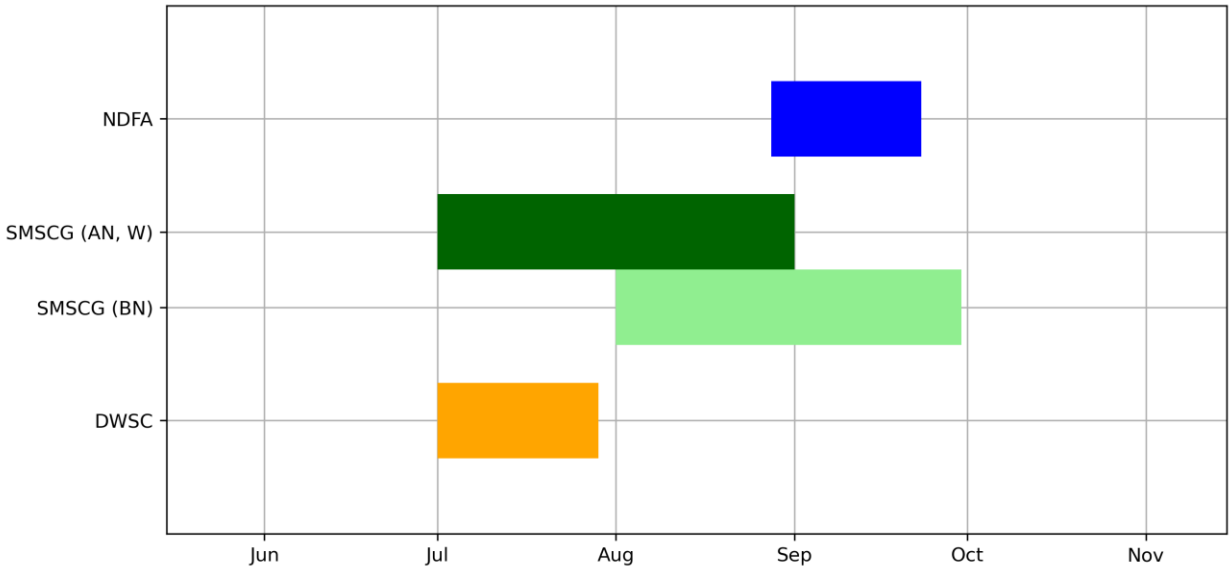

Figure 3 Management action timeline

Habitat Suitability Relationships

A number of studies have reported conditions associated with Delta Smelt presence (e.g., Feyrer et al. 2011; Sommer and Mejia 2013; Nobriga et al. 2008). We use the approach of Bever et al. (2016), which proposes a Habitat Suitability Index (HSI), referred to as "Station Index" in Bever et al. (2016). We also propose a modification to this approach using a temperature threshold discussed in Sommer and Mejia (2013) based on advice from Ted Sommer. We make the HSI estimates based on the following monthly abiotic parameters:

- Current Speed: monthly maximum depth-averaged current speed (m s^{-1})
- Salinity Suitability: Percent of time during a month with salinity < 6 psu
- Turbidity Suitability: monthly-averaged Secchi depth < 0.5 m
- Temperature Suitability: Percent of time during a month with temperature < 25 degrees C

These habitat properties are combined to estimate two different habitat suitability metrics. The first is

$$HSI_B = C_1 S + C_2 V \; if \; Secchi < 0.5$$
$$HSI_B = C_3 \times (C_1 S + C_2 V) \; if \; Secchi \geq 0.5 \quad (1)$$

where HSI_B is from Habitat Suitability Index from Bever et al. (2016), S is the percent time that salinity is less than 6 psu, V is the peak monthly current speed in m s^{-1}, $Secchi$ is Secchi depth in meters, and the constants are C_1 = 0.67, C_2 = 0.33 and C_3 = 0.42. Note that HSI_B is discontinuous at Secchi depth of 0.5 meters. An additional habitat suitability index is introduced based on input from Ted Sommer, consistent with Sommer et al. (2013). Specifically, HSI is calculated by adding a temperature effect to the Bever et al. (2016) approach

$$HSI = HSI_B \times T \quad (2)$$

where T is percent time that temperature is less than 25 degrees C. These two habitat suitability approaches are applied at a monthly time interval based on model predictions in each element in the model domain.

MODEL DESCRIPTIONS

Two models were used in this analysis. Two-dimensional simulations were performed using the RMA Bay-Delta model, which utilizes the RMA2 and RMA11 computational engines. The RMA Bay-Delta model extends from the Golden Gate through the San Francisco Estuary up the Sacramento River above the American River confluence, and up the San Joaquin River to Vernalis (see Figure 4).

Three-dimensional model simulations were performed using the RMA San Francisco Estuary UnTRIM model, which extends from the coastal ocean through the San Francisco Estuary up the Sacramento River above the American River confluence, and up the San Joaquin River to Vernalis (see Figure 5).

The boundary conditions applied to the models are nearly identical for the two the models.

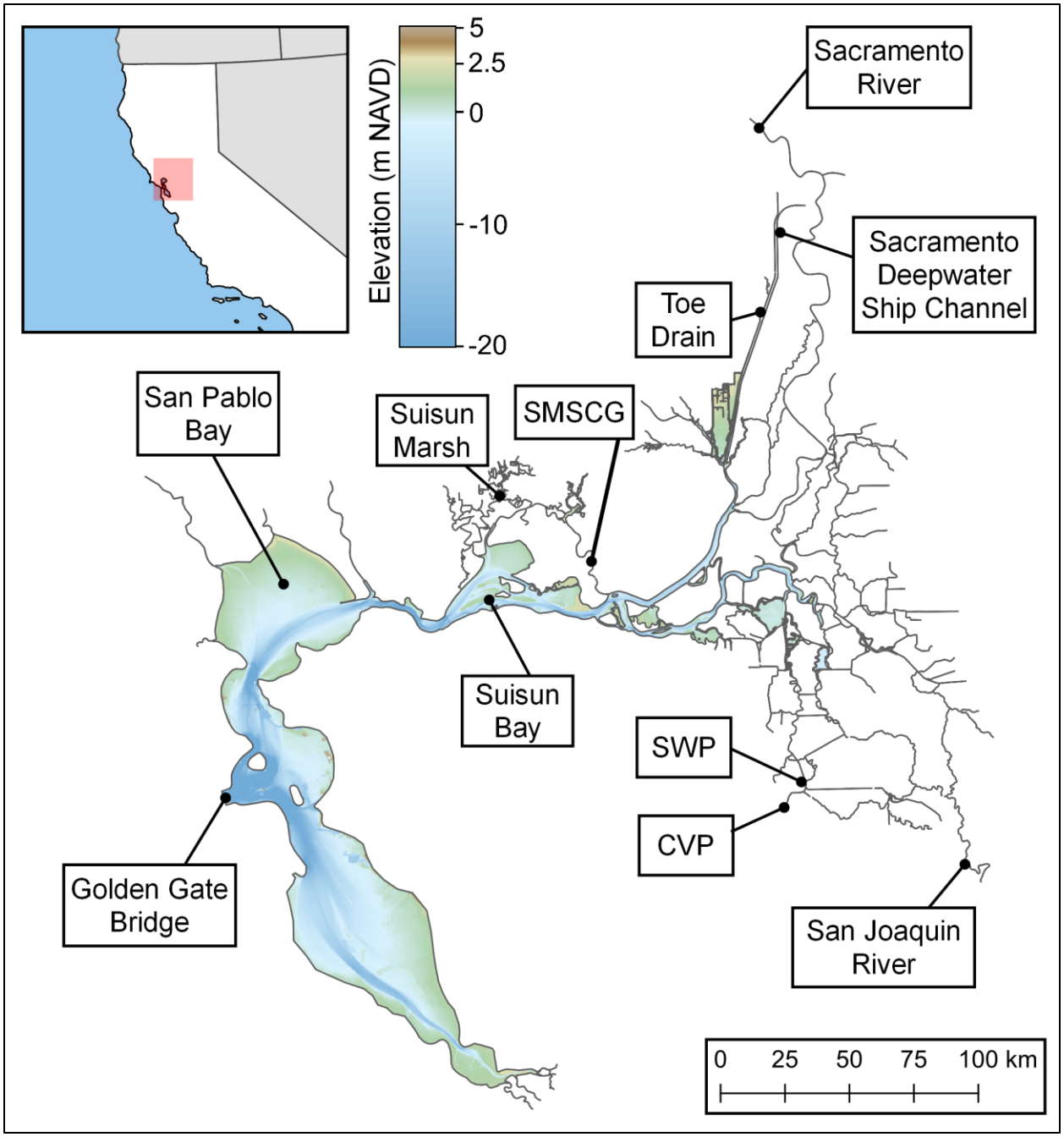

Figure 4 RMA Bay-Delta model domain

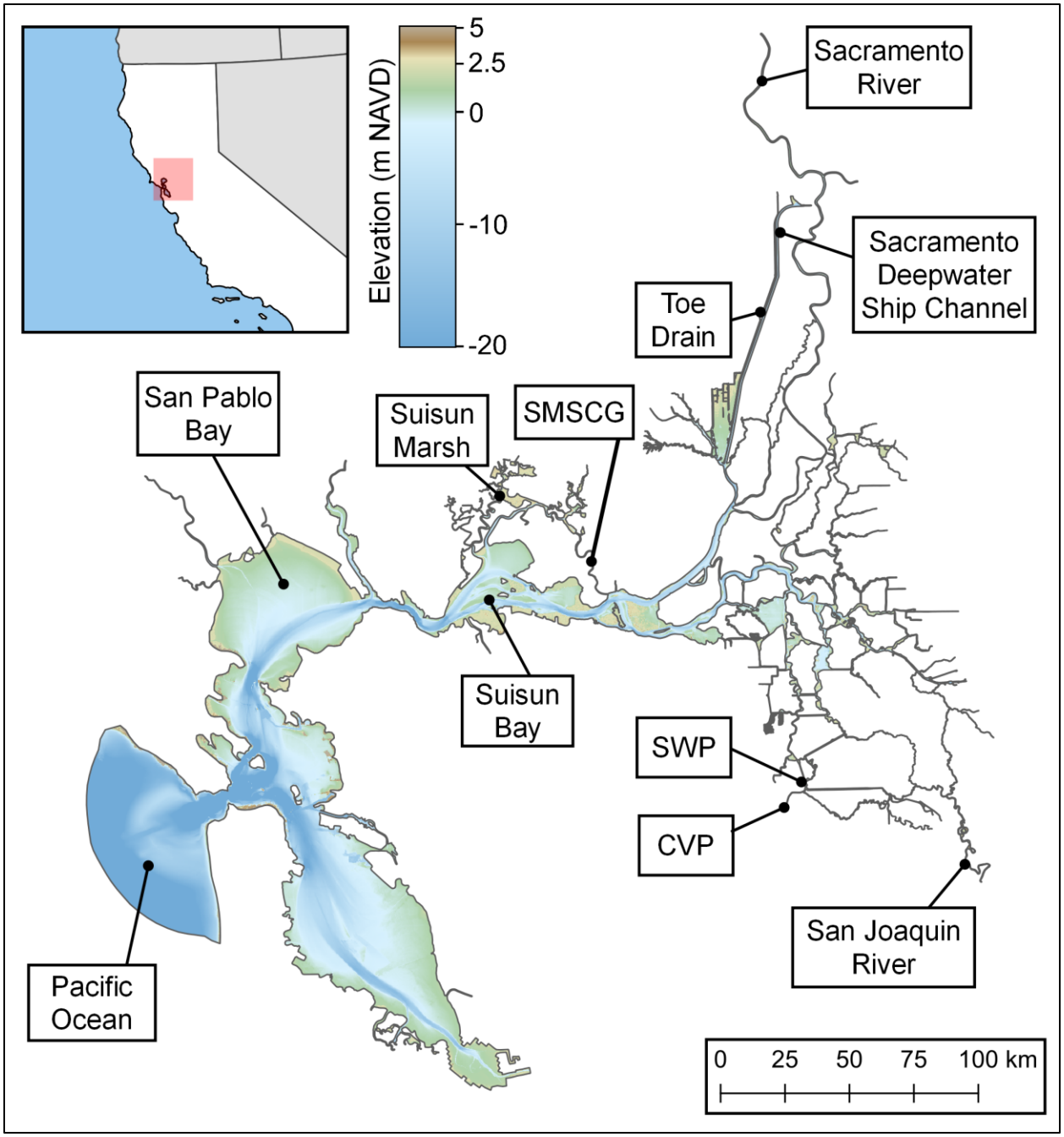

Figure 5 RMA UnTRIM San Francisco Estuary model domain

Model Grids

A hydrodynamic model grid consists of a set of geographical information that define the spatial extent and resolution of the predictions of the model. The primary components are nodes (points in space), sides defined by lines between adjacent nodes, and polygonal elements with nodes as vertices. A hydrodynamic model predicts water level, velocity, salinity and other properties on these nodes and elements. For each model, four model grids were developed to represent

- Pre-2018 conditions
- 2018 conditions (with restoration in Decker Island and Winter Island),
- 2019 conditions (including restoration in Yolo Flyway Farms, Decker Island and Winter Island)
- Post-2019 conditions (including restoration in Tule Red, Yolo Flyway Farms, Decker Island and Winter Island).

The locations of restoration areas are shown in Figure 6.

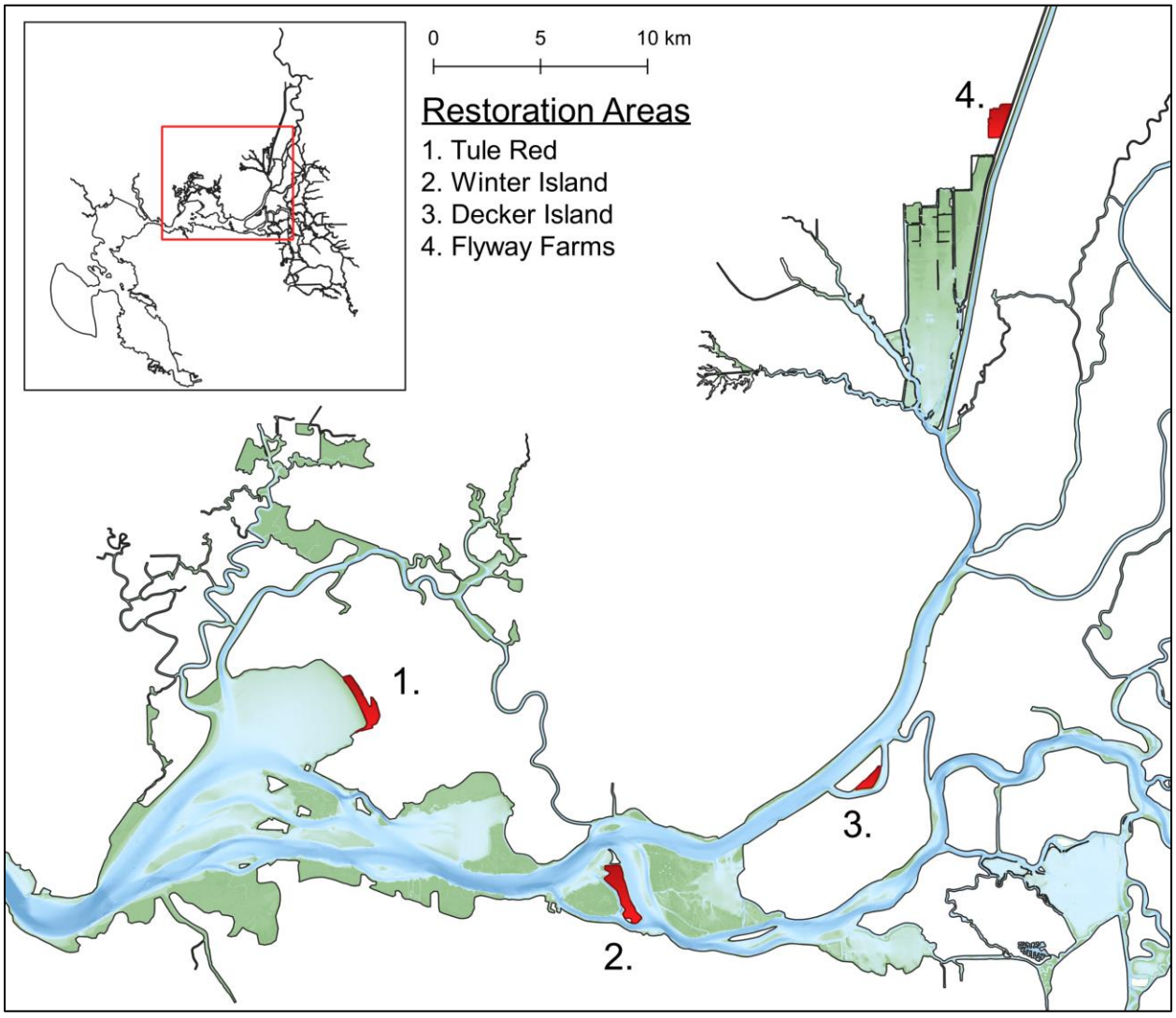

Figure 6 Recent restoration areas included in model grids

The model grids representing 2018 and 2019 conditions were used for the 2018 (Below Normal) and 2019 (Wet) historical simulations, respectively, and the grids representing pre-2018 conditions were applied to the earlier period historical simulations.

The model grids representing post-2019 conditions were used for management action scenario simulations and include all recently completed restoration sites.

The study area includes Suisun Bay, Suisun Marsh, and the Delta. The model domain also includes the San Francisco Bay, although it is not a focus of the study. Since this study is focused on summer/fall conditions, the majority of the Yolo Bypass is not included in the model domain. Inflows to the Toe Drain and the Cache Slough Complex are represented in the model.

Boundary Conditions

Typical boundary condition locations for the two-dimensional RMA Bay-Delta model and the UnTRIM RMA San Francisco Estuary model are shown in Figure 7 and Figure 8.

Inputs to both the two- and three-dimensional models included water surface elevation at the ocean (seaward) boundary, inflows in the estuary, water exports, consumptive use on Delta Islands (DICU), agricultural returns, managed pond diversions and returns, and gate and barrier operations. The salinity and temperature of these inflows were also specified. Spatially variable evaporation, precipitation and wind speed were applied in both models. The wind was specified as constant within each of several zones (Figure 9).

Net Delta Outflow (NDO) for each of the simulation periods is plotted in Figure 10. Detailed boundary conditions for the historical simulations are provided in the model calibration/validation reports (https://dshm.rmanet.app/overview/rma_calibration_reports/calReport_2018_RMA_2D-1D_CalibrationReport.pdf and https://dshm.rmanet.app/overview/rma_calibration_reports/calReport_2019_RMA_2D-1D_CalibrationReport.pdf). Major scenario boundary conditions are provided in Appendix B.

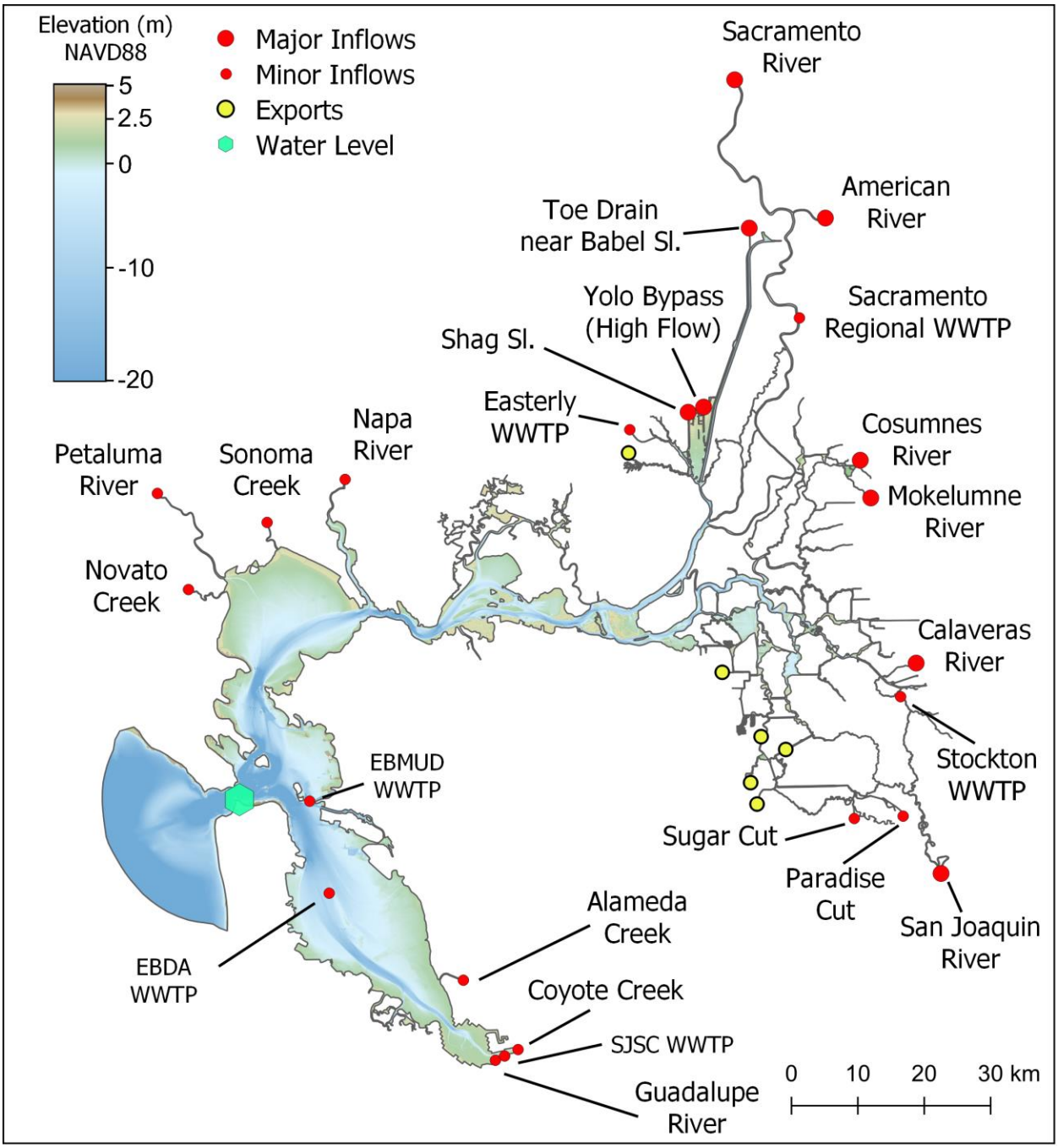

Figure 7 Flow and water level boundary condition inputs to the RMA multidimensional models of the San Francisco Estuary. With few exceptions the same boundary information is used for both the RMA2 and the RMA UnTRIM SF Estuary model.

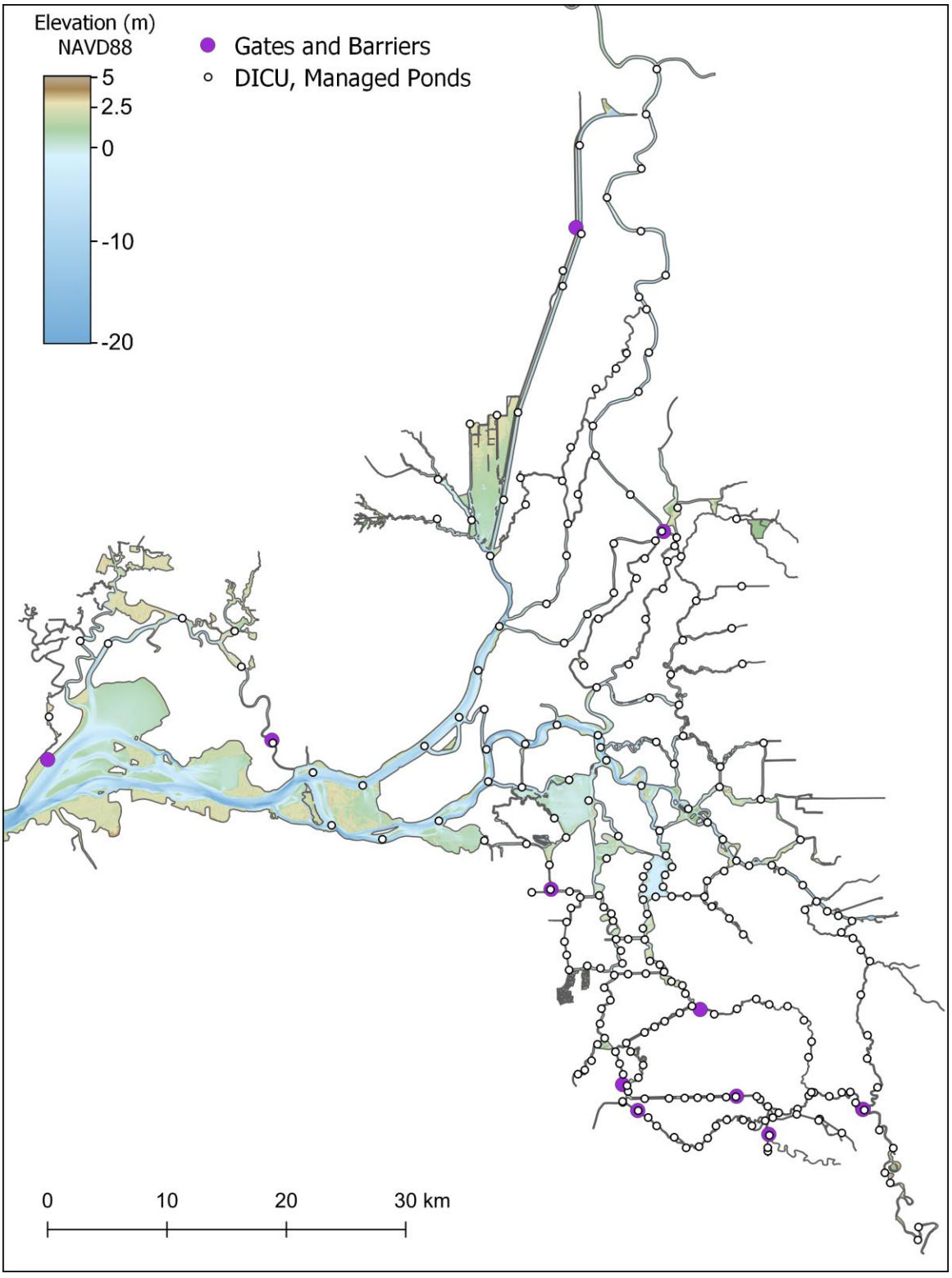

Figure 8 Gate and barrier, DICU and managed pond boundary condition inputs to the RMA multidimensional models of the San Francisco Estuary. The same boundary information is used for both the RMA2 and the RMA UnTRIM SF Estuary model.

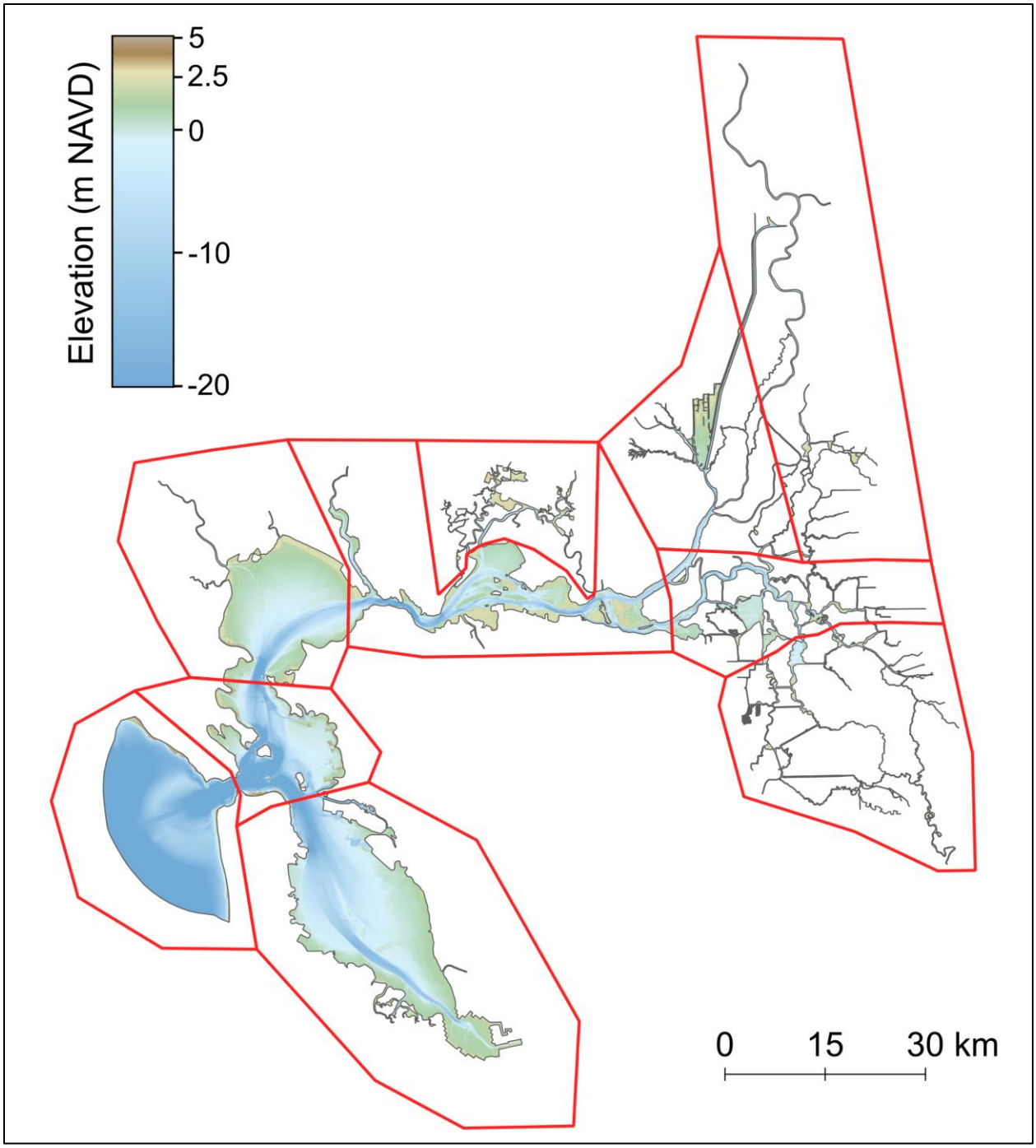

Figure 9 Wind and atmospheric data zones used by the hydrodynamic and temperature models

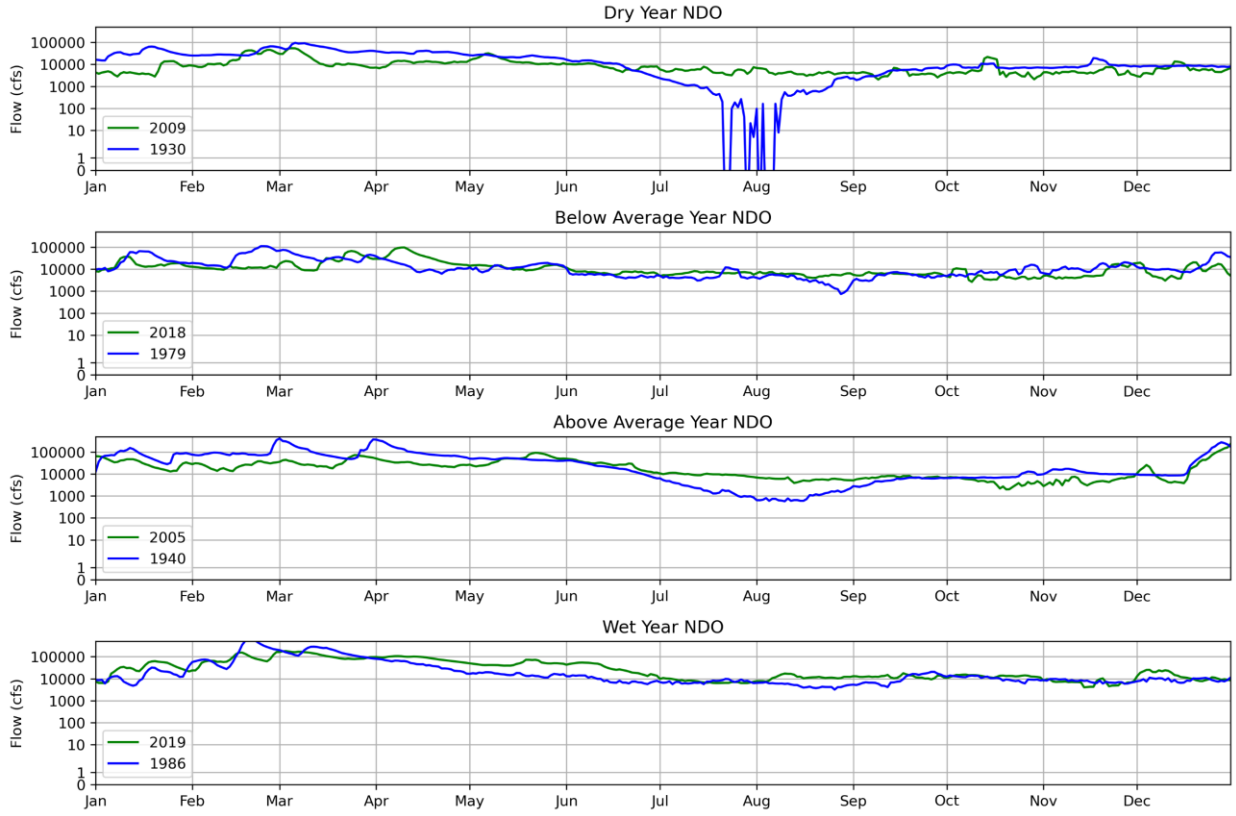

Figure 10 Net Delta Outflow for Dry, Below Normal, Above Normal and Wet years for Historical (green) and scenario (blue) simulations.

RMA Bay-Delta Model - RMA2/RMA11

The RMA Bay-Delta model was applied to assess HSI impacts related to current speed, salinity and temperature. The model utilizes the finite element method to simulate 2D depth-averaged / 1D cross-sectionally averaged flow and salinity for a 7.5-minute computational time step. The RMA Bay-Delta model is a widely accepted tool that is effective at predicting hydrodynamics and water quality throughout the Delta (see Calibration reports https://dshm.rmanet.app/overview/rma_calibration_reports/calReport_2018_RMA_2D-1D_CalibrationReport.pdf and https://dshm.rmanet.app/overview/rma_calibration_reports/calReport_2019_RMA_2D-1D_CalibrationReport.pdf). The model has been applied to flow and salinity impacts analyses for numerous restoration projects in the Bay-Delta system, including BDCP, Regional Salinity, Suisun Marsh PEIR/EIS, Prospect Island, Little Egbert Tract, Lookout Slough, McCormack-Williamson Tract, Decker Island, Winter Island, Dutch Slough, Chipps Island, Mallard Farms, Tule Red, Grizzly King, Potrero Marsh, Bradmoor Island, Arnold Slough, Hill Slough and Wings Landing (see for example RMA, 2009, 2012, 2013, 2015a and 2015b, 2020). The RMA Bay-Delta model has undergone continual development over more than 20 years to reflect currently available data and meet project needs. Similarly, since their original development in the 1970's, the RMA2 and RMA11 computational models have been updated over the years to best utilize the latest scientific knowledge and technology, and to meet new project needs.

RMA2 Model Formulation

Hydrodynamics were simulated using RMA2, a two-dimensional depth-averaged finite element model that solves the shallow water equations in primitive variables to provide temporal and spatial descriptions of velocities and water depths throughout the subject area. The program uses a finite element approach with Galerkin's criterion applied to the method of weighted residuals. For the two-dimensional approximations, the model employs 6-node triangular and 8-node quadrilateral elements. Three-node line elements are used for approximating one-dimensional channel flow. Quadratic shape functions are used to interpolate the velocity variables while linear shape functions are used for the depth. The quadratic functions allow for a curved element edge geometry. Because these equations can be highly non-linear, they are solved by a Newton-Raphson iterative technique. Time-dependent solutions employ a Crank-Nicholson implicit finite difference scheme. The time step used for modeling the depth-averaged flow and water quality transport in the Delta is 7.5 minutes.

The model uses the Smagorinsky formulation for modeling of turbulent momentum transfer. RMA2, capable of simulating the de-watering of tidal flats, is well-suited for modeling of inter-tidal hydrodynamics in the marshes and mudflats that characterize the Bay-Delta system.

A full description of the governing equations for flow and additional RMA2 model details can be found in Flooded Islands Pre-feasibility Study, RMA Delta Model Calibration Report (RMA, 2005).

RMA11 Model Formulation

The results of the RMA2 flow simulation (x and y velocity components, and depth of water) are saved at 15-minute intervals for all nodal locations to a binary file. The flow result file may then be used by the finite element water quality model, RMA11, to compute salinity and other constituent transport.

RMA11 solves a set of differential equations representing the conveyance of dissolved or suspended material by advection and turbulent mixing. These equations are derived from a statement of conservation of mass. Eddy diffusion is also used to approximate the complex process of time-dependent transport by turbulent mixing. In the intertidal water quality simulation mode, advection is the dominant transport mechanism. Turbulent diffusion occurs in the presence of velocity and concentration gradients. Calibrated scaling constants are developed for the longitudinal and transverse diffusion terms. The scaling constant for the longitudinal diffusion is multiplied by the current velocity to develop the longitudinal diffusion coefficient. Scaling constants are derived from local (regional) calculated dispersion at different delta outflow volumes, as estimated in Gross et al. (2010). For a particular region (e.g., San Pablo Bay) Gross et al. (2009) dispersion estimates were fitted to Delta outflow using a logarithmic function, and the resulting equation was assigned to elements of the grid in nearby regions. During model computation, regional dispersion was then derived from daily measured net Delta outflow and used as the scaling constant for a particular day. The transverse diffusion coefficient is set in the user input as some fraction of the longitudinal coefficient.

When modeling water temperature, the model must consider the heat sources and sinks at the air-water and sediment-water interfaces. The approach used in RMA-11 is to assume that heat is transferred from various energy sources. So that:

$$H_N = H_{SN} + H_{AN} - (H_B + H_E + H_C) - H_{BED}$$

where

H_{SN} = Net shortwave influx, ($kJ/m^2/hr$)

H_{AN} = Net longwave influx, ($kJ/m^2/hr$)

H_B = Longwave back radiation, ($kJ/m^2/hr$)

H_E = Evaporative flux, ($kJ/m^2/hr$)

H_C = Conductive flux, ($kJ/m^2/hr$)

H_{BED} = Heat exchange with the sediment bed, ($kJ/m^2/hr$)

The full description of the heat balance equations is presented in Appendix A. The primary meteorological input requirements are air temperature, wind speed, relative humidity (or dew point temperature) and cloud cover. Shortwave solar radiation at the water surface can be estimated from sun position and atmospheric conditions (clouds and dust), but typically net solar radiation measurements are directly available from local climate stations.

At times, water temperatures in the field may vary in the vertical dimension or stratify. RMA11 only computes depth-averaged water temperature.

A three-dimensional model component was included in the study to identify locations where management actions may influence processes not represented by the depth-averaged modeling tools, such as temperature stratification.

Hydrodynamics, salinity and temperature were simulated using the three-dimensional RMA UnTRIM San Francisco Estuary Model (Andrews et al. 2017, Gross et al. 2019, Kimmerer et al. 2019). UnTRIM solves the discretized Reynolds-averaged shallow water equations on an unstructured grid (Casulli and Walters 2000). It allows for wetting and drying of computation cells, and sub-grid scale representation of bathymetry (Casulli and Stelling 2010). Vertical turbulent mixing in the model is parameterized using a k-ε closure, which solves one equation for turbulent kinetic energy (k) and another for turbulent dissipation (ε) using published parameter values (Warner et al. 2005). The unstructured grid model domain extends from the coastal ocean through the San Francisco Estuary including the Delta. The vertical dimension is represented by a z-layer formulation with 1 meter spacing down to -20 meters NAVD and gradually stretching to larger spacing in deep regions, mostly in Central San Francisco Bay and the coastal ocean. The RMA UnTRIM San Francisco Estuary model has an atmospheric heat flux formulation based primarily on the formulation applied by Rayson et al. (2015).

All scenario simulations used a 60-second time step and saved model output at a 30-minute interval.

CALIBRATION/VALIDATION OF MODELS

Hydrodynamic Model Validation

Since both the two-dimensional RMA Bay-Delta model and the three-dimensional RMA UnTRIM San Francisco Estuary model have previously been calibrated to several simulation periods, there were limited changes to approach, grid, boundary condition types or parameters. Some adjustments were made to update aspects of the UnTRIM model and make the UnTRIM and RMA2 model configurations more consistent with each other. For one example, newly restored areas were added to the UnTRIM model grid as appropriate. The same flow boundary condition data were used for both models to the extent feasible.

Metrics which were used in the calibration include correlation coefficient (R), bias, root mean square error (RMSE) and a model skill metric (Willmott 1981), as have been used in previous publications (e.g., Gross et al. 2019). The calibration stations used for the 2019 (Wet) period are shown in Figure 11.

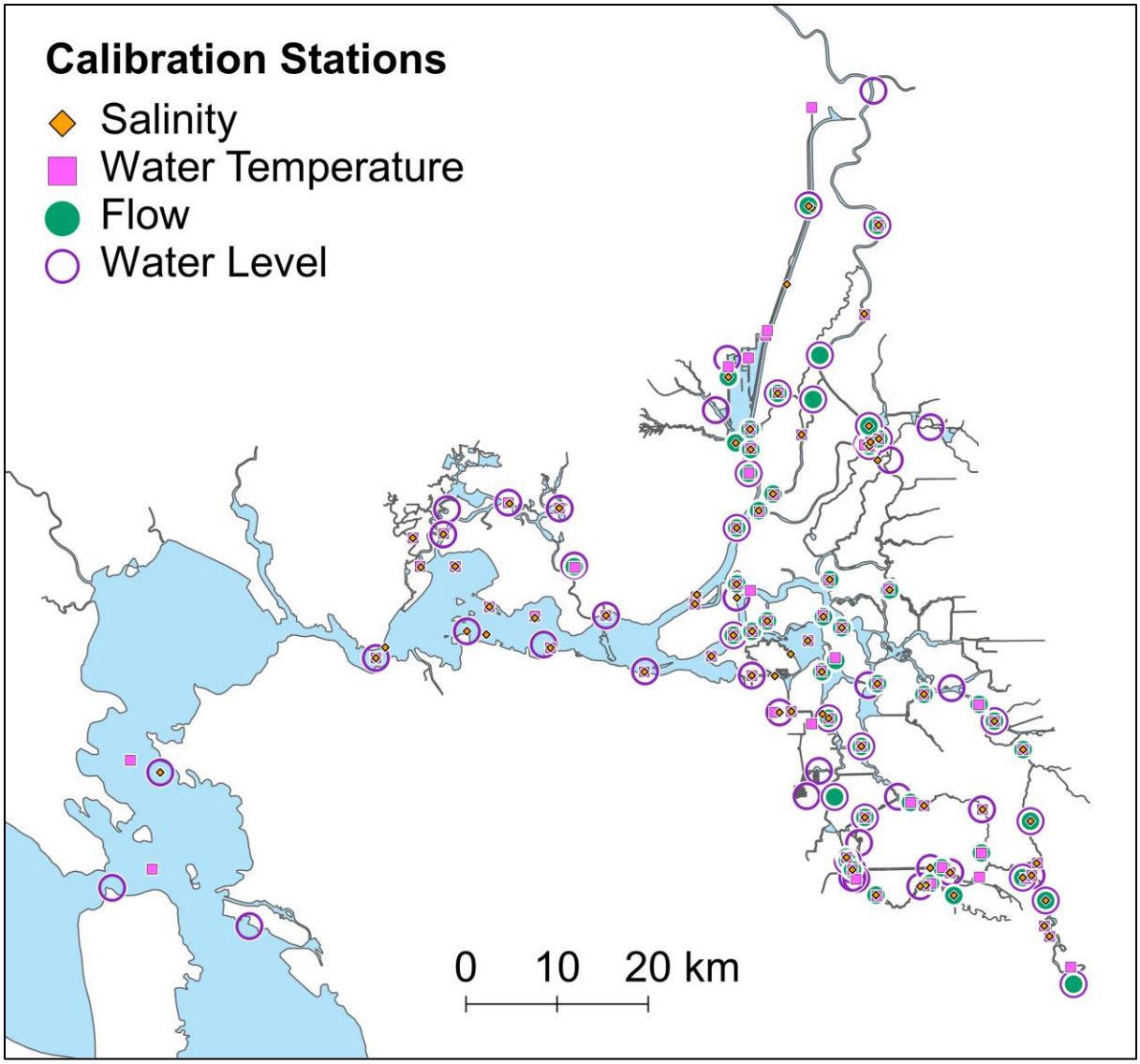

Figure 11 Validation/calibration output stations in the model domain for the 2019 (W) period

Detailed calibration reports Calibration reports for the two years with most data availability (2018 [Below Normal] and 2019 [Wet]) are available for both the two-dimensional model and three-dimensional model through the Shiny App (https://dshm.rmanet.app/overview/rma_calibration_reports/calReport_2018_RMA_2D-1D_CalibrationReport.pdf, https://dshm.rmanet.app/overview/rma_calibration_reports/calReport_2019_RMA_2D-1D_CalibrationReport.pdf, https://dshm.rmanet.app/overview/rma_calibration_reports/calReport_2018_UnTRIM_CalibrationReport.pdf, https://dshm.rmanet.app/overview/rma_calibration_reports/calReport_2019_UnTRIM_CalibrationReport.pdf)

Two- and Three-dimensional Salinity Model Validation

The RMA Bay-Delta model has been applied for salinity analysis of the Delta and Suisun Bay/Marsh for a number of modeling studies over the years, most typically to quantify the salinity impacts of various tidal restoration projects. The suitability of the model for reproducing observed salinities has been demonstrated for the four water year types.

The salinity regime in the Delta varies over the year, and for each water year type. Except for Critically Dry year types (e.g., 2014-2015), the Delta typically freshens with the winter time inflows, with salinity building back during the late spring to fall as Delta outflow decreases and salinity intrudes from the west. Although the seasonal time frame of summer-fall habitat analysis is June 1 – October 31, the salinity simulations were started in the wet season. The summer-fall salinity conditions are governed by the wet season freshening of the Delta and the salinity intrusion that develops as the year progresses. Management action scenarios used CalSim II-derived boundary conditions, which differ from historical conditions. The model of those scenarios was run to include the wet season inflows to allow the Delta salinity regime to naturally develop ("spin-up") for the summer-fall period. Therefore, the salinity verification included the wet season start to ensure the model reproduced the evolution of the salinity regime as the year progressed.

The same general approach, inputs and salinity dataset was used to validate the RMA UnTRIM San Francisco Estuary model for Below Normal and Wet water year types. The three-dimensional model simulates salinity and water temperature at the same time as water level and currents to allow them to influence density distribution which, in turn, influences horizontal circulation and vertical mixing.

Temperature Model Calibration and Validation

Water temperature is influenced by inflow boundary conditions, but primarily driven by meteorological conditions, specifically air temperature, wind speed, relative humidity, solar radiation and cloud cover. Meteorological data sources included DWR's CIMIS network, NOAA met stations, local airports, DWR CDEC and Mesowest. Some results from NOAA's North American Regional Reanalysis (NARR) were also utilized.

The summer and fall meteorological conditions vary notably over the domain of the model, with cooler temperatures over the San Francisco Bay and higher temperatures in the inland Delta regions. Temperatures over Suisun Bay region are intermediate, but the region is characterized in the summer by high westerly wind conditions. The meteorological forcing is applied to the model by region using the observed data characteristic to the region (Figure 9).

Simulation water temperature is less sensitive to antecedent conditions than salinity, as the temperature is forced over the entire surface of the model. The time frame of interest for the calibration is the summer-fall Delta Smelt Habitat period of June 1 through October 31. Starting the temperature simulations by April provides sufficient spin-up for the temperature results. The summer-fall temperature runs were performed for each water year type with the depth-averaged model and two water year types (Wet and Below Normal) with the three-dimensional model.

The RMA UnTRIM San Francisco Estuary model has an atmospheric heat flux formulation based primarily on the formulation applied by Rayson et al. (2015). This model requires atmospheric forcing inputs including solar radiation, air temperature, relative humidity and cloudiness. These were applied in a zonal approach where the inputs are time varying but uniform within each zone and vary spatially from zone to zone. The same meteorological inputs were used for the three-dimensional UnTRIM model as the depth-averaged RMA11 model.

MODEL INPUTS FOR SCENARIO SIMULATIONS

Scenario simulations used a combination of CalSim II and DSM2 outputs and historical data. Historical simulation model inputs are detailed in the 2D model calibration reports, available through the Shiny App (https://dshm.rmanet.app/overview/rma_calibration_reports/calReport_2018_RMA_2D-1D_CalibrationReport.pdf and https://dshm.rmanet.app/overview/rma_calibration_reports/calReport_2019_RMA_2D-1D_CalibrationReport.pdf). Major inflows and export boundary conditions for the scenario simulation are detailed in Appendix B.

CalSim II

Evaluation of management scenarios was based on four different water years covering Dry, Below Normal, Above Normal, and Wet water year types selected from the CalSim II results (see Table 3).

Table 3 Summary of CalSim II periods evaluated.

Water Year Type	CalSim II (CS) Year	X2 at 80 km
Dry	1930	No
Below normal	1979	No
Above normal	1940	Yes
Wet	1986	Yes

CalSim II results specifically representing the No Action alternative and the Suisun Marsh Salinity Control Gates Operation management actions were provided by Reclamation. These CalSim II results correspond to a contemporary regulatory environment (as of December 27, 2017) and a project year 2030 level of development (LTO EIS). The simulations are performed using precipitation from water year 1922 through 2003. Table 3 provides the historical and CalSim II years selected for each water year type. Above Normal and Wet water years included an action to maintain an X2 of 80 km in September and October. Boundary conditions for the remaining management action scenarios were developed by adding the appropriate flow actions.

CalSim II results provided monthly data for all major Delta inflows and exports. Monthly San Joaquin River EC inputs were also provided. A summary of CalSim II records applied to Delta boundary conditions is provided in Table 4.

Table 4 CalSim II records applied to Delta boundary conditions

Boundary Location	CalSim II Record	Boundary Type
Sacramento River	C169 + D168B + D168C*	Inflow
San Joaquin River	C639 + R644*	Inflow
Yolo Bypass	C157	Inflow
Cosumnes River	C501	Inflow
Mokelumne River	I504	Inflow
Calaveras River	C508 + R514	Inflow
CVP	D418	Diversion
Contra Costa at Rock Slough	D408_RS	Diversion
Contra Costa at Old River	D408_OR	Diversion
Contra Costa at Victoria Canal	D408_VC	Diversion
North Bay Aqueduct	D403A + D403B + D403C + D403D	Diversion
Freeport Diversions	D168B + D169C	Diversion
Stockton Diversions	D514A + D514B	Diversion
Antioch Diversions	D406B	Diversion

*Used daily smoothed record from DSM2

DSM2

With the CalSim II results as inputs, DSM2 was run to generate some Delta boundary conditions that are not available from CalSim II. Specifically, these include 15-minute Clifton Court flows and south Delta barrier operations. The daily smoothed inflows for the Sacramento and San Joaquin rivers that are used in DSM2 were also utilized in lieu of the original monthly flows from CalSim II.

Historical

Historical observations were used to set boundary conditions for the historical simulations. For the scenario simulations, some of the model boundary conditions are not available from CalSim II or DSM2. For these cases, historical data were used, if available for the particular year. Otherwise, boundary conditions from the historical simulation period of the same water year type were applied. Data sources included:

- USGS (https://maps.waterdata.usgs.gov/mapper/index.html)
- CDEC (https://cdec.water.ca.gov/)
- CIWQS (https://ciwqs.waterboards.ca.gov/ciwqs/readOnly/PublicReportEsmrAtGlanceServlet?inCommand=reset)
- NOAA (https://tidesandcurrents.noaa.gov/waterlevels.html?id=9414290)

Tide

NOAA observed historical Golden Gate tide data were applied in the historical simulations and Wet (1986 CS) scenario simulation. Predicted tides were applied to earlier CS periods (1979 and before) when observed data were unavailable.

Inflows

Historical flows were applied to both historical and scenario simulations for:

- Yolo Bypass Toe Drain
- All managed wetlands inflows and withdrawals (estimated)
- All wastewater treatment plants
- All inflows downstream of Martinez and in South SF Bay

Water Quality

Historical observed EC/salinity and water temperature data, where available, were applied to inflows for all historical simulations. For the scenario simulations, EC/salinity and temperature boundary conditions from the historical simulation

period of the same water year type were applied, except for San Joaquin River EC, which is available from CalSim II.

Atmospheric

Observed historical atmospheric data were applied in the historical simulations. For the scenario simulations, atmospheric boundary conditions from the historical simulation period of the same water year type were applied. All atmospheric data were applied by region, as shown in Figure 9. Meteorological data sources included DWR's CIMIS network, NOAA met stations, local airports, DWR CDEC and Mesowest. Some results from NOAA's North American Regional Reanalysis (NARR) were also utilized.

MODEL RESULTS

The full array of model outputs from this study have been made publicly accessible through the Shiny App (https://dshm.rmanet.app/overview/). These results indicate that management actions cause some changes in predicted abiotic fields. The effects are generally at a regional or smaller scale (not estuary-wide) and there is minimal spatial overlap in effects.

3D model results were depth-averaged prior to habitat suitability calculations. Tidal time scale (15-minute) results were post-processed using python tools to produce monthly results on an unstructured grid. Scenario results were differenced to create maps of differences between scenarios. All results were converted to raster format.

Current Speed

For HSI calculations, modeled peak monthly depth-averaged current speeds are extracted throughout the model domain. An example of the current speed metric is shown in Figure 12. Figure 13 shows the difference in current speed metric between the NDFA+SMSCG+DWSC and No Action scenarios, where the SMSCG action increases the peak current speed at the downstream end of Montezuma Slough and reduces current speed in Nurse Slough.

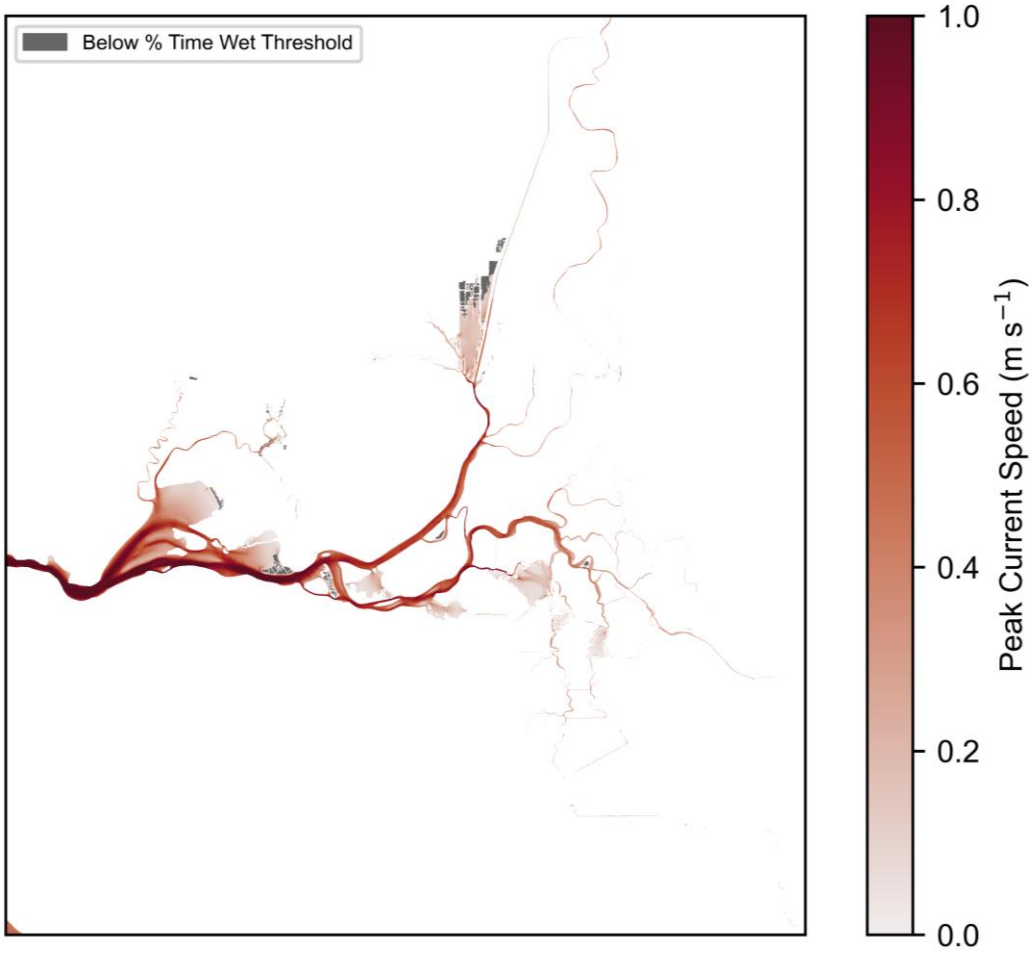

Figure 12 Example current speed metric from 2D model output: peak August, Below Normal (1979 CS) current speed for the No Action scenario

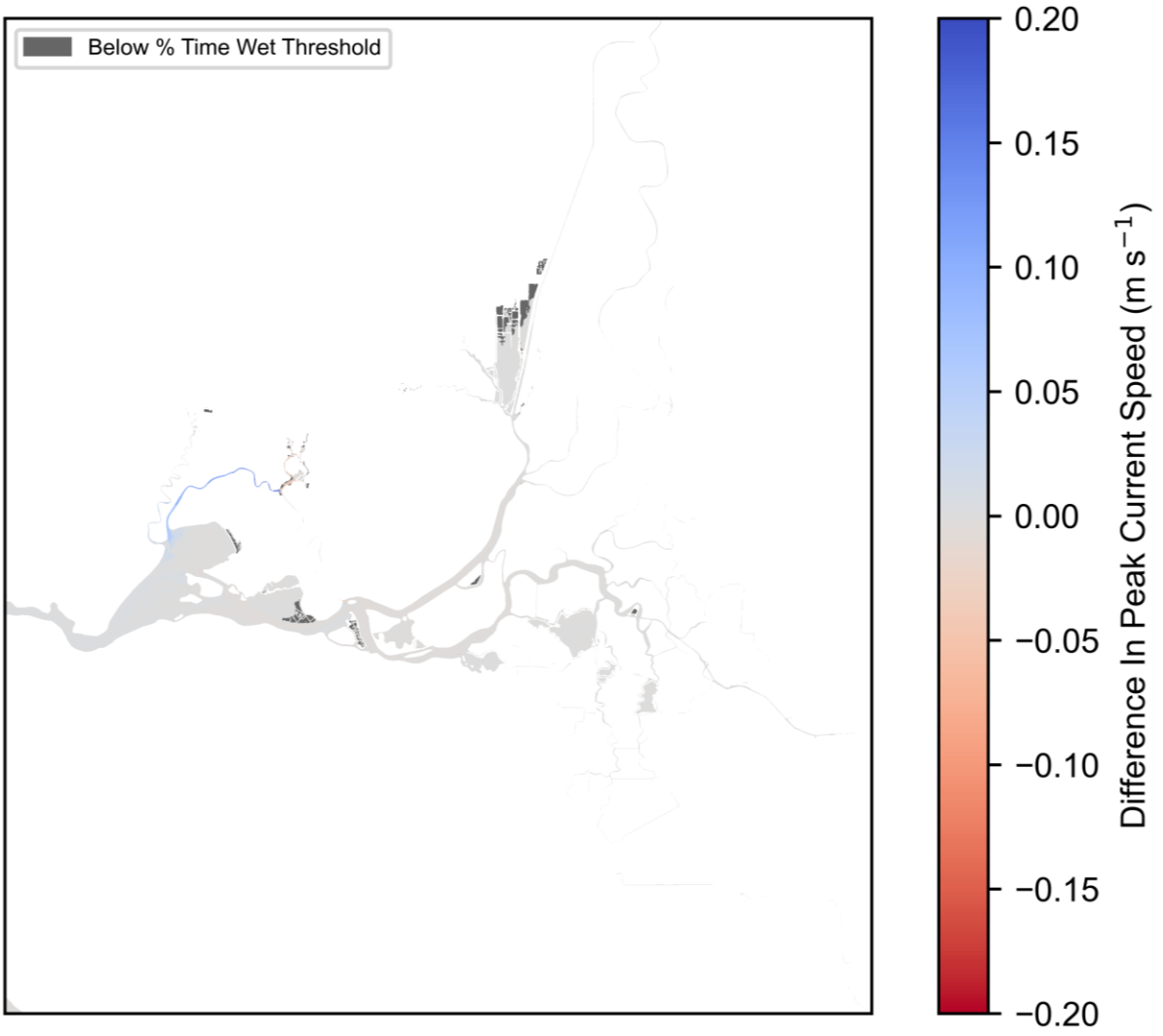

Figure 13 Example current speed metric difference from 2D model output: Difference between NDFA+SMSCG+DWSC and No Action August, Below Normal (1979 CS) peak current speed

Salinity

Salinity was simulated directly in the 3D model, while EC was simulated in the 2D model and converted to salinity using standardized equations from UNESCO (Fofonoff and Millard 1983). An example of monthly-averaged salinity computed by the 2D model is shown in Figure 14. Figure 15 shows the difference in monthly-averaged salinity between the NDFA+SMSCG+DWSC and No Action scenarios, where the SMSCG action increases salinity between the Sacramento – San Joaquin confluence and Suisun Bay and decreases salinity in Suisun Marsh, downstream of Nurse Slough, and into Suisun Bay.

2D modeled salinity time series at Beldon's Landing in Montezuma Slough were analyzed to determine the percent of time that salinity was below 6 psu and 4 psu threshold values each month. The SMSCG action can have large impacts at Beldon's Landing, while the flow actions have little to no impact. Results for the 6 psu threshold are summarized in Table 5 for June through October. There are no management actions in June and therefore no impacts on Beldon's Landing salinity. Results for the 4 psu threshold are summarized in Table 6. The SMSCG action increases the time salinity is below the 6 psu threshold by 70 – 100% during August and September. Smaller increases occur in July (0 – 5%) and October (6 – 15%). For the Above Normal (1940 CS) and Wet (1986 CS) years, when the SMSCG action begins in July, there is about a 90 – 95% increase in the time salinity is below the 4 psu in July. Regardless of July or August action start date, the time below 4 psu in August is increased by 90 – 100% and in September by 10%. Salinity exceeds 4 psu throughout October for all cases.

For HSI calculations, modeled salinity results were post-processed to fraction of time each month that salinity is less than 6 psu throughout the model domain. An example of this metric is shown in Figure 16. Figure 17 shows the difference in salinity suitability metric between the NDFA+SMSCG+DWSC and No Action scenarios, where, due to the salinity changes described above, the salinity metric is increased between the confluence region and just upstream of Suisun Bay and reduced in Suisun Marsh, downstream of Nurse Slough.

Qualitative comparisons between 2D and 3D salinity modeling results can be made through the Shiny App. An example comparison for the No Action August, Below Normal (1979 CS) salinity and salinity suitability is shown in Figure 18. At this time the 3D model predicts greater salinity intrusion east of Suisun Bay, resulting in lower salinity suitability.

2D monthly-averaged salinity suitability, defined as percent time < 6 PSU, showed the largest changes in the Suisun Marsh and Confluence subregions (EDSM subregions shown in Figure 19) as a result of the SMSCG action. In the three water years during which it occurred (all excluding Dry), the SMSCG action brought salinity suitability above 60% during August and above 50% in September, from below 30% without the action (Figure 20). CalSim II flows used during modeling allowed for a corresponding slight decrease in salinity suitability in the confluence region in SMSCG scenarios, with a maximal reduction of ~10% in September of the Below Normal year.

Table 5 Percent of time 2D modeled salinity at Beldon's Landing is less than 6 psu each month from June through October

Year/Type	Scenario	% of time Beldon's Landing Salinity < 6 psu				
		Jun	Jul	Aug	Sep	Oct
Dry (1930 CS - No SMSCG action)	No Action	89%	11%	0%	0%	77%
	NDFA	89%	11%	0%	0%	77%
	DWSC	89%	11%	0%	0%	77%
	NDFA+DWSC	89%	11%	0%	0%	77%
Below Normal (1979 CS - SMSCG action begins in Aug)	No Action	100%	89%	10%	0%	65%
	NDFA	100%	89%	10%	0%	65%
	SMSCG	100%	89%	100%	100%	71%
	DWSC	100%	89%	10%	0%	65%
	NDFA+SMSCG	100%	89%	100%	100%	71%
	SMSCG+DWSC	100%	89%	100%	100%	72%
	NDFA+DWSC	100%	89%	10%	0%	65%
	NDFA+SMSCG+DWSC	100%	89%	100%	100%	72%
Above Normal (1940 CS - SMSCG action begins in Jul)	No Action	100%	99%	32%	6%	65%
	NDFA	100%	99%	32%	6%	65%
	SMSCG	100%	100%	100%	93%	80%
	DWSC	100%	99%	32%	6%	65%
	NDFA+SMSCG	100%	100%	100%	93%	80%
	SMSCG+DWSC	100%	100%	100%	93%	80%
	NDFA+DWSC	100%	99%	32%	6%	65%
	NDFA+SMSCG+DWSC	100%	100%	100%	93%	80%
Wet (1986 CS - SMSCG action begins in Jul)	No Action	100%	95%	27%	9%	78%
	NDFA	100%	95%	27%	9%	78%
	SMSCG	100%	100%	100%	95%	88%
	DWSC	100%	95%	27%	9%	78%
	NDFA+SMSCG	100%	100%	100%	95%	88%
	SMSCG+DWSC	100%	100%	100%	95%	88%
	NDFA+DWSC	100%	95%	27%	9%	78%
	NDFA+SMSCG+DWSC	100%	100%	100%	95%	88%

Table 6 Percent of time 2D modeled salinity at Beldon's Landing is less than 4 psu each month from June through October

Year/Type	Scenario	% of time Beldon's Landing Salinity < 4 psu				
		Jun	Jul	Aug	Sep	Oct
Dry (1930 CS - No SMSCG action)	No Action	1%	0%	0%	0%	0%
	NDFA	1%	0%	0%	0%	0%
	DWSC	1%	0%	0%	0%	0%
	NDFA+DWSC	1%	0%	0%	0%	0%
Below Normal (1979 CS - SMSCG action begins in Aug)	No Action	92%	21%	0%	0%	0%
	NDFA	92%	21%	0%	0%	0%
	SMSCG	92%	21%	91%	10%	0%
	DWSC	92%	21%	0%	0%	0%
	NDFA+SMSCG	92%	21%	91%	10%	0%
	SMSCG+DWSC	92%	21%	91%	10%	0%
	NDFA+DWSC	92%	21%	0%	0%	0%
	NDFA+SMSCG+DWSC	92%	21%	91%	10%	0%
Above Normal (1940 CS - SMSCG action begins in Jul)	No Action	76%	2%	0%	0%	0%
	NDFA	76%	2%	0%	0%	0%
	SMSCG	75%	97%	100%	10%	0%
	DWSC	76%	2%	0%	0%	0%
	NDFA+SMSCG	75%	97%	100%	10%	0%
	SMSCG+DWSC	75%	97%	100%	10%	0%
	NDFA+DWSC	76%	2%	0%	0%	0%
	NDFA+SMSCG+DWSC	75%	97%	100%	10%	0%
Wet (1986 CS - SMSCG action begins in Jul)	No Action	85%	6%	0%	0%	0%
	NDFA	85%	6%	0%	0%	0%
	SMSCG	85%	98%	100%	9%	0%
	DWSC	85%	6%	0%	0%	0%
	NDFA+SMSCG	85%	98%	100%	9%	0%
	SMSCG+DWSC	85%	98%	100%	9%	0%
	NDFA+DWSC	85%	6%	0%	0%	0%
	NDFA+SMSCG+DWSC	85%	98%	100%	9%	0%

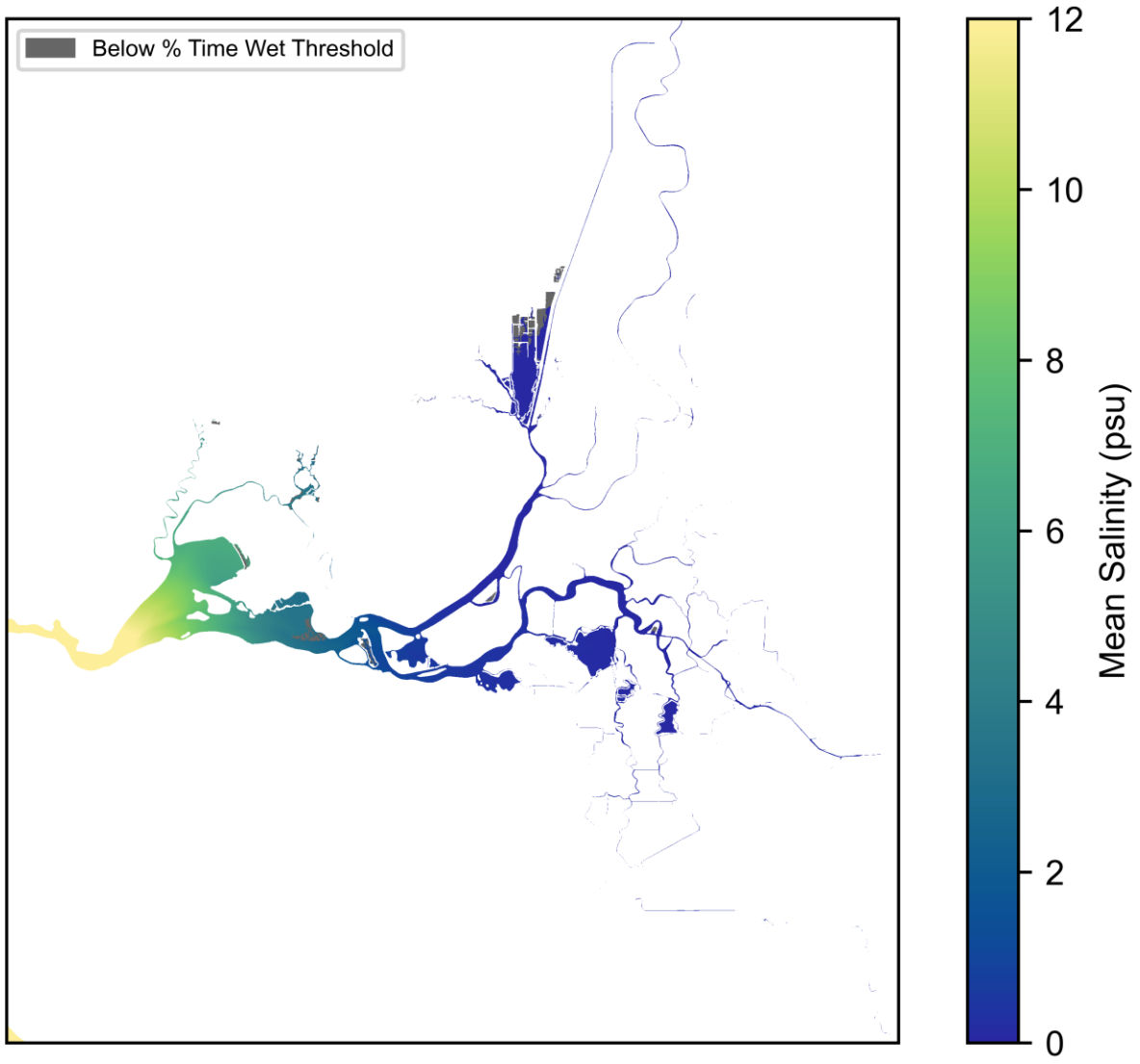

Figure 14 Example monthly-averaged salinity from 2D model output: August, Below Normal (1979 CS) No Action scenario

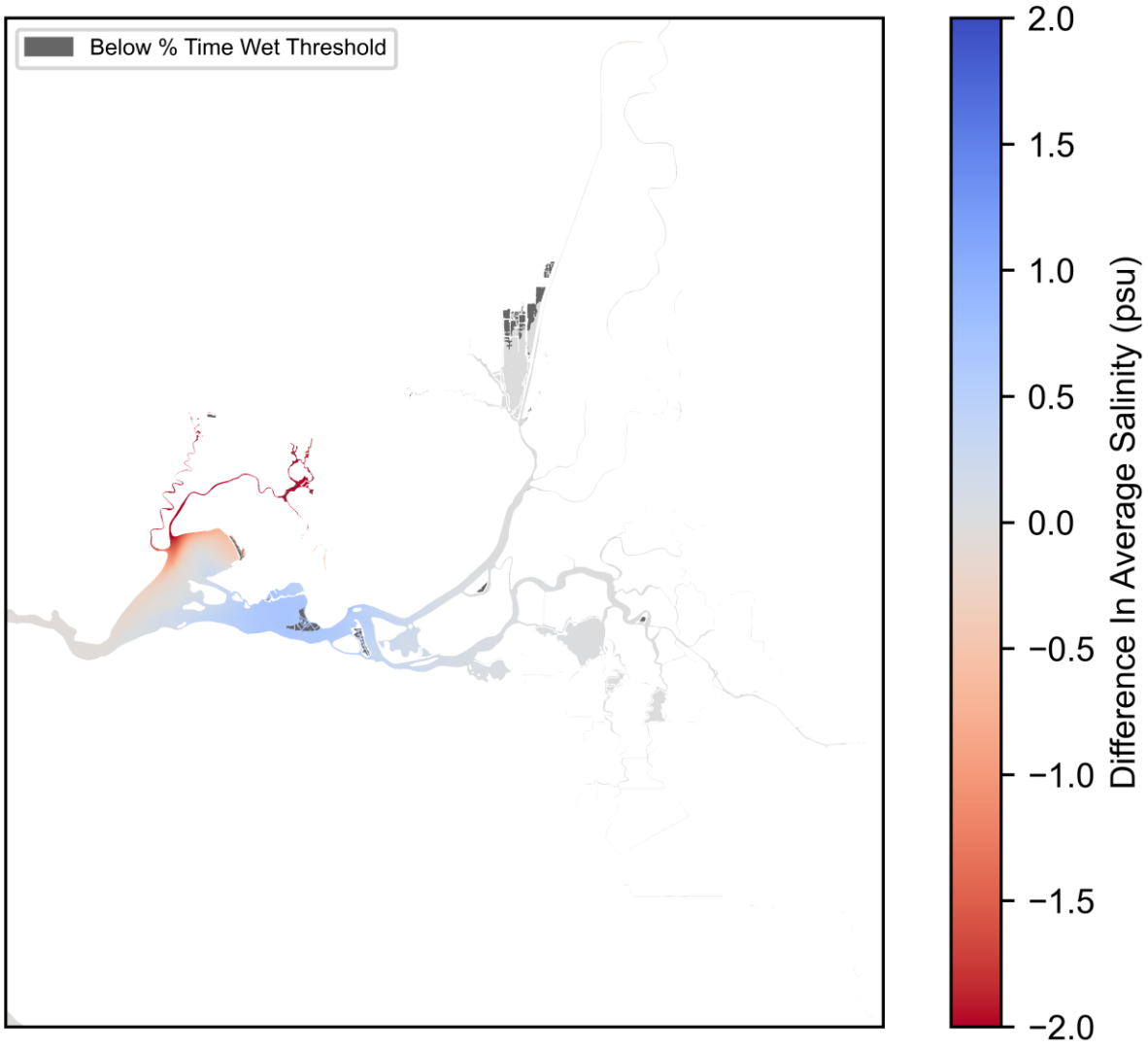

Figure 15 Example salinity difference from 2D model output: difference between NDFA+SMSCG+DWSC and No Action August, Below Normal (1979 CS) monthly-averaged salinity

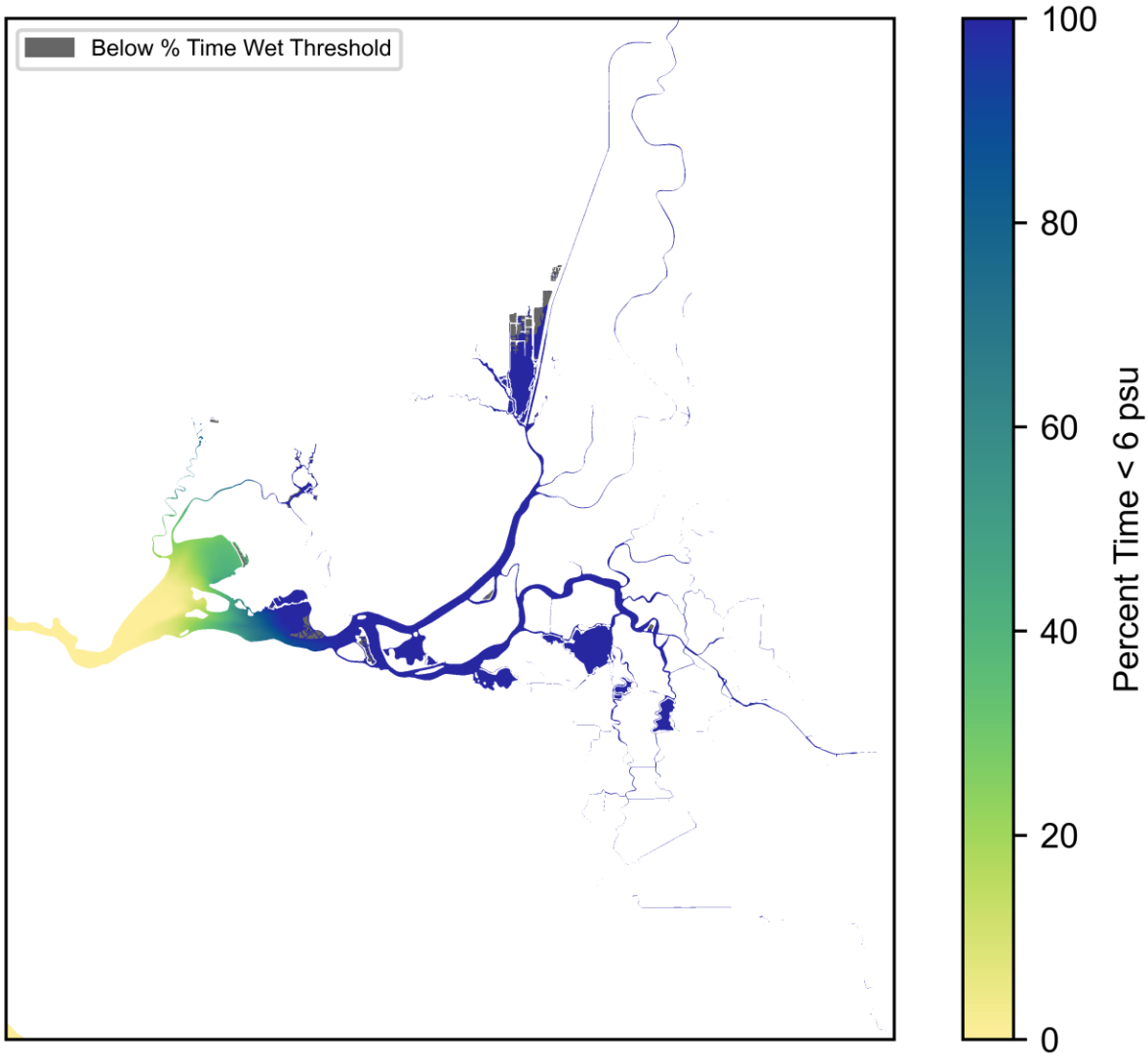

Figure 16 Example salinity suitability metric from 2D model output: percent time salinity < 6 psu during August, Below Normal (1979 CS) for the No Action scenario

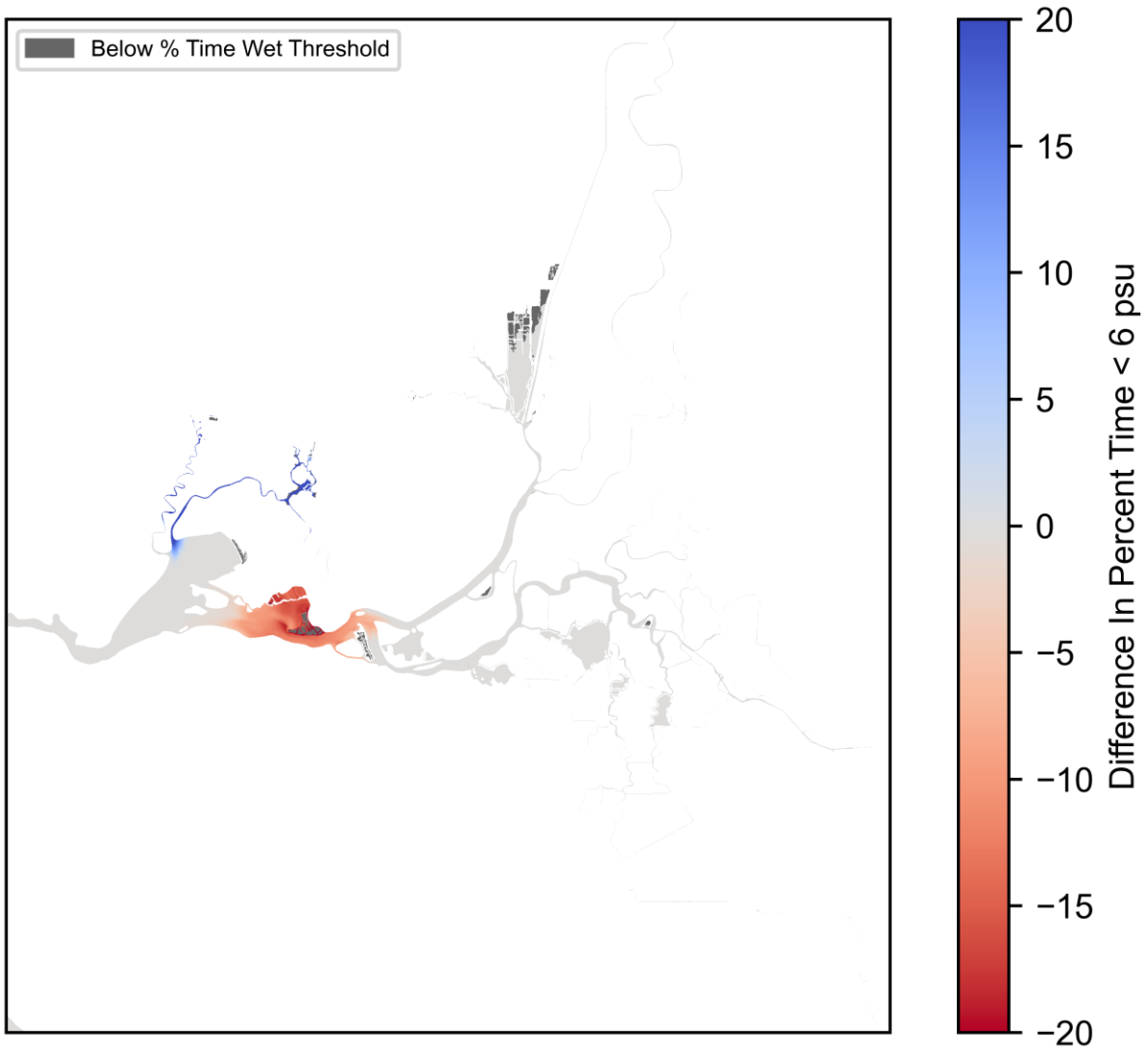

Figure 17 Example salinity suitability metric difference from 2D model output: difference between NDFA+SMSCG+DWSC and No Action August, Below Normal (1979 CS) percent time salinity < 6 psu

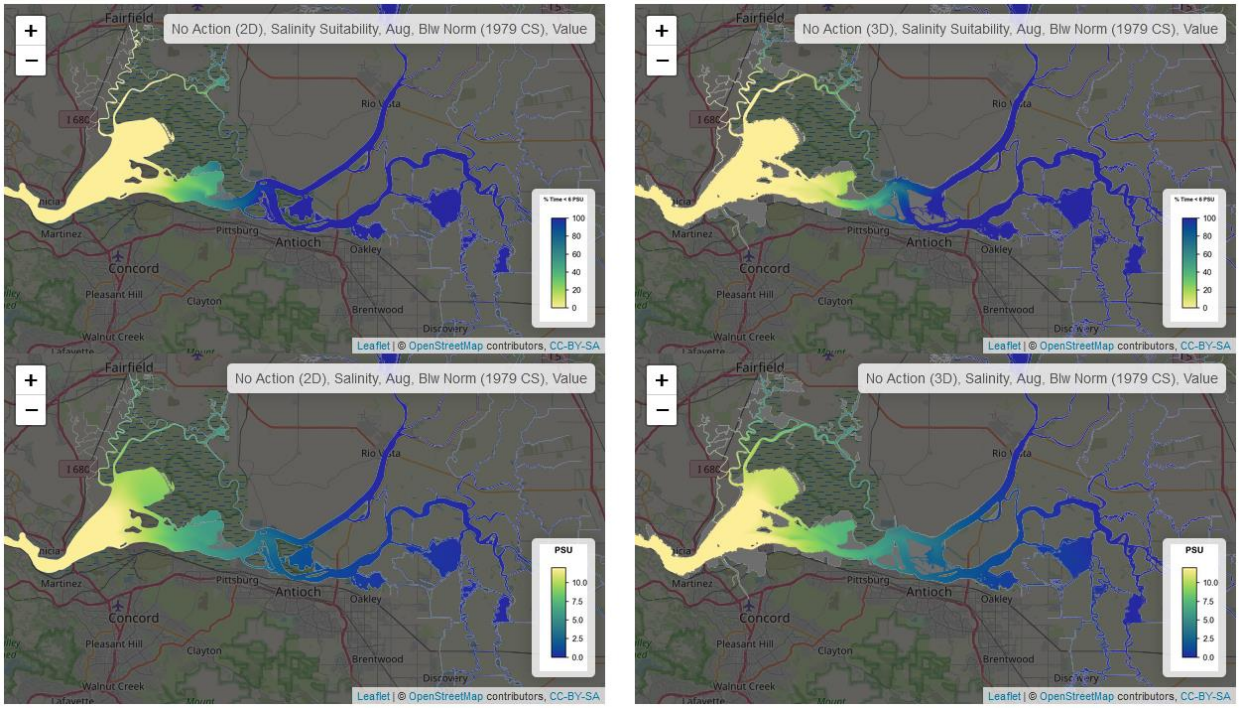

Figure 18 Example Shiny App comparison of 2D and 3D salinity and salinity suitability model results for August Below Normal (1979 CS), No Action

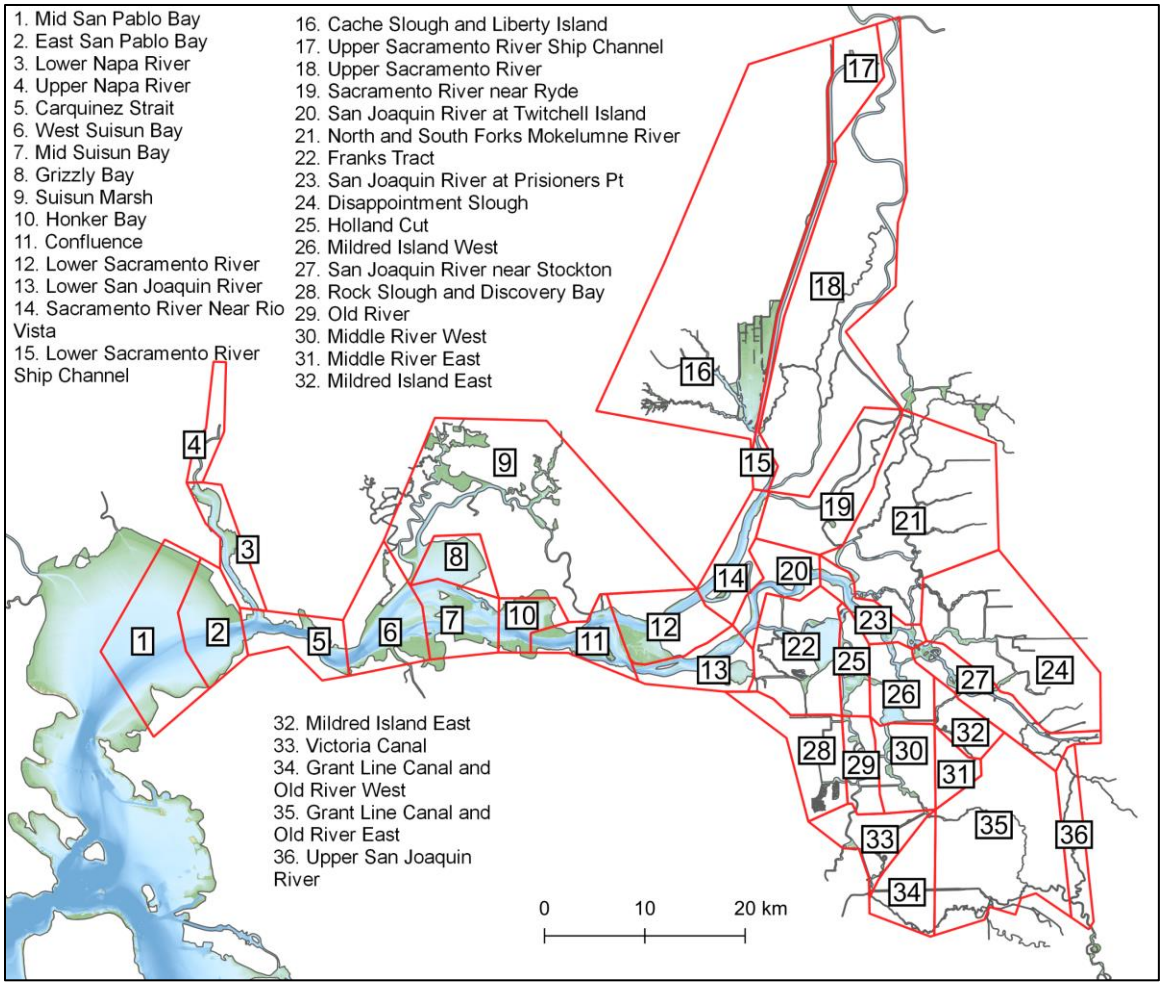

Figure 19 Enhanced Delta Smelt Monitoring (EDSM) program subregions used in tabulation of Habitat Suitability Index (HSI)

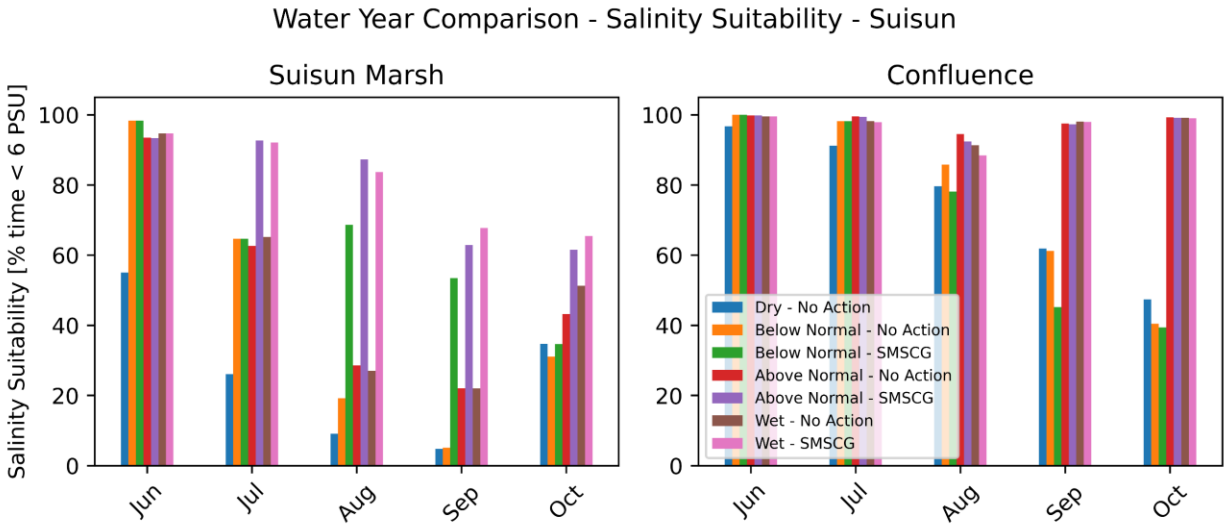

Figure 20 Volume-averaged monthly salinity suitability (% time > 6 psu) for EDSM subregions most influenced by the SMSCG actions, for four water-year types. Note that SMSCG operations were not simulated for the Dry year.

Water Temperature

For HSI calculations, predicted water temperature results are post-processed to fraction of time each month that temperature is less than 25 degrees C throughout the model domain. Examples of monthly-averaged water temperature and the water temperature suitability metric are shown in Figure 21 and Figure 22, respectively. Figure 23 shows the difference in July, Below Normal (1979 CS) monthly-averaged temperature suitability metric between the NDFA+SMSCG+DWSC and No Action scenarios in the Cache Slough Complex, where the DWSC action shifts the temperature and temperature suitability metric distribution in the DWSC.

Qualitative comparisons between 2D and 3D temperature modeling results can be made through the Shiny App. An example comparison for the No Action July, Below Normal (1979 CS) temperature and temperature suitability results in the Cache Slough Complex is shown in Figure 24. Gray areas indicate that water depths are too shallow to be included in habitat suitability calculations. The gray area in the northern part of Cache Slough Complex is much greater in the 3D model, due to the use of a depth threshold for the 3D model in addition to the % time wet threshold that was used for the 2D model. The 2D model temperatures are slightly higher. Compared with the 3D model, the 2D model predicts a larger area of potential habitat with slightly lower temperature suitability.

Monthly volume-averaged temperature suitability, defined as percent time less than 25 C, varied most in the Upper Ship Channel due to the DWSC action, where warm water was displaced downstream (Figure 25). In the Upper Ship Channel,

temperature suitability increased to above 40% from 0% in July and to slightly above 0% in August. There was a corresponding slight decrease in temperature suitability downstream in the Lower Ship Channel. There were negligible changes to water temperature and temperature suitability in the Cache Slough and Liberty Island, and Sacramento River near Rio Vista Regions. The NDFA action produced negligible changes in volume-averaged temperature suitability.

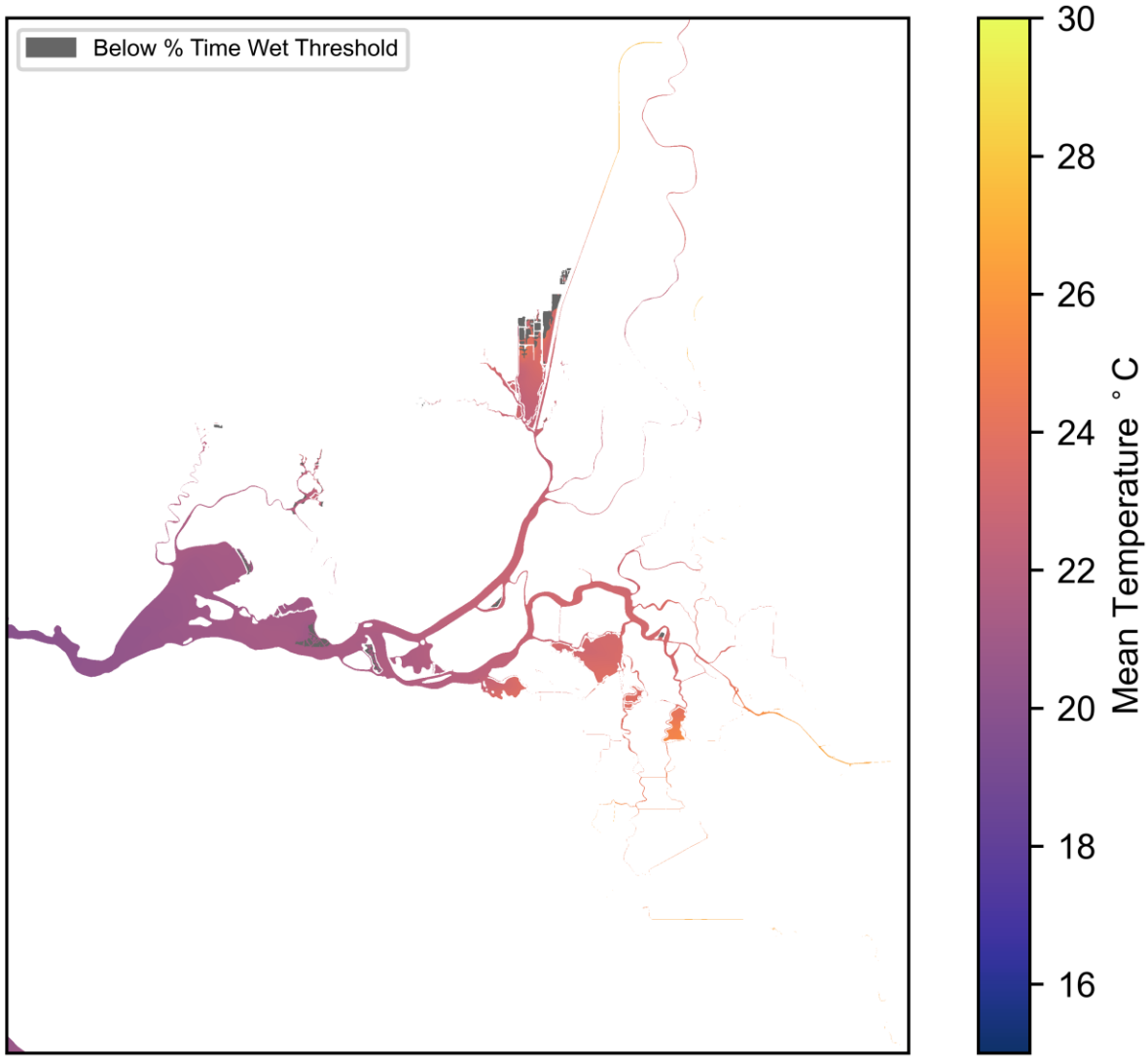

Figure 21 Example monthly-averaged temperature from 2D model output: July, Below Normal (1979 CS) No Action scenario

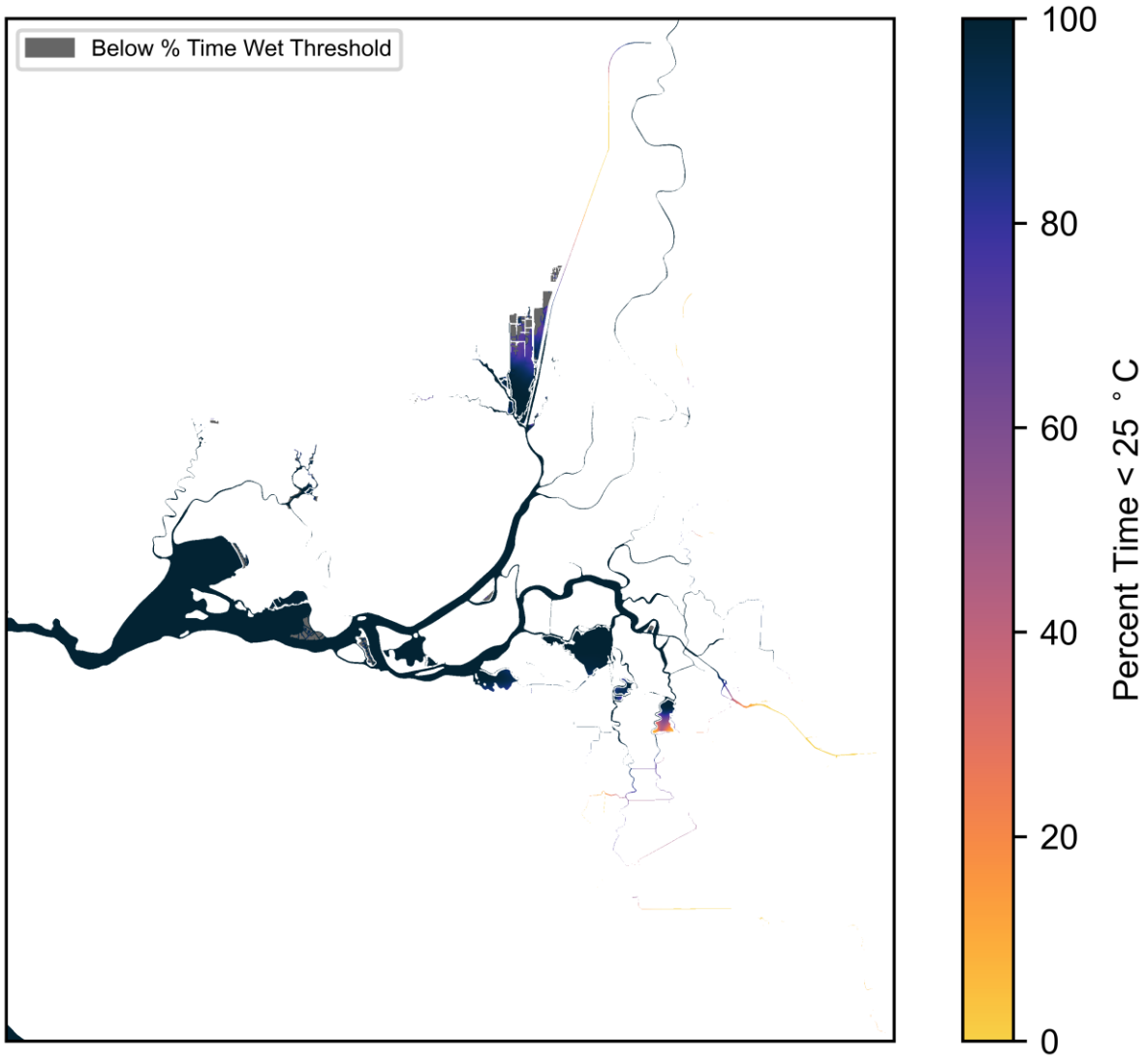

Figure 22 Example water temperature suitability metric from 2D model output: percent time water temperature < 25 ° C during July, Below Normal (1979 CS) for the No Action scenario

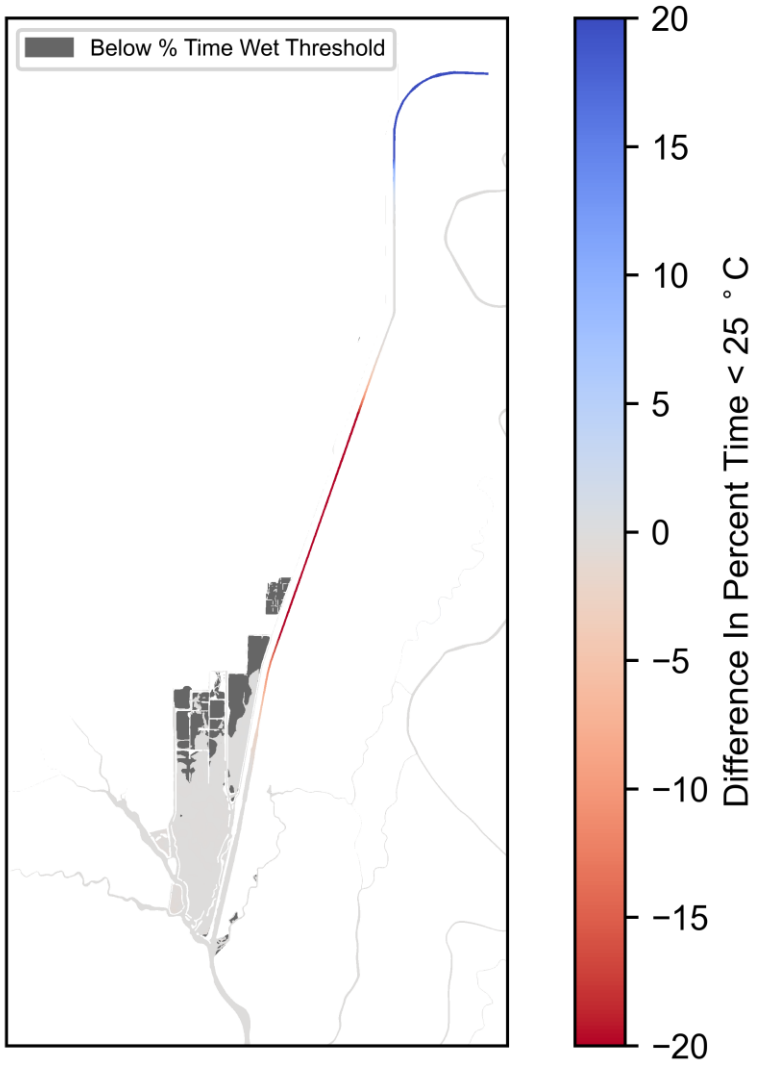

Figure 23 Example water temperature suitability metric difference from 2D model output: difference between NDFA+SMSCG+DWSC and No Action July, Below Normal (1979 CS) percent time water temperature < 25 ° C in Cache Slough Complex

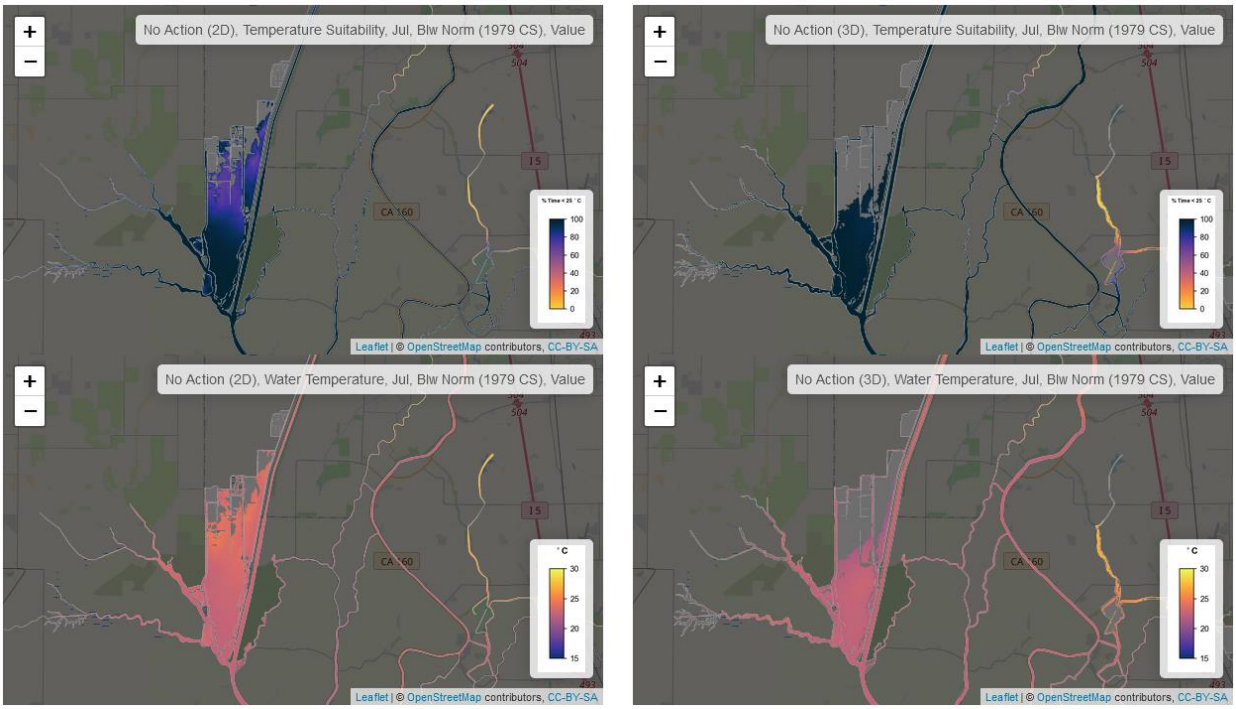

Figure 24 Example Shiny App comparison of 2D and 3D temperature and temperature suitability model results for July Below Normal (1979 CS), No Action

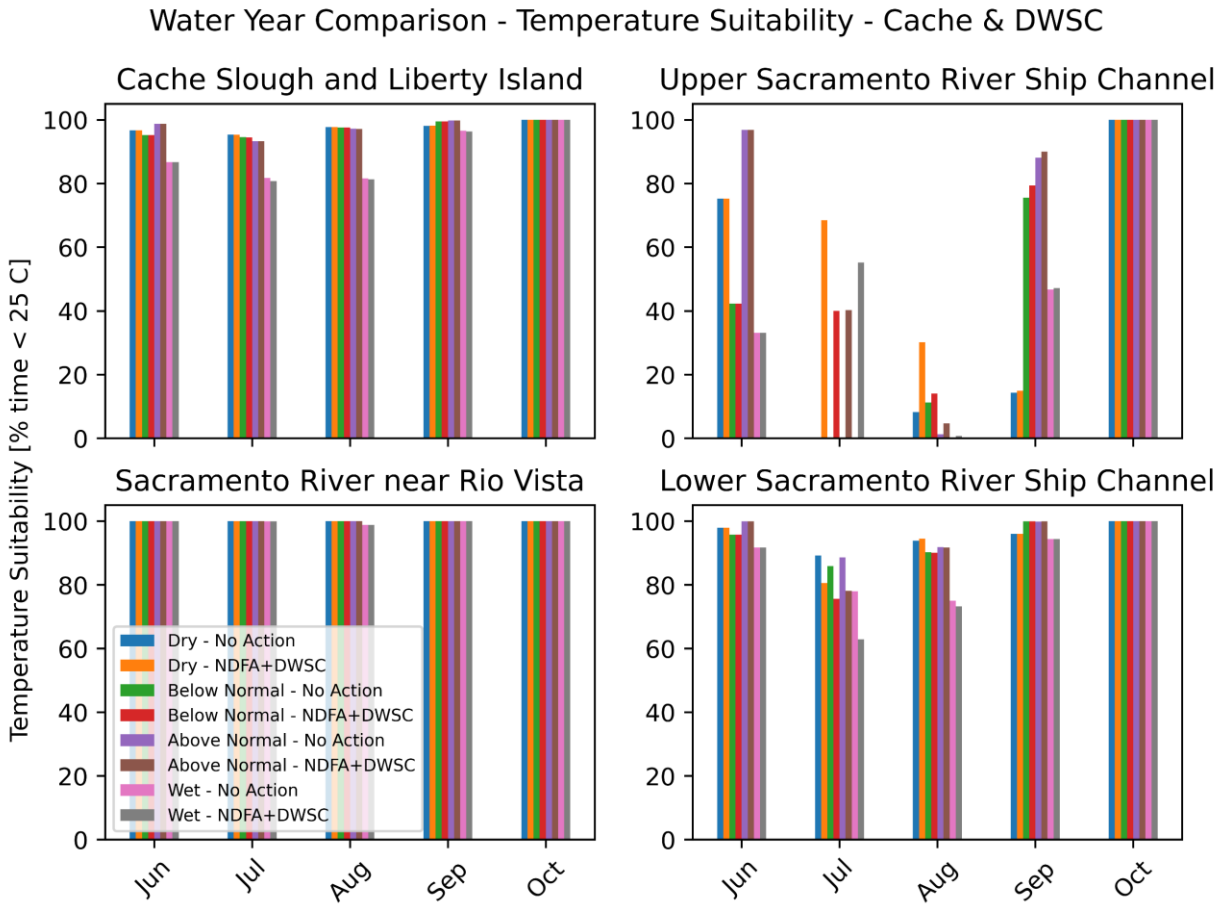

Figure 25 Volume-averaged monthly temperature suitability (% time < 25 C) for EDSM subregions near Cache Slough, spanning four different water year flow types.

Turbidity – Secchi Depth

Secchi depth was estimated by interpolating observed continuous turbidity data over the model domain. An example of monthly Secchi depth with turbidity station locations is shown in Figure 26.

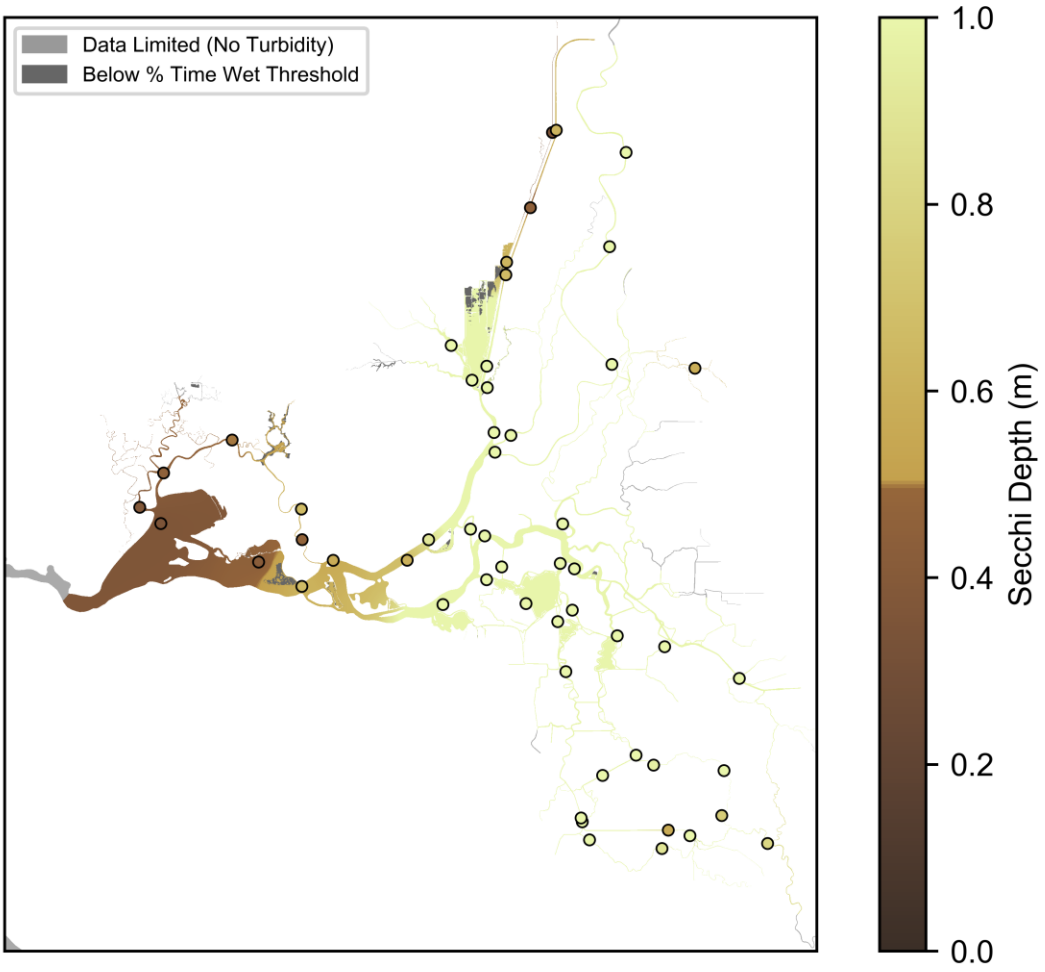

Figure 26 Example interpolated monthly-averaged Secchi depth for August, Below Normal (2018 Historical). Circles show monthly-averaged values at turbidity stations used in the interpolation.

Because sufficient turbidity data were only available for recent years, Secchi depths calculated for 2018 (Below Normal) were used for all Below Normal and Dry year analyses and 2019 (Wet) Secchi depths were used for Wet and Above Normal year analyses. Secchi depth was calculated from turbidity (typically NTU) time series data at the stations. To compute a monthly average, *Turbidity* (NTU) was transformed into *SecchiDepth* (m) according to a relationship developed for the Sacramento-San Joaquin Delta by Pete Smith (pers. comm.):

$$SecchiDepth = \frac{4.8228}{Turbidity^{0.7518}}$$

Paired *Secchi Depth* and *Turbidity* data were obtained during the California Department of Fish and Wildlife Fall Midwater Trawl (FMWT) surveys in 2009-11 and Spring Kodiak Trawl (SKT) in 2011-12. This relationship largely agrees with other published and available turbidity-Secchi relationships for different regions, but has the benefit of fitting data from our study region (Figure 27). Interestingly, three of the fitted curves, including the curve used here, all cross at the HSI threshold of 0.5 m Secchi depth at a Turbidity value of 20 NTU.

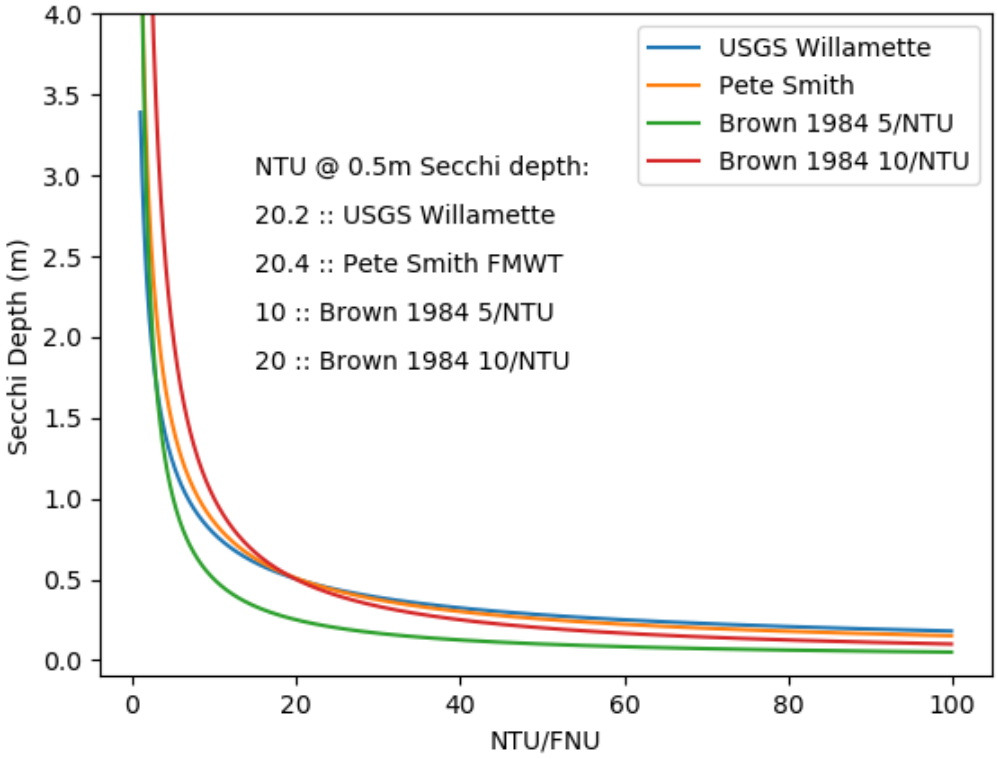

*Figure 27 Available Turbidity-Secchi Depth relationships. Pete Smith curve (R^2=0.9439; pers. comm.) was used to convert Turbidity to Secchi Depth for this study. The USGS Willamette curve is Secchi Depth = 11.123*Turbidity$^{-0.637}$. Brown (1984) found two relationships that bounded their paired observations, Secchi Depth = 5/Turbidity, and Secchi Depth = 10/Turbidity.*

HABITAT SUITABILITY INDEX RESULTS

The full array of HSI results from this study have been made publicly accessible through the Shiny App (https://dshm.rmanet.app/overview/).

All HSI results utilize depth-averaged monthly results from the 2D model and 3D model for which results were averaged over the vertical dimensions. Scenario HSI results were differenced to create maps of differences between scenarios. All results were converted to raster format. Example plots of monthly-averaged HSI and HSI difference from No Action are provided in Figure 28 and Figure 29.

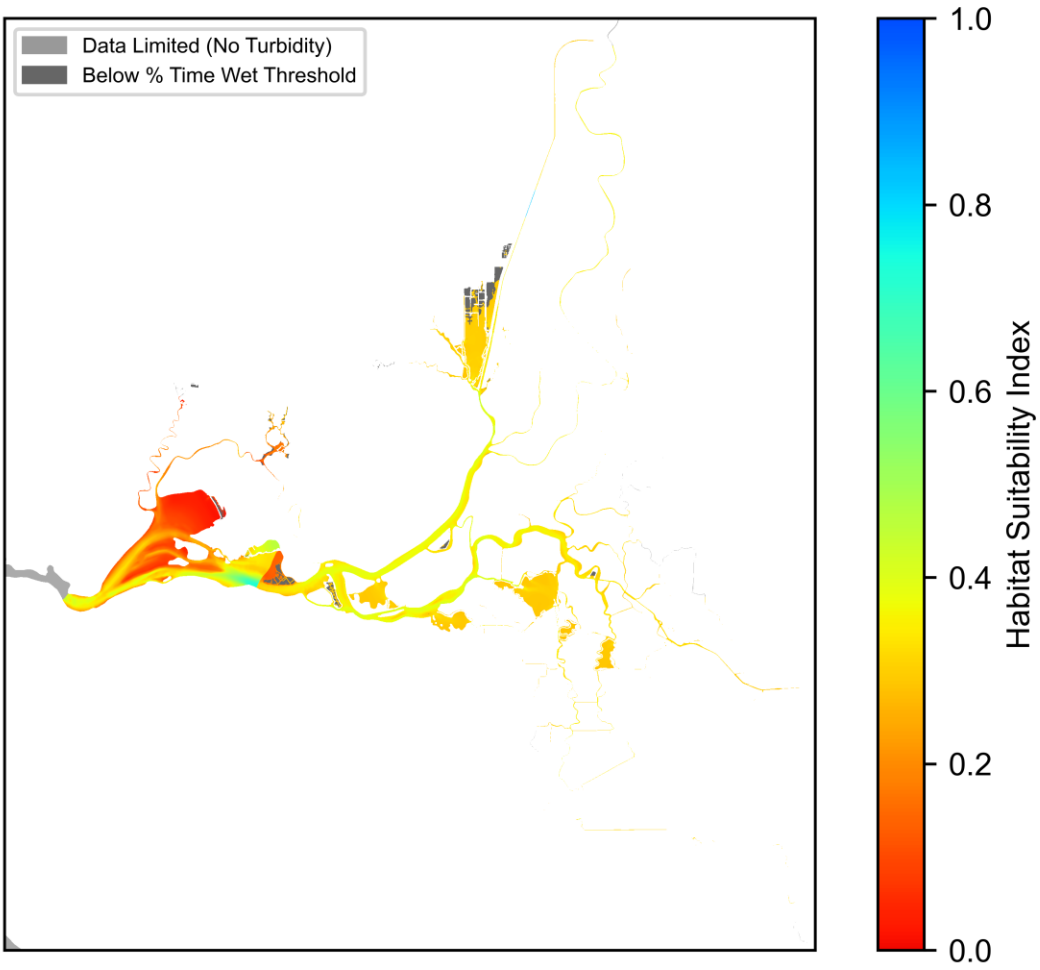

Figure 28 Example monthly-averaged HSI from 2D model output: August, Below Normal (1979 CS) No Action scenario

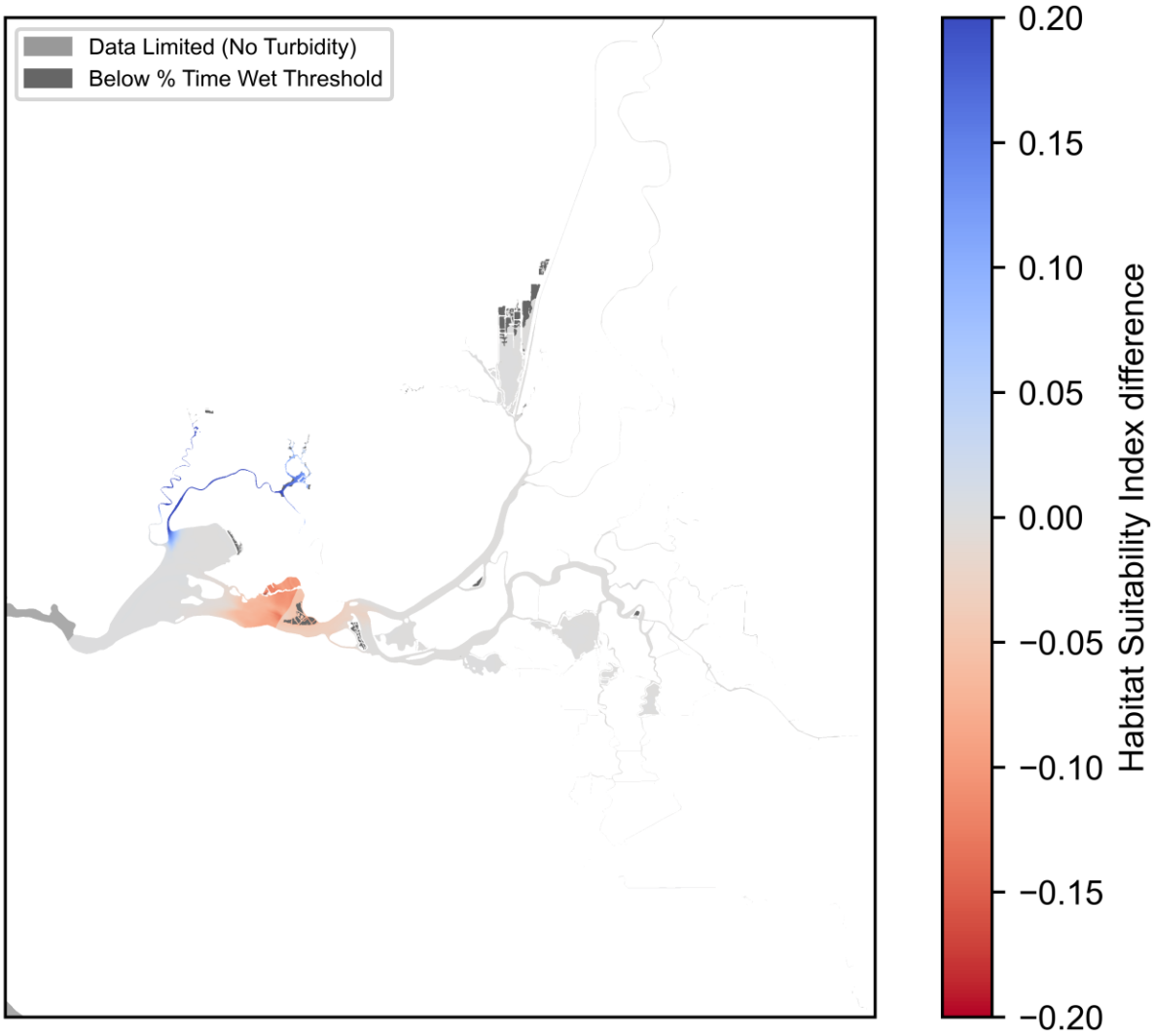

Figure 29 Example HSI difference from 2D model output: difference between NDFA+SMSCG+DWSC and No Action August, Below Normal (1979 CS) monthly-averaged HSI

Management actions cause some changes in predicted HSI. The effects are generally at a regional or smaller scale (not estuary-wide) and there is minimal spatial overlap in effects. General observations of the management effects on HSI:

- Suisun Marsh Salinity Control Gate operation
  - Lowered salinity in Suisun Marsh, improving HSI in Suisun Marsh (Figure 30)
  - Increased salinity in eastern Suisun Bay, decreasing HSI (Figure 30)
  - Increased current speed at the western end of Montezuma Slough, improving HSI
  - Decreased current speed at the eastern end of Montezuma Slough, decreasing HSI
- Deepwater Ship Channel Flow Augmentation

    - Shifted temperature distribution in DWSC, causing habitat to shift northward in the DWSC (Figure 31)
    - May affect turbidity but not currently modeled
- North Delta Flow Action
    - Increased current speed in Toe Drain, causing no discernible difference in HSI

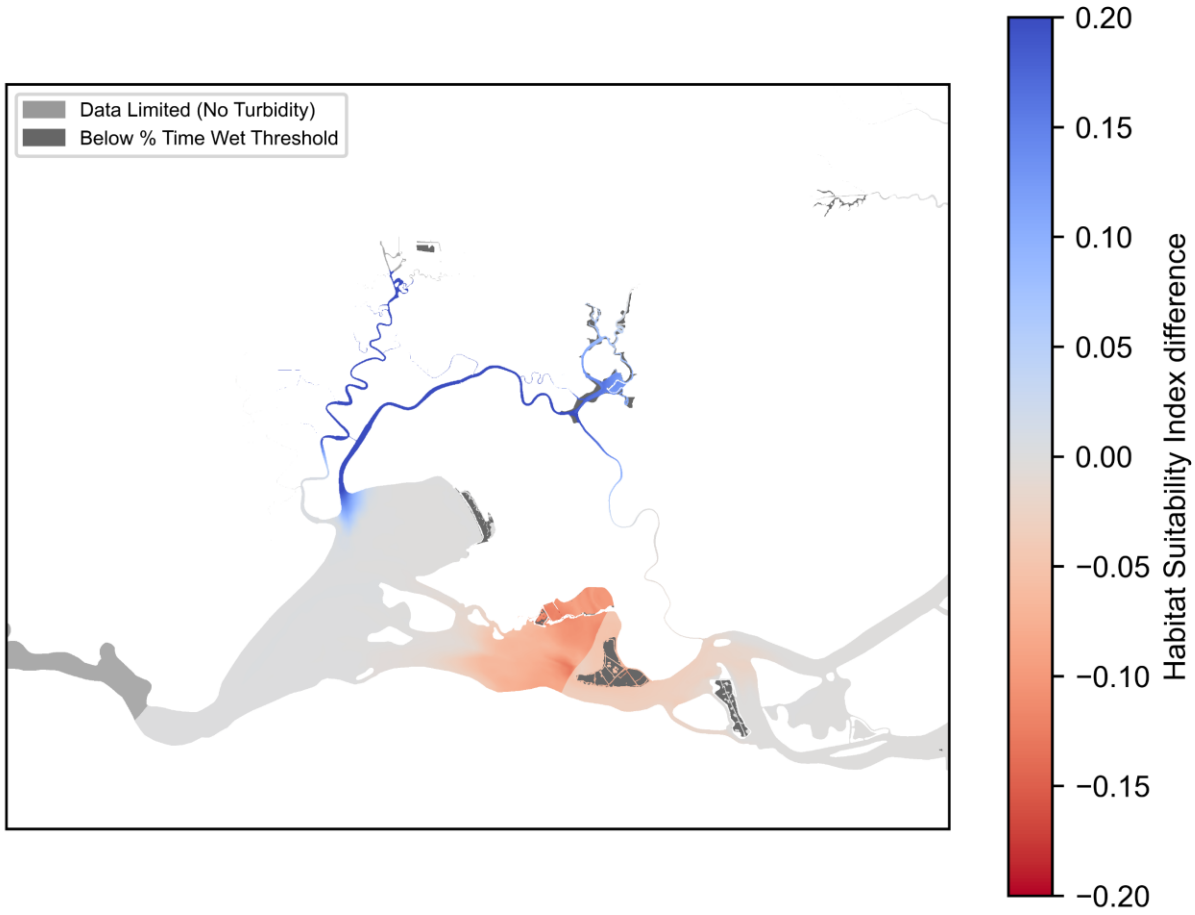

Figure 30 Example HSI difference from 2D model output in Suisun Marsh: difference between NDFA+SMSCG+DWSC and No Action August, Below Normal (1979 CS) monthly-averaged HSI

Table 7 Comparison of Base and SMSCG model scenarios in Suisun Marsh subregion. Monthly-averaged Habitat Suitability (HSI) and the salinity suitability component of HSI (% time less than 6 PSU) are compared, weighted by volume, for the Below Normal water year (1979 CS). HSI ranges from 0-1, and salinity suitability is in units of %.

Scenario	Metric	July	August	September	October
Base	HSI	0.582	0.206	0.153	0.320
SMSCG	HSI	0.582	0.511	0.420	0.345
No Action	% Time < 6 PSU Salinity	64.7	19.2	5.1	31.0
SMSCG	% Time < 6 PSU Salinity	64.7	68.6	53.4	34.6

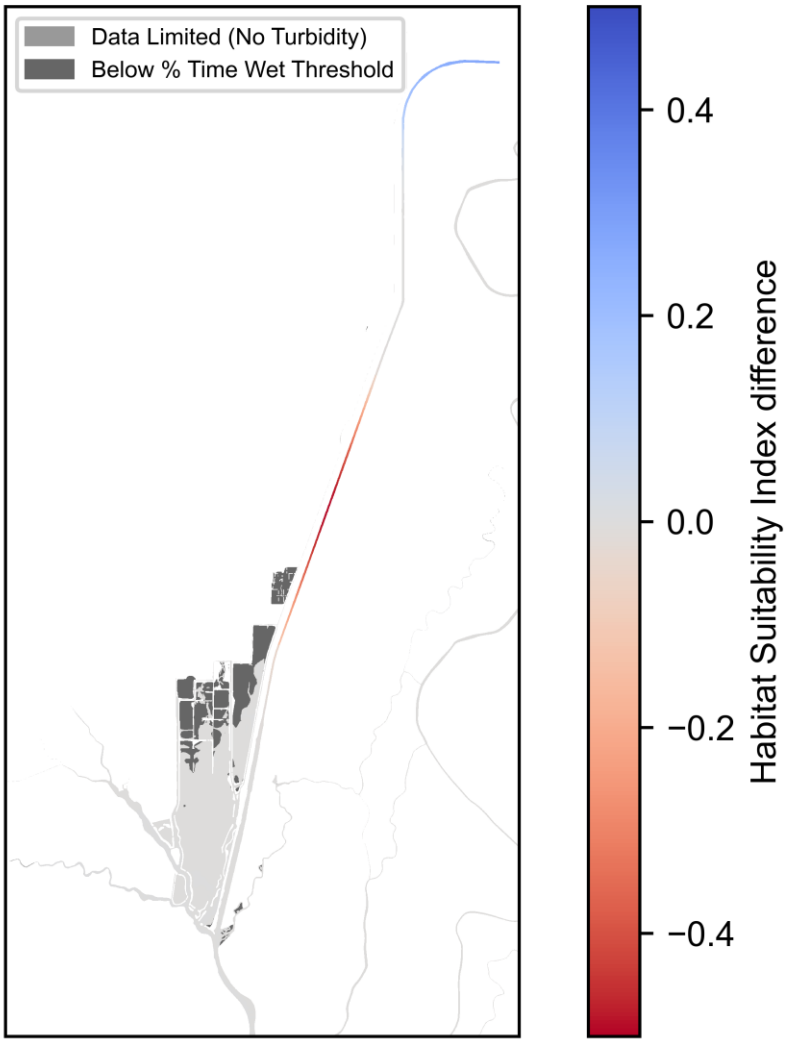

Figure 31 Example HSI difference from 2D model output in Cache Slough Complex: difference between DWSC and No Action July, Below Normal (1979 CS) monthly-averaged HSI

Habitat Suitability Index (HSI), calculated as volume-averaged monthly index across the four EDSM regions (Figure 32), showed little change as a result of different

combinations of actions (Figure 33-Figure 36); scenarios that included the SMSCG action showed slight increase in HSI in the West region where the action occurred. However, narrowing in on the EDSM subregions (Figure 19) closer to the actions, HSI in Suisun Marsh increased during Jul-Oct in water years where the SMSCG action occurred, with a >100% increase in August and September (Figure 37). In the Upper Ship Channel subregion, the DWSC action increased the average HSI above zero to between 0.1-0.2 in August, but had little impact outside that month (Figure 38).

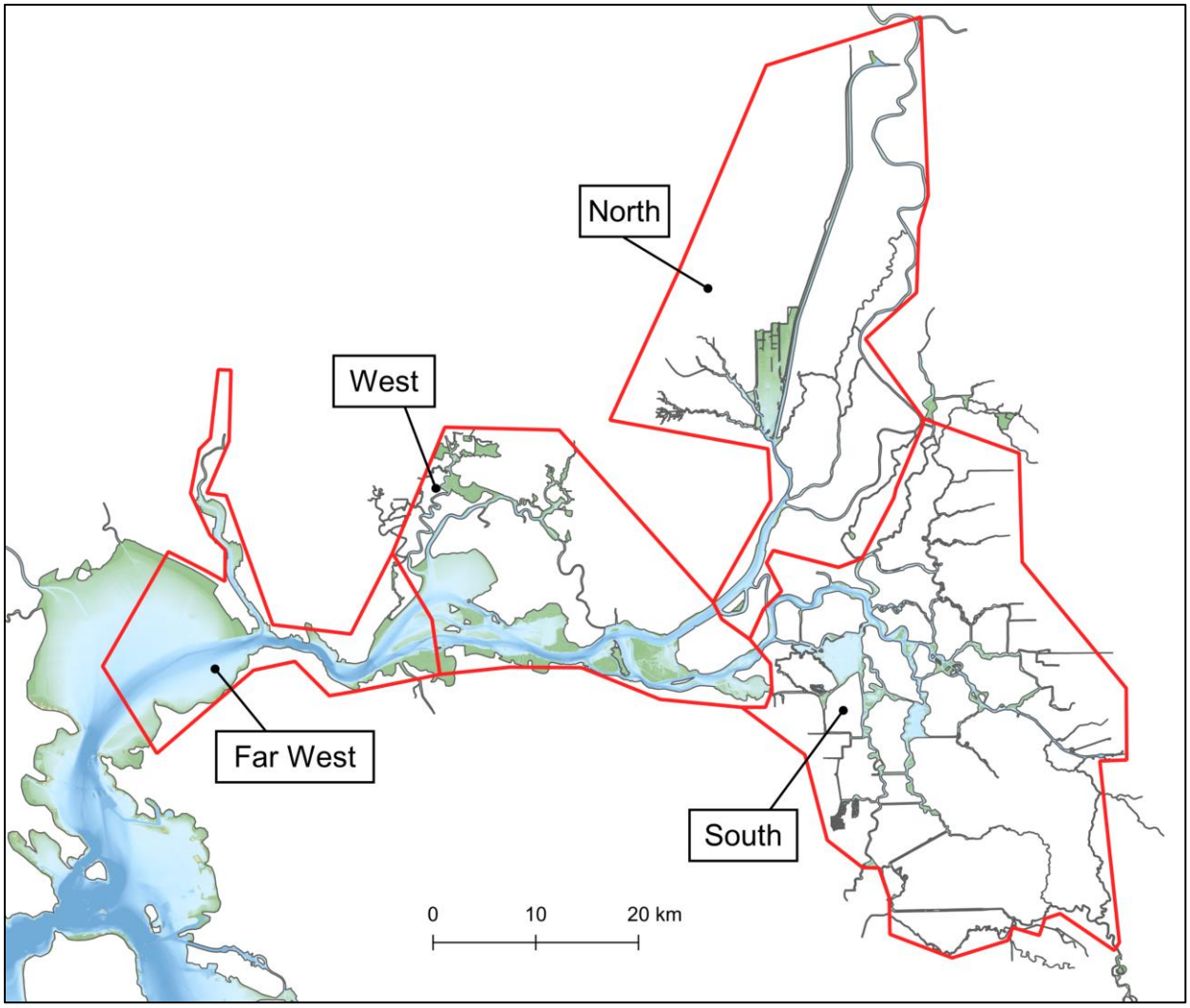

Figure 32 Broad regions used in tabulation of Habitat Suitability Index (HSI), corresponding to the regions of the Enhanced Delta Smelt Monitoring (EDSM) program

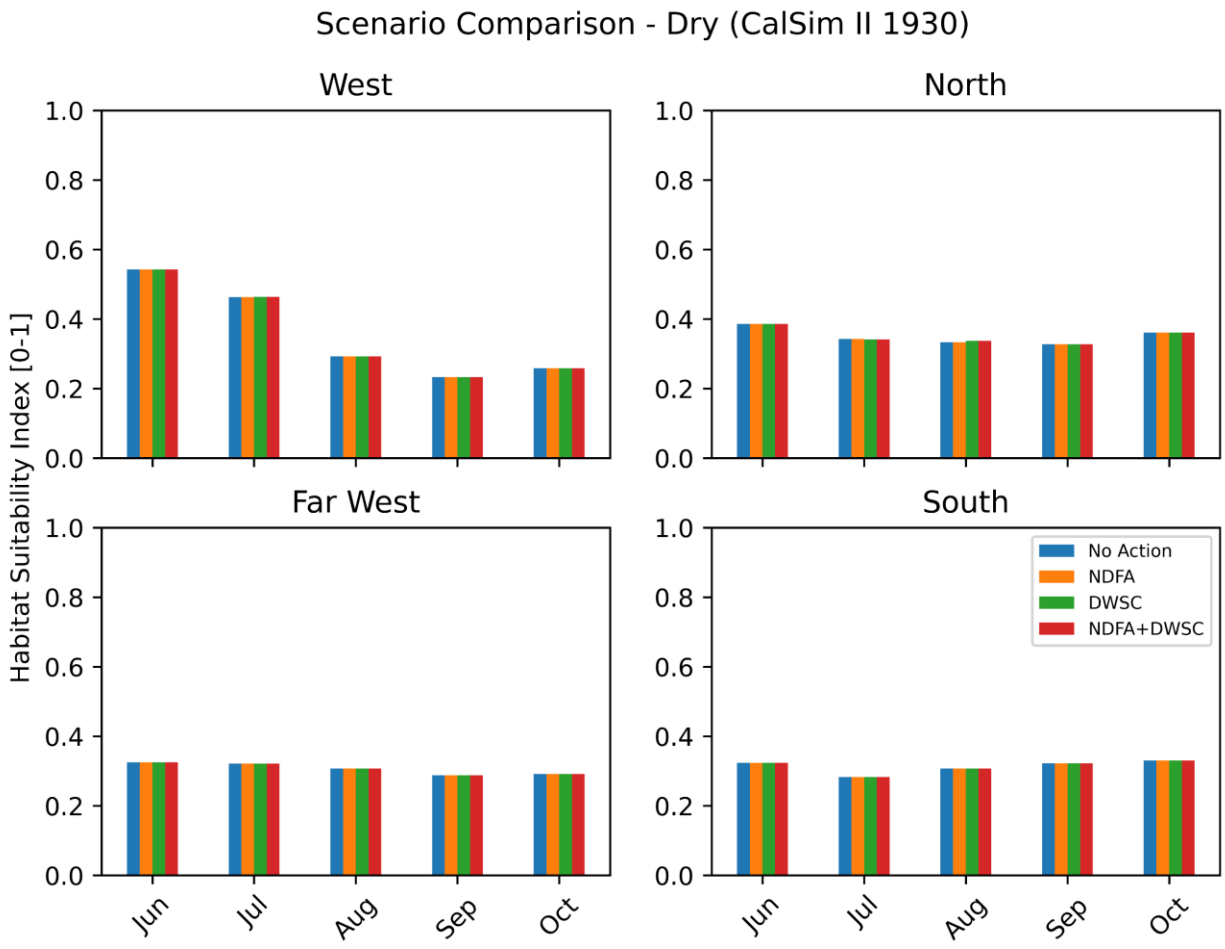

Figure 33 Dry water year (1930 CS) volume-averaged Habitat Suitability Index in EDSM regions for different action scenarios. No SMSCG actions took place in the Dry year.

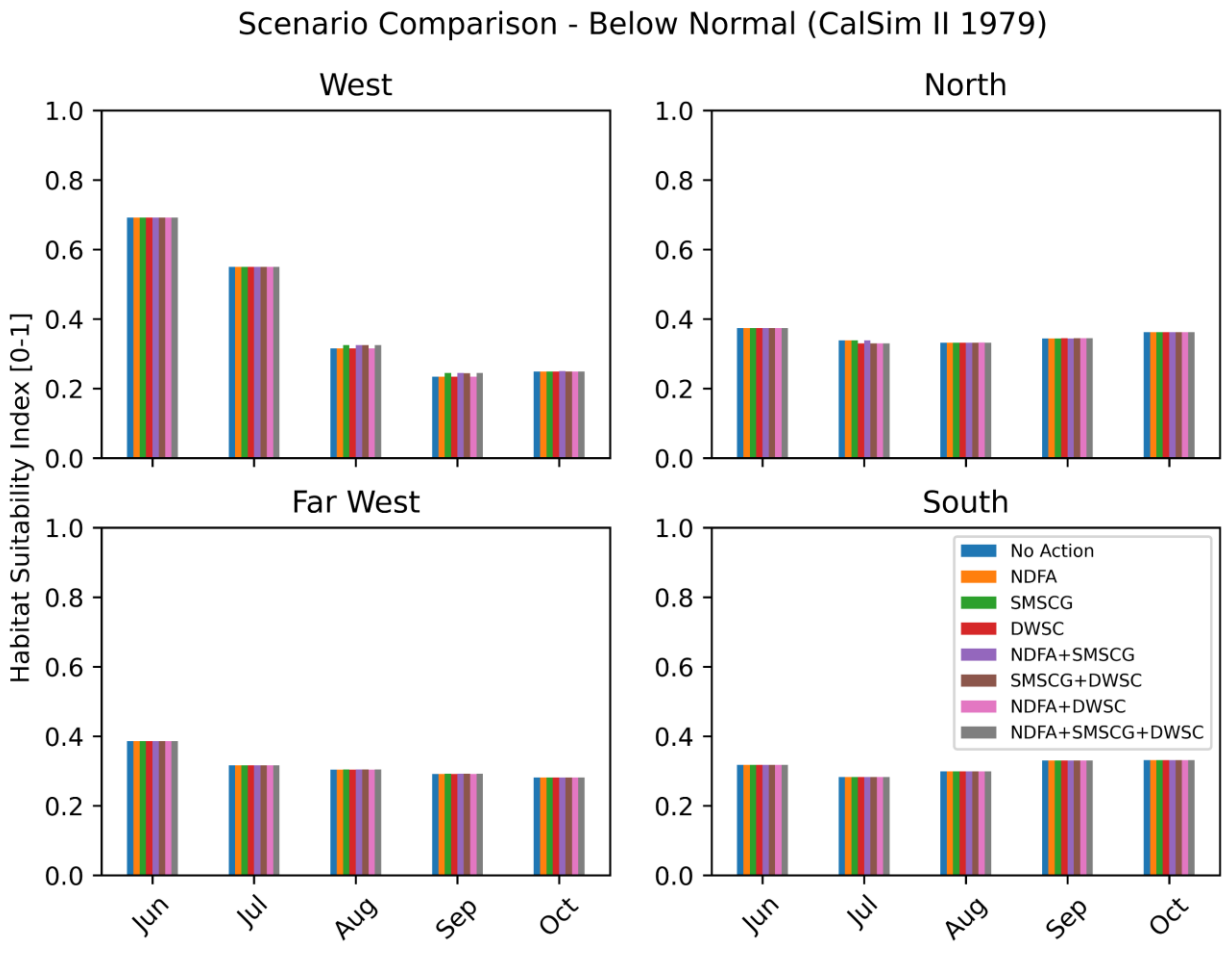

Figure 34 Below Normal water year (1979 CS) volume-averaged Habitat Suitability Index in EDSM regions for different action scenarios.

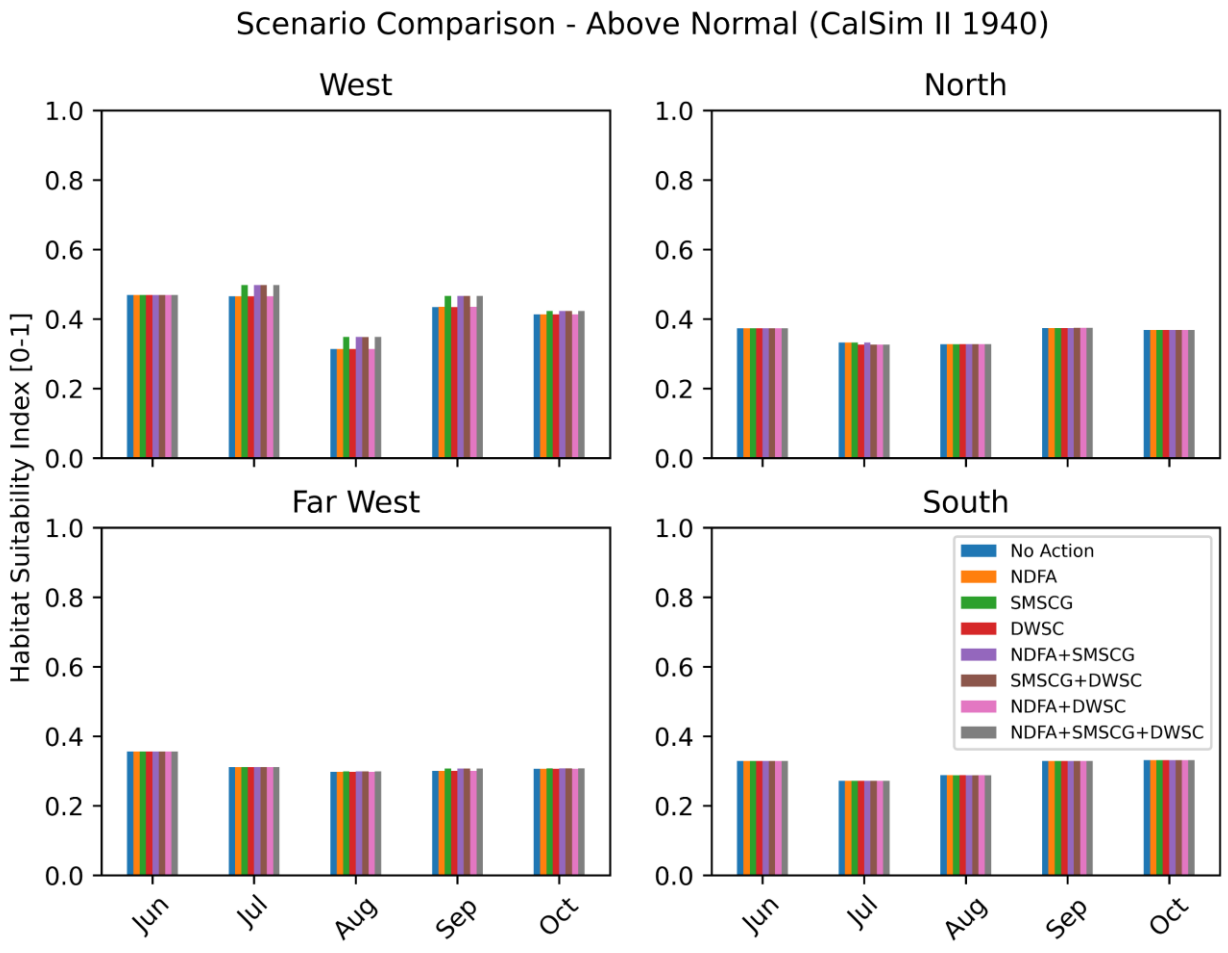

Figure 35 Above Normal water year (1940 CS) volume-averaged Habitat Suitability Index in EDSM regions for different action scenarios.

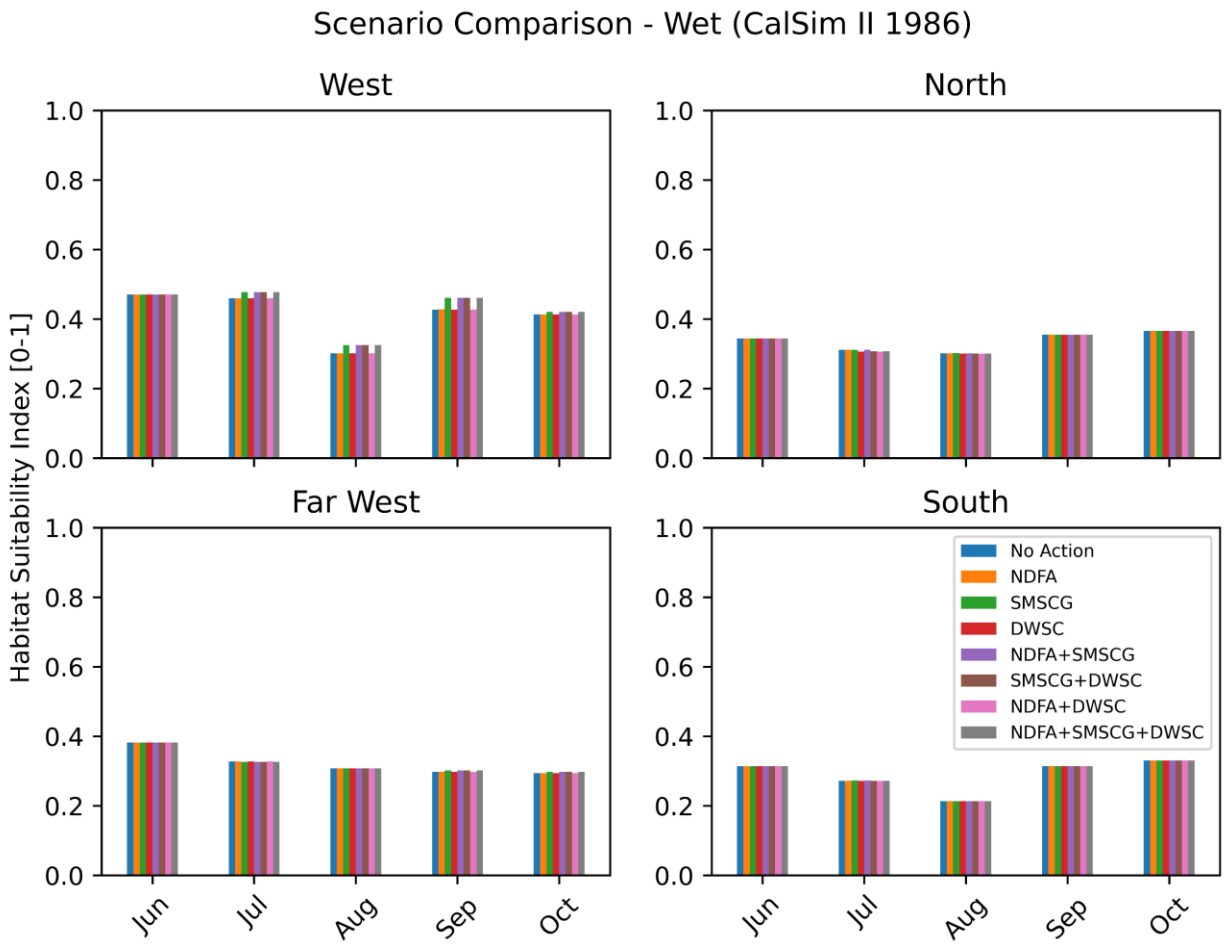

Figure 36 Wet (1986 CS) water year volume-averaged Habitat Suitability Index in EDSM regions for different action scenarios.

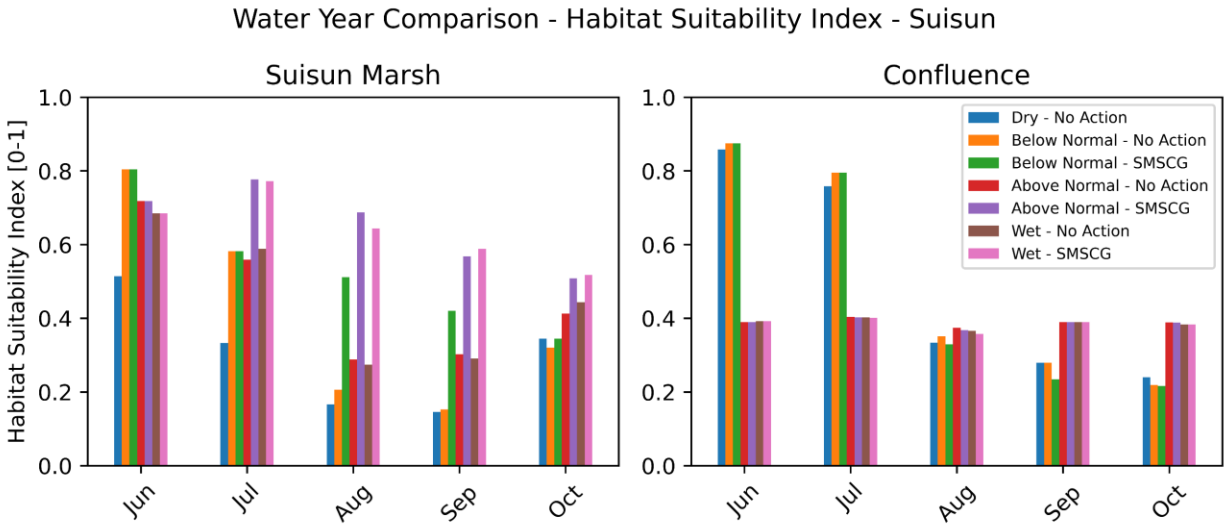

Figure 37 Volume-averaged monthly HSI for EDSM subregions most affected by the SMSCG action. HSI increased over 100% in August and September in Suisun Marsh with the SMSCG action.

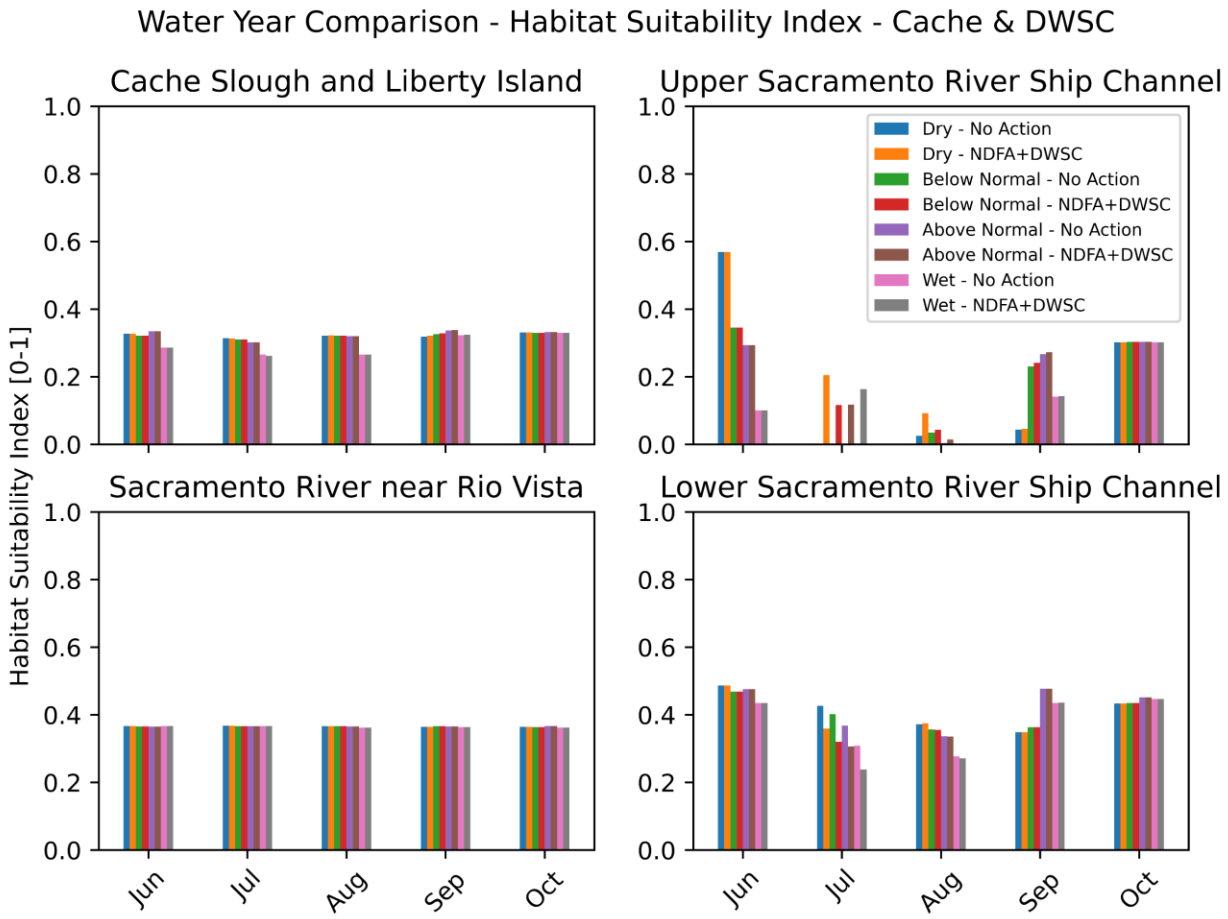

Figure 38 Volume-averaged monthly HSI for EDSM subregions near the location of the NDFA and DWSC actions. Lowered temperatures due to cold inflowing water caused a small increase above zero in HSI in the Upper Sacramento River Ship Channel and caused a smaller decrease in HSI in the Lower Sacramento River Ship Channel as the warm water was advected seaward.

THREE-DIMENSIONAL EFFECTS

Three-dimensional effects of management actions can be explored in multiple ways. One is by comparing results from the depth-averaged (2D) modeling and the three-dimensional modeling. This is useful but the differences between models may result from differences in formulation and grid resolution, among other factors, in addition to resolution of three-dimensional physical processes. Therefore, we also explore whether the three-dimensional results show salinity and temperature stratification or other three-dimensional patterns.

As noted previously, comparison of two-dimensional and three-dimensional predictions can be readily explored in the Shiny App. An example comparison of

HSI and temperature results from both model platforms is given in Figure 24. Both models were also be used to estimate differences between action scenarios and the No Action scenario and these differences can also be explored in the Shiny App. An example of temperature differences resulting from management actions is given in Figure 39. Exploration of results generally indicates qualitative similarity in predictions of abiotic fields and management effects. One significant difference noted is that the 3D model sometimes predicts higher temperature in the Suisun Marsh relative to the 2D model (Figure 40). Since Figure 40 shows predictions for a historical year, we can evaluate which model is more consistent with temperature observations. The 2D model was more consistent while the 3D model overpredicted temperature locally in the Suisun Marsh. So, in this specific case, the differences were not due to three-dimensional effects but to better model performance of the 2D model. The difference likely results from scaling of wind speed to account for marsh shading that was implemented differently in the two models.

We explored temperature and salinity stratification in regions and times potentially affected by management actions. The Deepwater Ship Channel transect along which we examined vertical variability of model predictions is shown in Figure 41. We focus the analysis on July, when the management action is expected to occur. An example of stratified conditions is given in the three-dimensional model results along the Deepwater Ship Channel in July 5, 2018 (Below Normal) at 17:00 (Figure 42). The typical dynamic is that density gradients strengthen during flood tide and stratification forms during ebb tide due to tidal straining. Flood tides are typically well-mixed. Salinity stratification is less pronounced in this region. When tidally-averaged, some vertical variability in temperature is still noted. However, a significant estuarine circulation pattern in longitudinal velocity is not clear (Figure 43).

Monthly-averaged vertical variability in 3D model predictions along the DWSC transect are plotted in Figure 44. While salinity stratification is small, temperature stratification is significant in the upper half of the DWSC. The vertical variability in longitudinal velocity likely results partially from wind forcing.

The Montezuma Slough transect along which we examined vertical variability of model predictions is shown in Figure 45. An example of salinity stratified conditions is present in the three-dimensional model results along the upper (east) portion of Montezuma Slough on August 2 at 22:00 (Figure 46) during an ebb tide after operation of the SMSCG commenced. Stratification typically forms during ebb tide due to tidal straining and density-driven flow and persists through slack water and part of the subsequent flood tide. In contrast, well-mixed conditions are typical

during peak flood tides. When tidally-averaged, some vertical variability in salinity is still noted (Figure 47). Days after commencement of the SMSCG operation, freshwater has moved further west along the transect and compressed salinity gradients in that region, leading to salinity stratification on ebb tides (Figure 48). On the west end of the slough an estuarine circulation pattern can be seen with longitudinal velocity directed seaward (toward the west end of the slough) at the surface and landward at depth (Figure 49 and Figure 50).

Taken together the analysis of three-dimensional results indicate that both salinity and temperature stratification in key areas of interest is transient and estuarine circulation and other exchange flow patterns are weak. This analysis suggests that overall circulation and transport patterns can be represented by a depth-averaged model. However, results also suggest some vertical variability in habitat quality which can be explored best with a three-dimensional model.

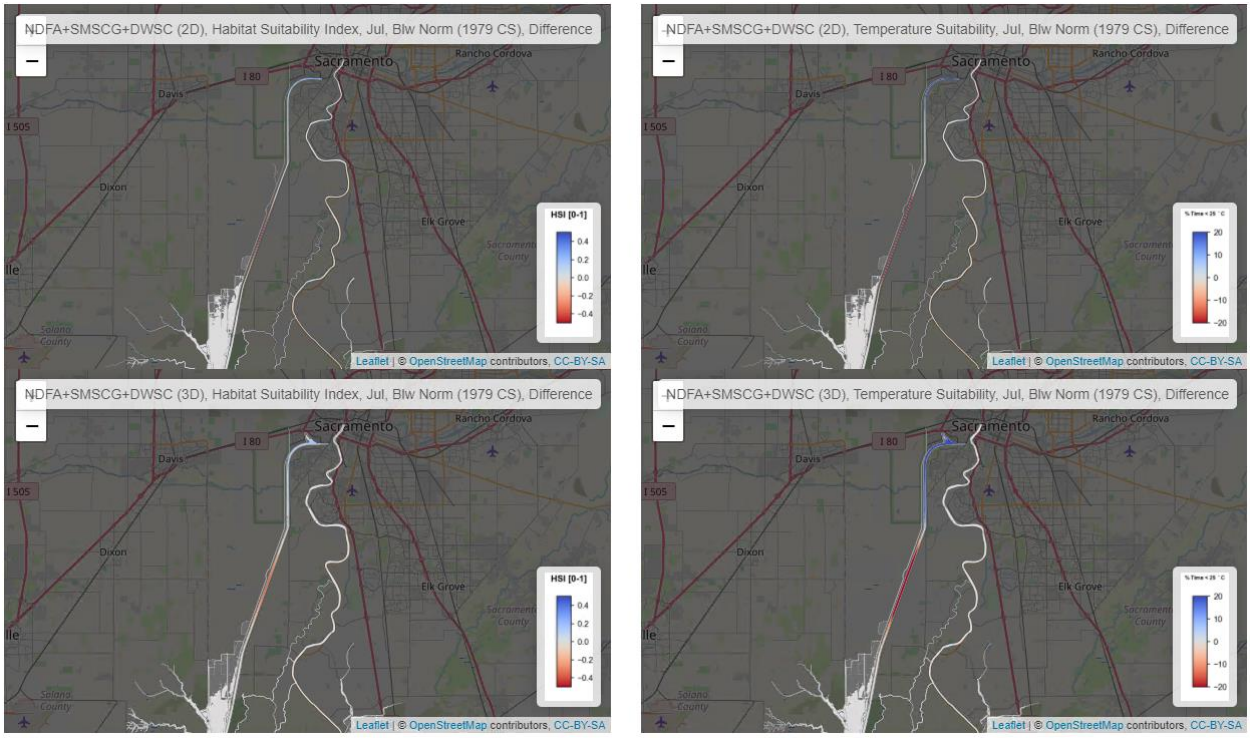

Figure 39 2D (top row) and 3D (bottom row) estimates of habitat suitability differences (left column) and temperature differences (right column) between the NDFA+SMSCG+DWSC scenario relative to the No Action scenario in July of a Below Normal water year (1979 CS)

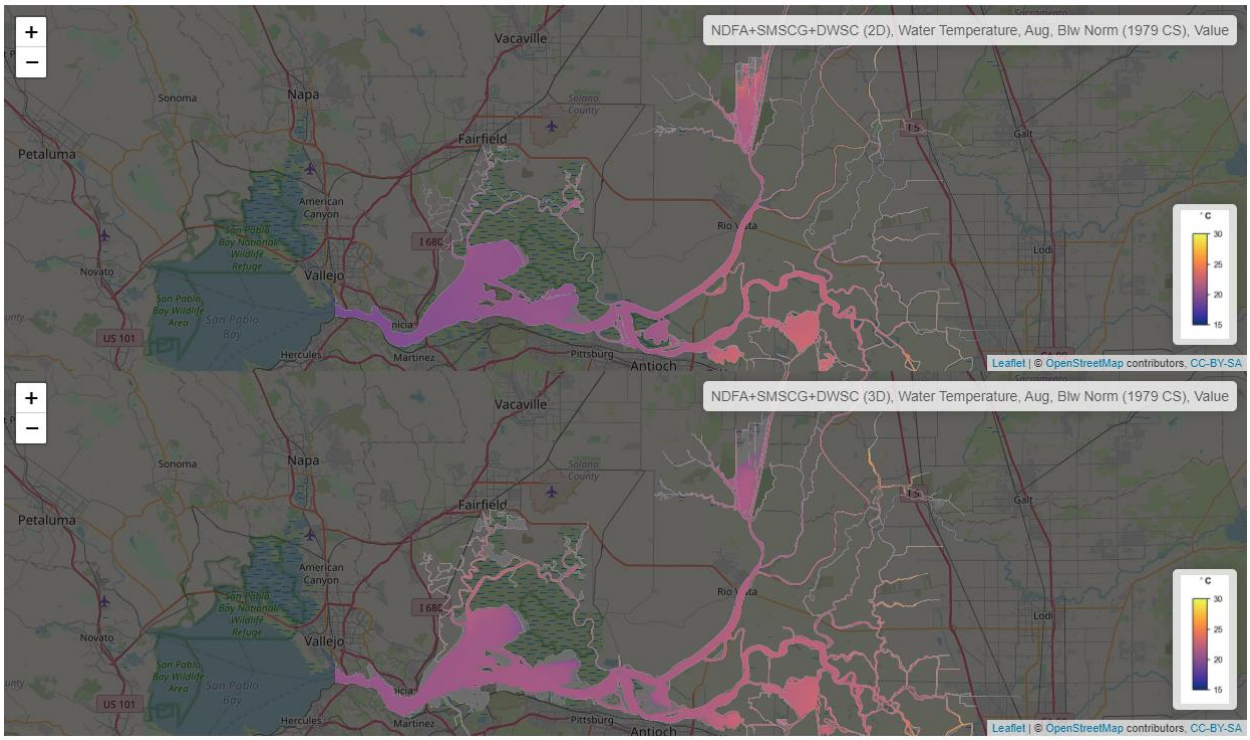

Figure 40 Temperature predictions for the 2D (top row) and 3D (bottom row) models in August of the historical Below Normal water year (2018)

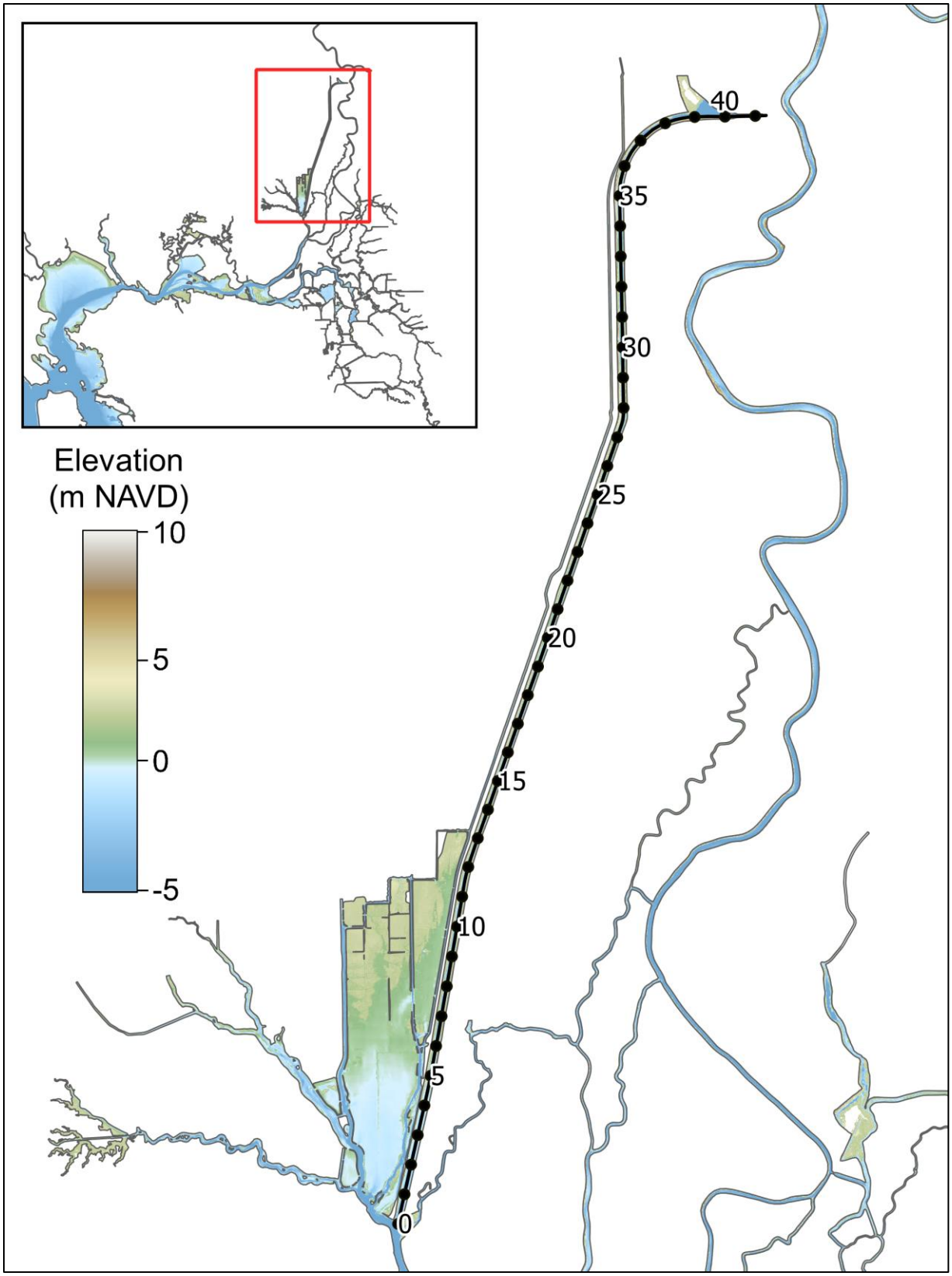

Figure 41 Transect for examination of vertical variability of three-dimensional model results in the Deepwater Ship Channel

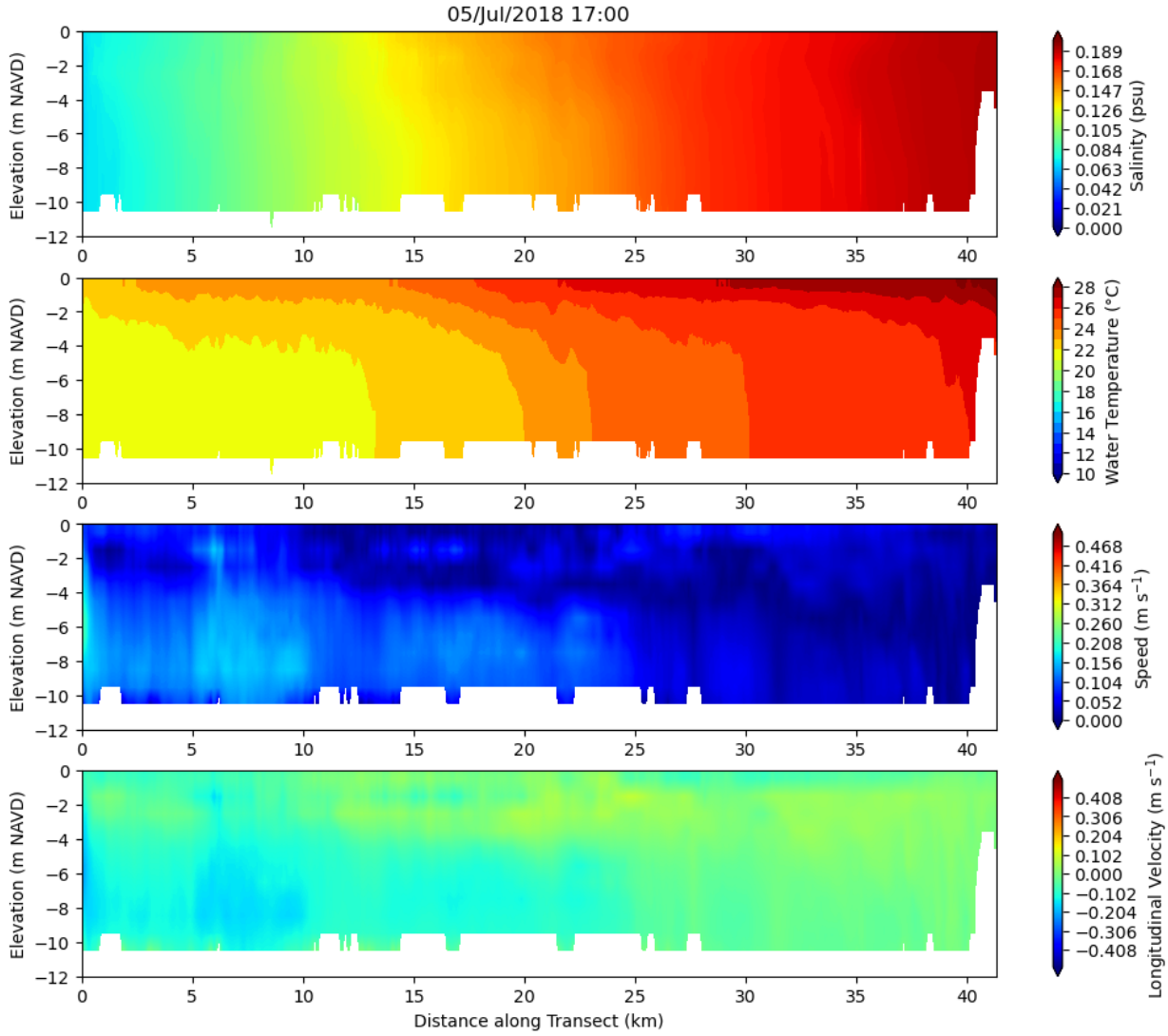

Figure 42 Three-dimensional model results along the Deepwater Ship Channel on July 5, 2018 (Below Normal Historical) at 17:00, during an ebb tide. The x-axis is distance along the ship channel (zero at the south end). The panels (from top) are salinity, temperature, speed and longitudinal velocity. Positive longitudinal velocity is out of the DWSC.

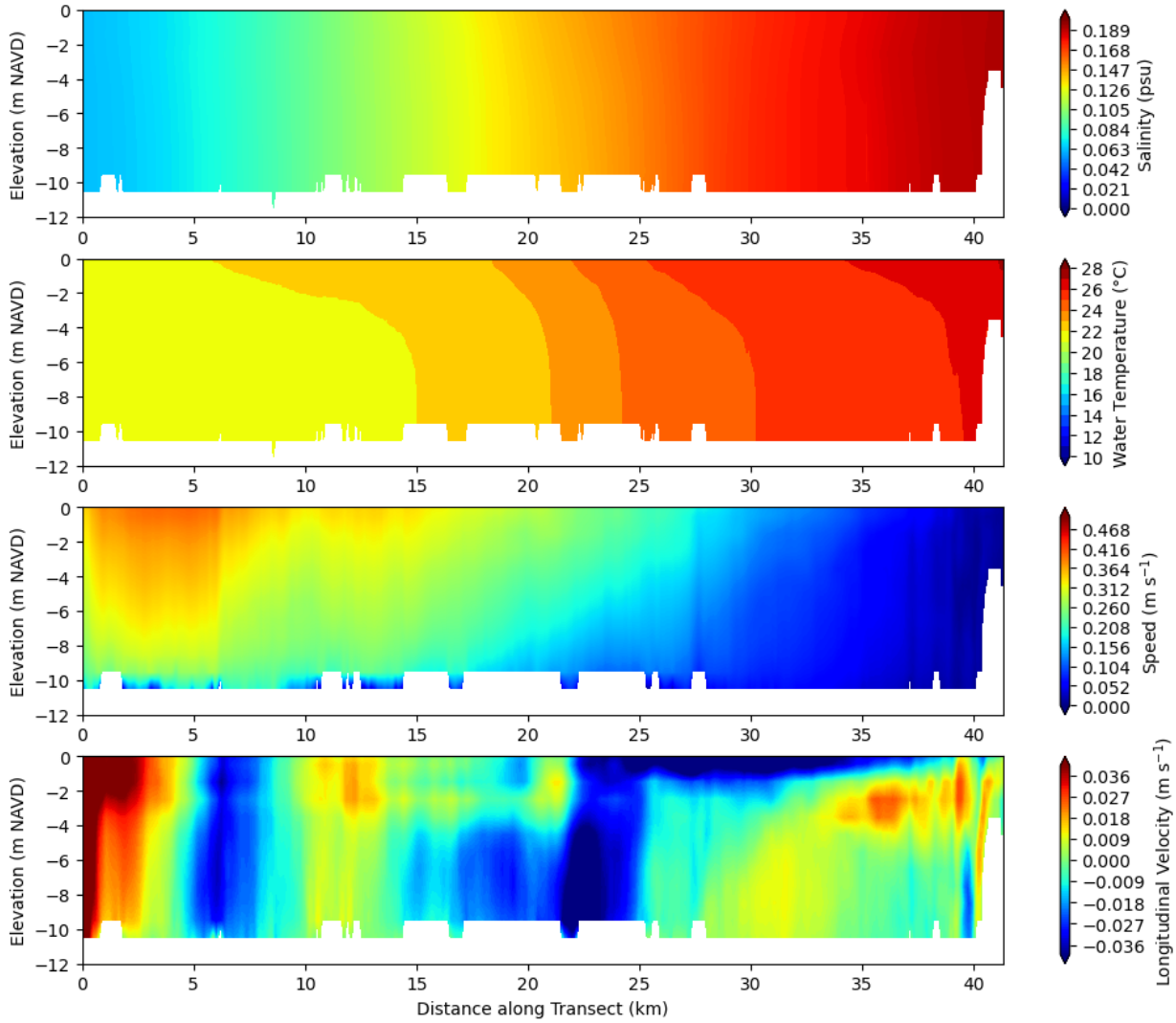

Figure 43 Tidally-averaged three-dimensional model results along the Deepwater Ship Channel on July 5, 2018 (Below Normal Historical). The x-axis is distance along the ship channel (zero at the south end). The panels (from top) are salinity, temperature, speed and longitudinal velocity. Positive longitudinal velocity is out of the DWSC.

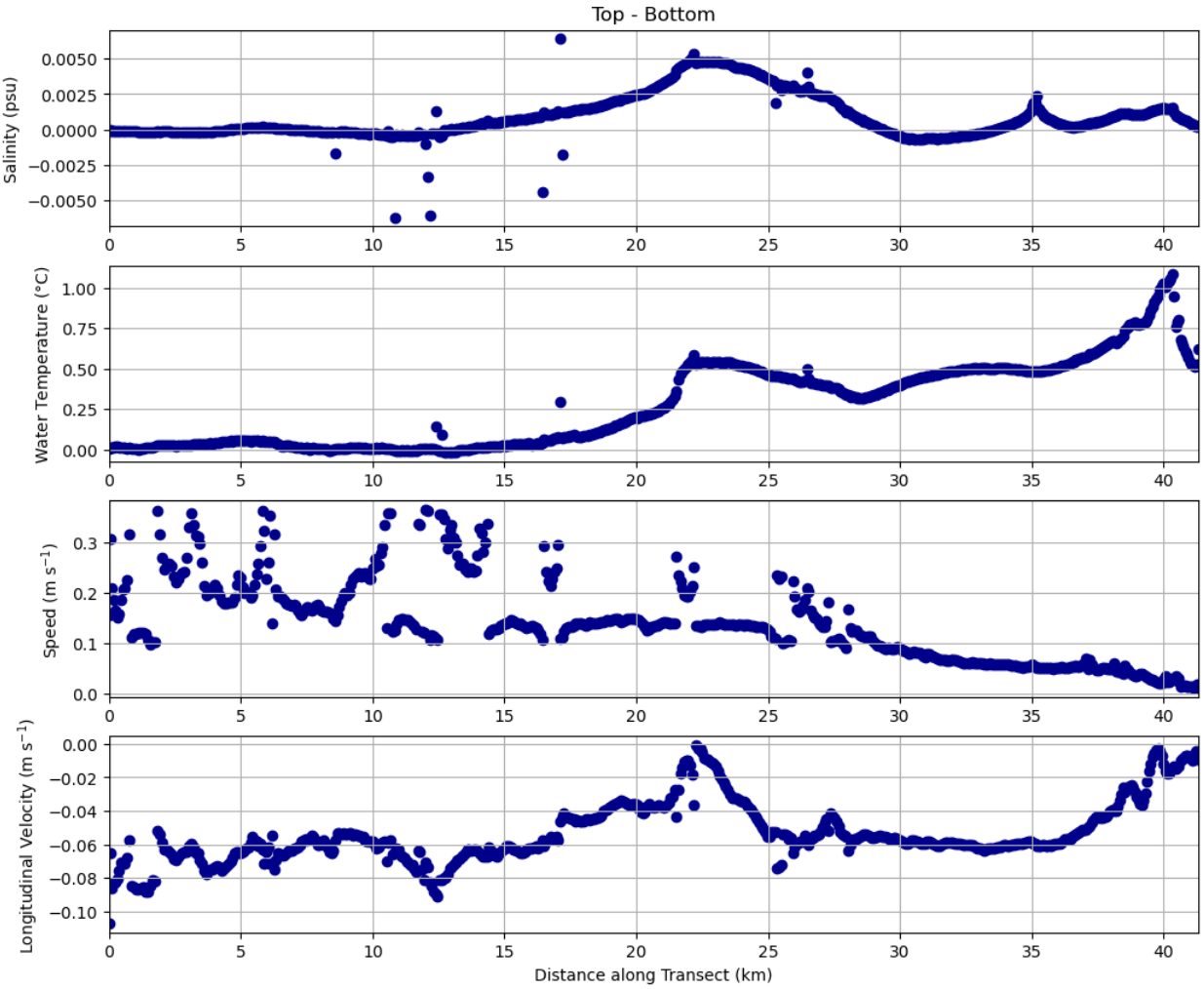

Figure 44 Monthly-averaged top layer to bottom layer difference in model predictions along the Deepwater Ship Channel transect for July, Below Normal (2018 Historical).

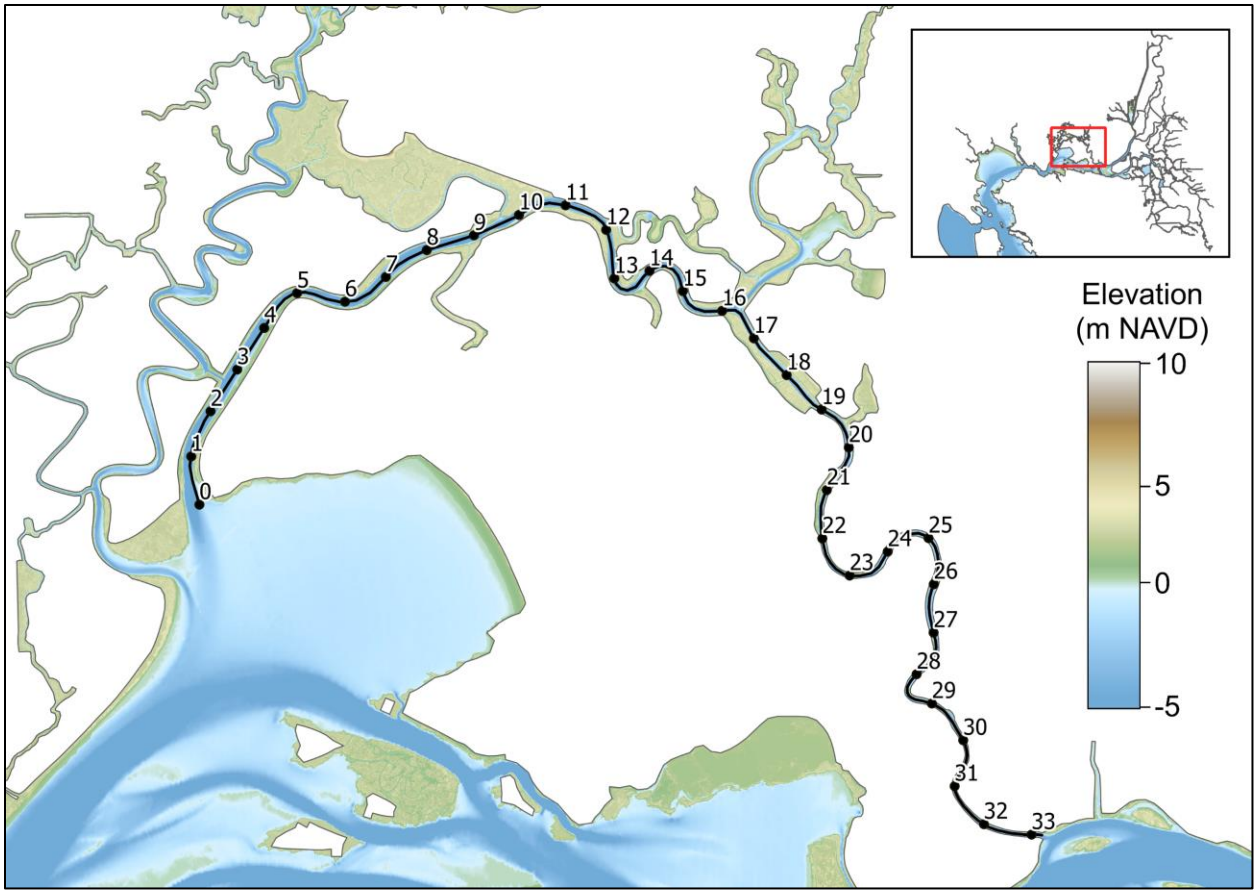

Figure 45 Transect for examination of vertical variability of three-dimensional model results in Montezuma Slough. The Suisun Marsh Salinity Control Gates are located at 29.5 km.

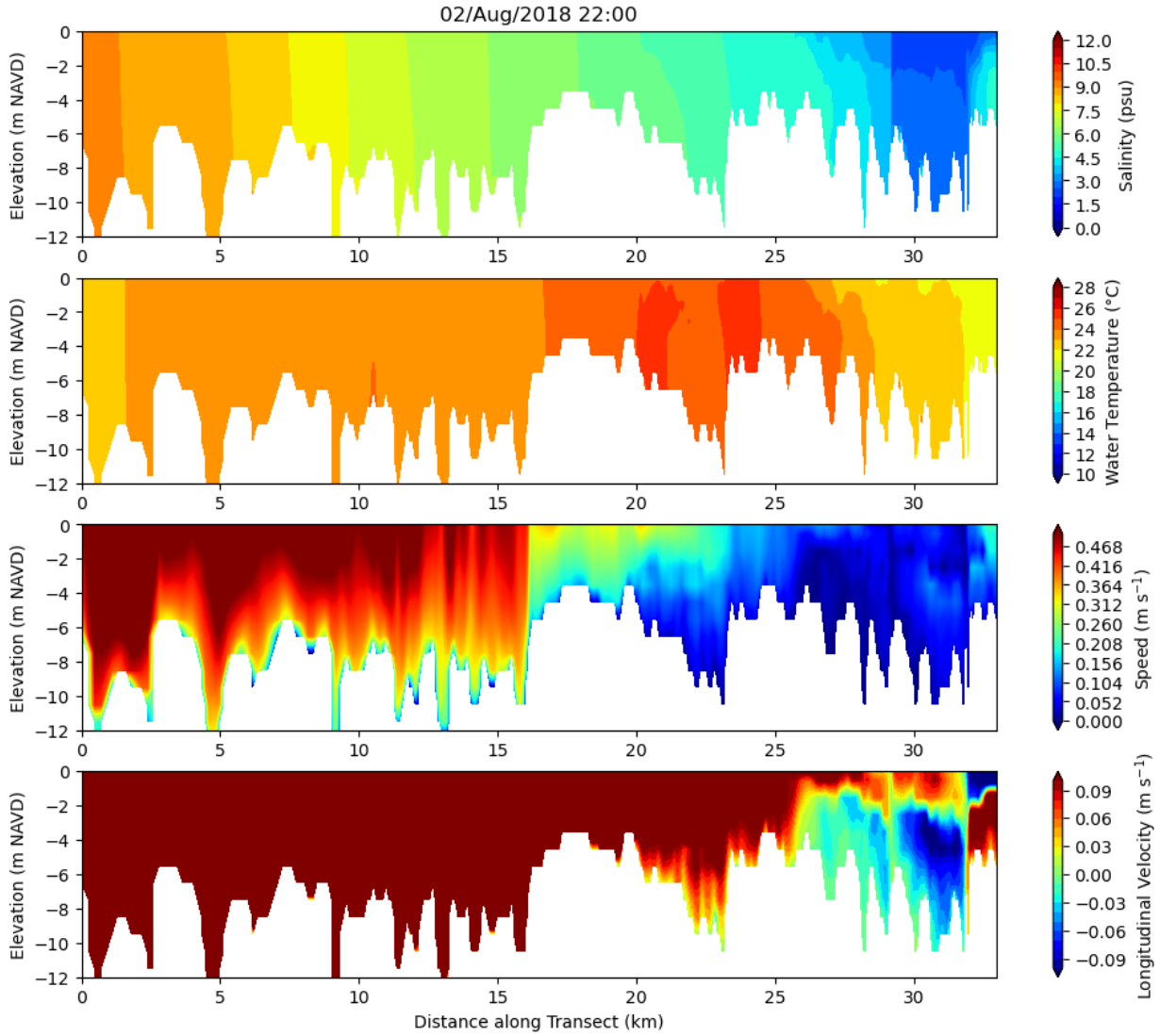

Figure 46 Three-dimensional model results along Montezuma Slough on August 2, 2018 (Below Normal Historical) at 22:00, during an ebb tide after the SMSCG operation was initiated. The x-axis is distance along the slough (zero at the west end). The panels (from top) are salinity, temperature, speed and longitudinal velocity.

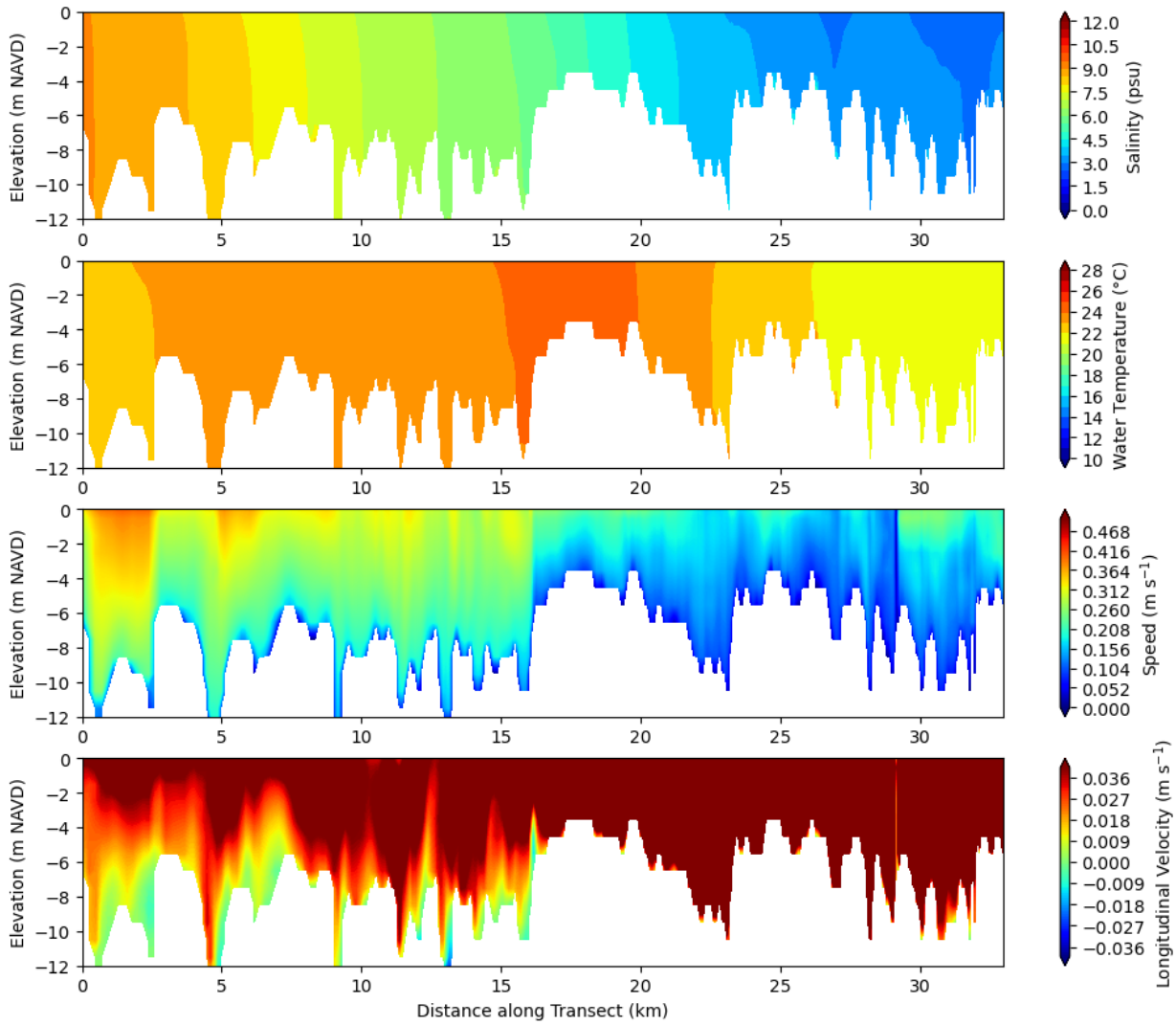

Figure 47 Tidally-averaged three-dimensional model results along Montezuma Slough on August 3, 2018 (Below Normal Historical), the day after the SMSCG operation was initiated. The x-axis is distance along the slough (zero at the west end). The panels (from top) are salinity, temperature, speed and longitudinal velocity.

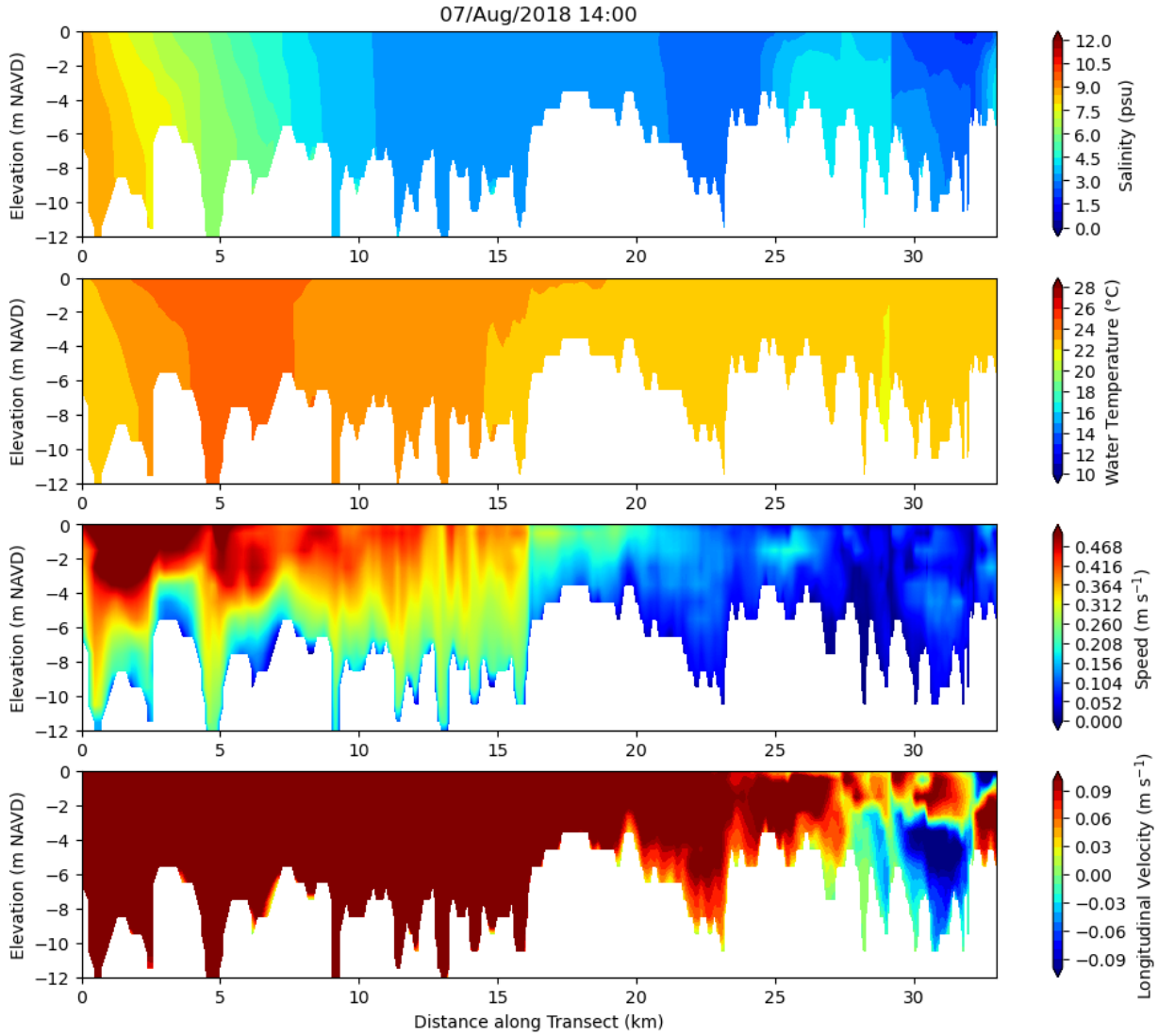

Figure 48 Three-dimensional model results along Montezuma Slough on August 7, 2018 (Below Normal Historical) at 14:00, during an ebb tide days after the SMSCG operation was initiated. The x-axis is distance along the slough (zero at the west end). The panels (from top) are salinity, temperature, speed and longitudinal velocity.

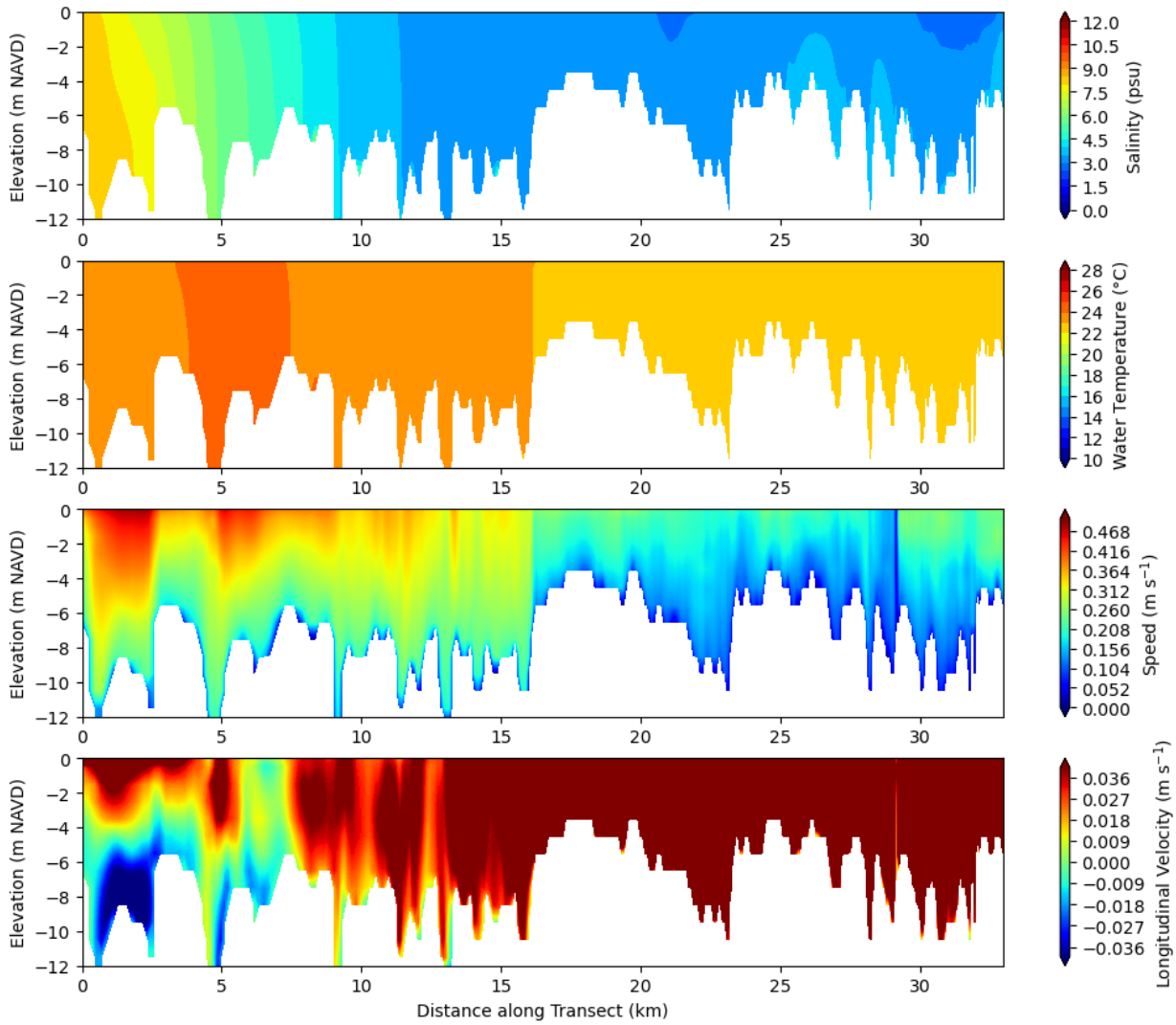

Figure 49 Tidally-averaged three-dimensional model results along Montezuma Slough on August 7, 2018 (Below Normal Historical), days after the SMSCG operation was initiated. The x-axis is distance along the slough (zero at the west end). The panels (from top) are salinity, temperature, speed and longitudinal velocity.

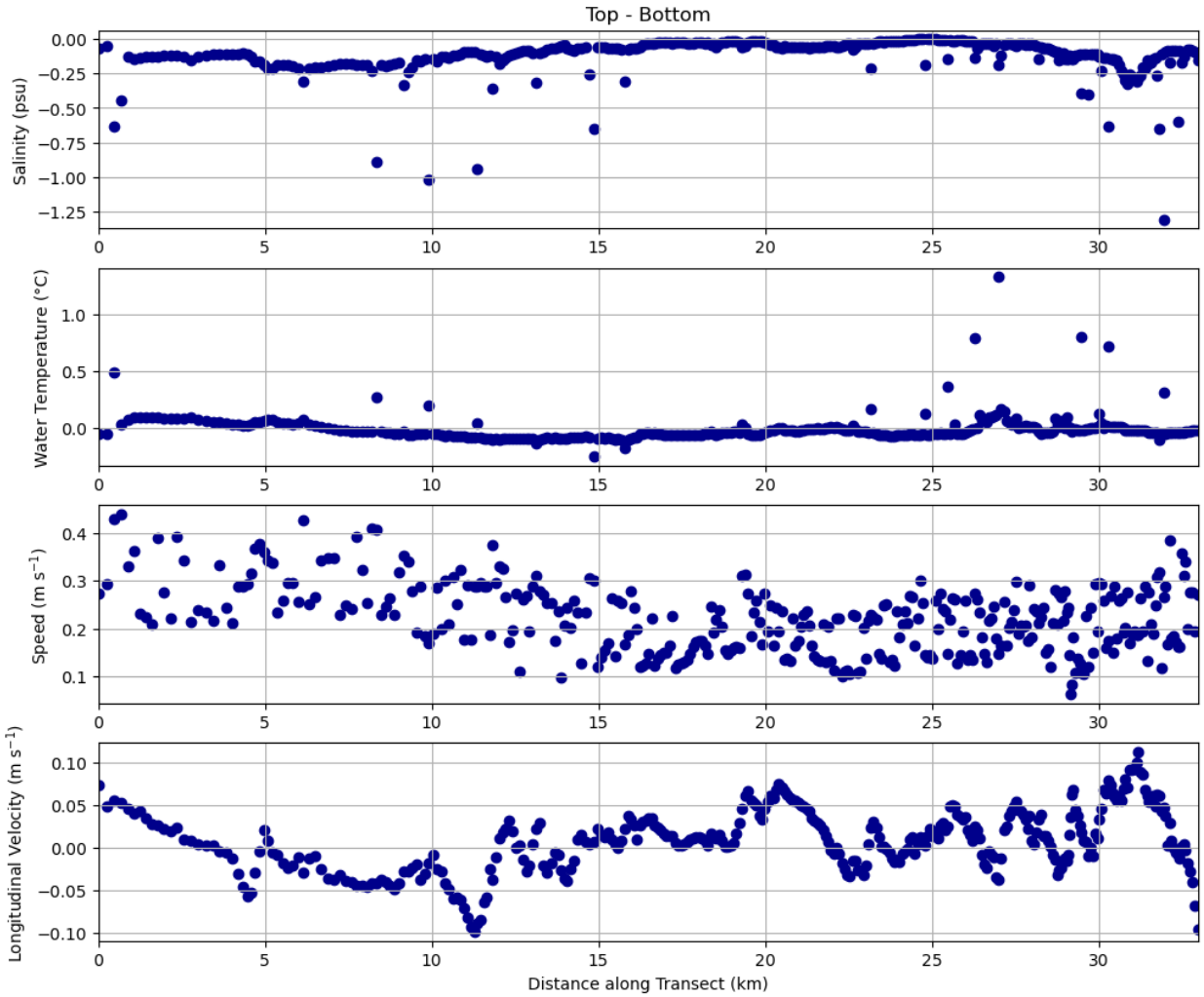

Figure 50 Monthly-averaged top layer to bottom layer difference in model predictions along the Montezuma Slough transect for August 2018 (Below Normal Historical).

REFERENCES

Andrews SW, Gross ES, Hutton PH. 2017. Modeling salt intrusion in the San Francisco Estuary prior to anthropogenic Influence. Continental Shelf Research 146: 58-81.

Bever AJ, MacWilliams ML, Herbold B, Brown LR, Feyrer FV. 2016. Linking Hydrodynamic Complexity to Delta Smelt (*Hypomesus transpacificus*) Distribution in the San Francisco Estuary, USA. San Francisco Estuary & Watershed Science.

Brown, R. 1984. Relationships between suspended solids, turbidity, light attenuation and algal productivity, Lake and Reservoir Management, 1(1): 198-205.

Casulli V, Stelling GS. 2010. Semi-implicit subgrid modelling of three-dimensional free-surface flows. Int. J. Numer. Methods Fluids 67, 441–449. http://dx.doi.org/10.1002/fld.2361.

Casulli V, Walters RA. 2000. An unstructured grid, three-dimensional model based on the shallow water equations. Int. J. Numer. Methods Fluids 32, 331–348.

Feyrer F, Nobriga M, Sommer T. 2007. Multi-decadal trends for three declining fish species: habitat patterns and mechanisms in the San Francisco Estuary, California, U.S.A. Can J Fish Aquat Sci [accessed 2021 Jan 07]; 136:1393–1405. http://dx.doi.org/10.1139/F07-048

Feyrer F, Newman K, Nobriga M, Sommer T. 2011. Modeling the effects of future outflow on the abiotic
habitat of an imperiled estuarine fish. Estuaries Coasts 34(1):120–128. doi: http://dx.doi.org/10.1007/
s12237-010-9343-9

Fofonoff NP, Millard Jr. RC. 1983. Algorithms for computation of fundamental properties of seawater. UNESCO technical papers in marine science 44. 58 p.

Frantzich J et al. 2019. Investigating Yolo Bypass as a Fall Food Web Subsidy for the Delta.

Gross ES, MacWilliams ML, Kimmerer WJ. 2009. Three-dimensional modeling of tidal hydrodynamics in the San Francisco Estuary. San Franc. Estuary Watershed Sci. 7 (2). http://escholarship.org/uc/item/9rv243mg

Gross E, Andrews S, Bergamaschi B, Downing B, Holleman R, Burdick S, Durand J. 2019. The Use of Stable Isotope-Based Water Age to Evaluate a Hydrodynamic Model. Water (11).

Kimmerer W, Wilkerson F, Downing B, Dugdale R, Gross E, Kayfetz K, Khanna S, Parker A,
Thompson J. 2019b. Effects of Drought and the Emergency Drought Barrier on the Ecosystem of the California Delta. San Fr. Estuary Watershed Sci. 17.

Moyle PB, Brown LR, Durand JR, Hobbs JA. 2016. Delta Smelt: life history and decline of a once-abundant
species in the San Francisco Estuary. San Francisco Estuary and Watershed Science; 14(2).

Nobriga ML, Sommer TR, Feyrer F, Fleming K. 2008. Long-term trends in summertime habitat suitability for Delta Smelt, Hypomesus transpacificus, San Franc Estuary Watershed Sci [accessed 2021 Jan 07]; 11(3).

Rayson MD, Gross ES, and Fringer OB. 2015. Modeling the tidal and sub-tidal hydrodynamics in a shallow, micro-tidal estuary. Ocean Modell., 89, 29–44, https://doi.org/10.1016/j.ocemod.2015.02.002.

RMA. 2005. Flooded Islands Feasibility Study: RMA Delta Model Calibration Report, June 2005.

RMA. 2009. Numerical Modeling in Support of Suisun Marsh PEIR/EIS, Technical Appendix, September 2009.

RMA. 2012. Appendix D: Prospect Island Tidal Restoration Project Calibration and Verification of Hydrodynamic Model Used for Phase 1 Preliminary Alternatives Screening. Technical Memorandum, June 2012. From, Stillwater Sciences and Wetlands and Water Resources, Inc. (2012). Prospect Island Tidal Restoration:

Synthesis of Phase 1 Screening-Level Modeling Evaluation of Conceptual Restoration Alternatives, Final Report, September 2012.

RMA. 2013. Prospect Island Tidal Restoration Project Calibration and Verification of Water Quality Model Used for Phase 2 Alternatives Evaluation. Technical Memorandum. Prepared for Wetlands and Water Resources, July 2013.

RMA. 2015a. Initial Modeling of Local and Regional Impacts of the Proposed Winter Island Tidal Marsh Restoration. Technical Memorandum, July 2015. https://coveredactions.deltacouncil.ca.gov/services/download.ashx?u=447f1b4a-3332-4af4-8b5b-6806ef11c7d6

RMA. 2015b. Salinity Modeling Analysis of the Proposed Tule Red Tidal Marsh Restoration, Grizzly Island, California. Technical Memorandum, November 2015. https://coveredactions.deltacouncil.ca.gov/services/download.ashx?u=228cf586-0206-44ba-bbf0-104f8a4f8fc9

RMA. 2020. Lookout Slough Tidal Habitat Restoration and Flood Improvement Project: Modeling EC Impacts. Technical Memorandum, July 2020.

Sommer T, Hartman R, Koller M, Koohafkan M, Conrad JL, MacWilliams M, et al. 2020. Evaluation of a large-scale flow manipulation to the upper San Francisco Estuary: Response of habitat conditions for an endangered native fish. PLoS ONE 15(10): e0234673. https://doi.org/10.1371/journal.pone.0234673

Sommer T, Mejia F, Nobriga M, Feyrer F, Grimaldo L. 2011. The spawning migration of Delta Smelt in the upper San Francisco Estuary. San Franc Estuary Watershed Sci [accessed 2021 Jan 07]; 9(2). https://doi.org/10.15447/sfews.2014v9iss2art2

Warner JC, Sherwood CS, Arango HG, Signell RP. 2005. Performance of four turbulence closure models implemented using a generic length scale method. Ocean Model. 8, 81–113. http://dx.doi.org/10.1016/j.ocemod.2003.12.003.

Willmott CJ. 1981. On the Validation of Models. Phys. Geogr. 2, 184–194.

APPENDIX A: RMA THERMAL MODELING EQUATIONS

In RMA-11, the dependent model variable used when simulating heat transport is the water temperature, T. When calculating heat fluxes using the conservation of energy equations, however, the truly consistent parameter which should be considered is the concentration of stored heat, C_H. This has units of kJ/m^3. The specific heat of water, c, and its density, ρ, are used to relate these two parameters.

$$C_H = c\,\rho\,T$$

where

C_H = Heat content of water, (kJ/m^3)

c = Specific heat of water, (4.19 kJ/kg/deg C)

ρ = Density of water, (1000 kg/m^3)

T = Water temperature, (deg C)

In addition to advective and dispersive heat transport, the RMA-11 temperature model considers heat sources and sinks at the air-water and sediment-water interfaces. The term for heat transfer at the water surface, G_{SFC}, is calculated as

$$G_{SFC} = \frac{H_N}{3600\ c\ \rho}$$

where

G_{SFC} = Surface boundary temperature source rate, (m deg C/s)

H_N = Net energy flux passing the air-water interface, (kJ/m^2/hr)

and 3600 is a conversion factor between seconds and hours. Similarly, the term for heat transfer at the bed, G_{BED}, is calculated as

$$G_{BED} = \frac{H_{BED}}{3600\ c\ \rho}$$

where

G_{BED} = Bed boundary temperature source rate, (m deg C/s)

H_{BED} = Net energy flux passing the sediment-water interface, (kJ/m^2/hr)

Then the temperature at every point in the model may be updated by solving an equation similar to

$$\frac{dT}{dt} = adv + disp + \frac{G_{SFC}}{h} + \frac{G_{BED}}{h}$$

where

t = Time, (s)

adv = Advective thermal flux, (deg C/s)

$disp$ = Dispersive thermal flux, (degC/s)

h = Water depth, (m)

The approach used in RMA-11 is to assume that heat is transferred from various energy sources which can be calculated individually. At the water surface

$$H_N = H_{SN} + H_{AN} - (H_B + H_E + H_C)$$

where

H_{SN} = Net shortwave radiation influx, (kJ/m^2/hr)

H_{AN} = Net longwave radiation influx, (kJ/m^2/hr)

H_B = Longwave back radiation flux, (kJ/m^2/hr)

H_E = Evaporative flux, (kJ/m^2/hr)

H_C = Conductive energy flux, (kJ/m^2/hr)

The sections that follow will describe how each of these components is calculated.

Net Shortwave Radiation Influx, H_{SN}

Incoming shortwave radiation is that which passes directly from the sun to the earth's surface. The magnitude of this term depends on the solar altitude, the

damping effect of scattering and absorption in the atmosphere, and shortwave reflection from the water surface. This can be expressed following Roesner et al. (1981) as

$$H_{SN} = H_0 \, a_\tau \, (1 - R_S) \, (1 - 0.65 \, C_L^2)$$

where

H_0 = Incoming solar shortwave to the earth's atmosphere, (kJ/m^2/hr)

a_τ = Atmospheric transmissivity, (non-dimensional)

R_S = Albedo of the water surface, (non-dimensional)

C_L = Cloudiness, (non-dimensional, expressed as a fraction 0–1)

Alternatively, solar radiation measured at the earth's surface may be input to the model directly. Because of the prevalence of terrestrial shortwave radiation sensors currently available in California,[1] this has become the preferred modeling method. For detailed equations on how to predict H_o, a_t, and R_S as a function of atmospheric conditions, time of year, time of day, and site latitude, see for example Wunderlich (1972).

Net Longwave Atmospheric Radiation Influx, H_{AN}

Longwave radiation is dependent mostly upon air temperature but also to a small degree on cloudiness. A small fraction of the longwave radiation is reflected by the water surface. This amount reflected is usually taken to be 3% of the incoming radiation. The net downwelling longwave radiative flux can be expressed following Wunderlich (1972), as

$$H_{AN} = 9.37\text{E-}06 \, \sigma \, T_R^6 \, (1 + 0.17 \, C_L^2) \, (1 - R_L)$$

where

[1] See, for example, the California Irrigation Management Information System (CIMIS) sensor system. http://cimis.water.ca.gov

σ = Stefan-Boltzman constant, (2.0412E-07 kJ/m^2/hr/deg K)

T_R = Absolute temperature of the air, (deg K)

R_L = Reflectivity of water surface, (0.03)

Longwave Back Radiation Flux, H_B

Longwave back radiation is the heat lost by the water through the air water interface. Using black body theory, the back radiation may be expressed as

$$H_B = \varepsilon_w \, \sigma \, T_{abs}^4$$

where

ε_w = Emissivity of water, (0.97)

T_{abs} = Absolute temperature of the water surface, (deg K)

Evaporative Heat Flux, H_E

Evaporation is also a significant source of heat loss from the water body to the atmosphere. The rate of evaporation is converted to heat lost using the latent heat of vaporization

$$H_E = \rho \, L_w \, E$$

where

E = Evaporation rate, (m/hr)

L_w = Water latent heat of vaporization, (kJ/kg)

= $2400 - 0.9 \, T_S$

T_S = Water surface temperature, (deg C)

The evaporation rate is usually expressed as a function of the difference between the saturation vapor pressure of the air, e_s, and the actual air water vapor pressure, e_a, and as function of local wind speed.

$$E = (a + b\,W)\,(e_s - e_a)$$

where

a, b = Empirical constants

W = Wind speed measured at 2 meters above the water surface, (m/s)

e_s = Saturation water vapor pressure of the air at the temperature of the water surface, (millibars)

= $8.8534\ \exp(0.054\ T_S) - 2.8345$ (Roesner et al., 1981)

e_a = Water vapor pressure in the air (millibars),

= $\frac{RH}{100}\ e_{s,a}$

RH = Relative humidity of the air, (%)

$e_{s,a}$ = Saturation water vapor pressure of the air, (millibars)

= $8.8534\ \exp(0.054\ T_a) - 2.8345$

T_a = Temperature of the air, (deg C)

Suggested values for a and b are given by Roesner (1969) as

a = 6.2E-06 m/hr/millibar

b = 5.5E-06 m/hr/millibar per m/s of wind speed

Conductive Heat Flux, H_C

Heat transferred between the water and the atmosphere due to temperature differences not related to water vapor exchange is known as conduction. It is usually assumed to be related to the same variables as evaporation and can be derived using a proportionality constant known as Bowen's ratio. Bowen's ratio is expressed as

$$B = \frac{H_C}{H_E} = C_B \left(\frac{T_S - T_a}{e_s - e_a}\right)\left(\frac{P_a}{P_{ref}}\right)$$

where

C_B = Empirical constant, (0.6096 millibars/deg C)

P_{ref} = Reference atmospheric pressure at sea level, (1013.25 millibars)

Then H_C may be calculated as (Martin and McCutcheon, 1999)

$$H_C = C_B \rho L_w (a + b W)\left(\frac{P_a}{P_{ref}}\right)(T_S - T_a)$$

Bed Thermal Flux, H_{BED}

Temperature simulations may produce unphysically high temperatures during the daytime hours and low temperatures during the nighttime hours in very shallow water and exposed intertidal areas. These large temperature fluctuations can be moderated by inclusion of a sediment bed layer in the temperature model.

The net energy flux passing the sediment-water interface, H_{BED}, can be modeled following Chapra et al. (2008) as a function of the bed-water temperature gradient and the thermal diffusivity of the sediments

$$H_{BED} = \rho_{bed}\, c_{bed}\, \alpha \left(\frac{T_{bed} - T}{h_{bed}}\right)$$

where

ρ_{bed} = Density of the bed sediments, (1000 kg/m^3)

c_{bed} = Specific heat of the bed sediments, (4.19 kJ/kg/deg C)

α = Thermal diffusivity of the bed sediments, (m^2/s)

h_{bed} = Depth of bed layer, (m)

T_{bed} = Temperature of the bed sediments, (deg C)

T = Modeled water temperature, (deg C)

The temperature of the bed sediments is explicitly modeled using an equation similar to

$$\frac{dT_{bed}}{dt} = -\frac{H_{BED}}{\rho_{bed}\, c_{bed}\, h_{bed}}$$

For simplicity, the bed layer is assumed to have a density and specific heat similar to water. This is a good assumption for saturated mud flats, but may not be as accurate when the underlying sediments are less porous (Chapra et al., 2008, Table 4).

The sediment bed is represented as a single lumped layer rather than a more complex vertically segmented system of individual sub-layers, as is common in some models. The parameters for the depth of the bed layer, h_{bed}, and the thermal diffusivity of the sediments, α, are model inputs which can be adjusted during calibration. Typical values for α are in the range 1.0E-7 to 8.0E-7 m^2/s (Chapra et al., 2008, Table 4). The depth of the bed layer can be adjusted in order to control the response time of the bed temperature to fluctuations in the overlying water temperature. Depths on the order of 2.2 m, 30 cm, and 12 cm will respond to temperature fluctuations on the order of annual, weekly, and diurnal time scales, respectively (Chapra et al., 2008).

References

Chapra, S., Pelletier, G., and H. Tao. 2008. "QUAL2K: A Modeling Framework for Simulating River and Stream Water Quality (Version 2.11): Documentation and Users Manual." Civil and Environmental Engineering Department, Tufts University. Medford, MA.

Martin, J.L. and S.C. McCutcheon. 1999. *Hydrodynamics and Transport for Water Quality Modeling*. Lewis Publishers, Boca Raton, FL.

Roesner, L. A. 1969. "Temperature Modeling in Streams", Lecture notes, Water Quality Workshop, Tennessee Valley Authority. Knoxville, TN.

Roesner, L.A., Giguere, P.R., and D.E. Evenson. 1981. "Computer Program Documentation for the Stream Quality Model QUAL-II." Report No. 600/9-81-014. Environmental Research Laboratory, Office of Research and Development, US Environmental Protection Agency. Athens, GA.

Wunderlich, W.O. 1972. "Heat and Mass Transfer Between a Water Surface and the Atmosphere." Report No. 0-6803. Tennessee Valley Authority, Division of Water Control Planning, Engineering Laboratory. Norris, TN.

APPENDIX B: SCENARIO BOUNDARY CONDITIONS

In the sections below, major inflow and export boundary conditions are plotted for each of the scenario simulation periods. For the SMSCG scenarios the Sacramento River inflows and the Clifton Court and CVP export flows differed slightly at times from No Action flows.

For the major river inflows, the smoothed CalSim II records that were used by DSM2 were used in the scenario simulations.

The model used 15-minute Clifton Court flows computed by DSM2. Daily values are plotted here for ease of viewing.

Delta Islands Consumptive Use (DICU) flows were taken from DSM2 and mapped to the 2D and 3D models based on DSM2 locations. The DICU values plotted below represent the net flow from diversions, drains and seepage, summed over all locations.

Dry Year (1930 CS)

Major inflows and exports for the Dry water year type (1930 CS) simulation period are plotted in Figure 51 and Figure 52, respectively. There were no SMSCG operations during this period.

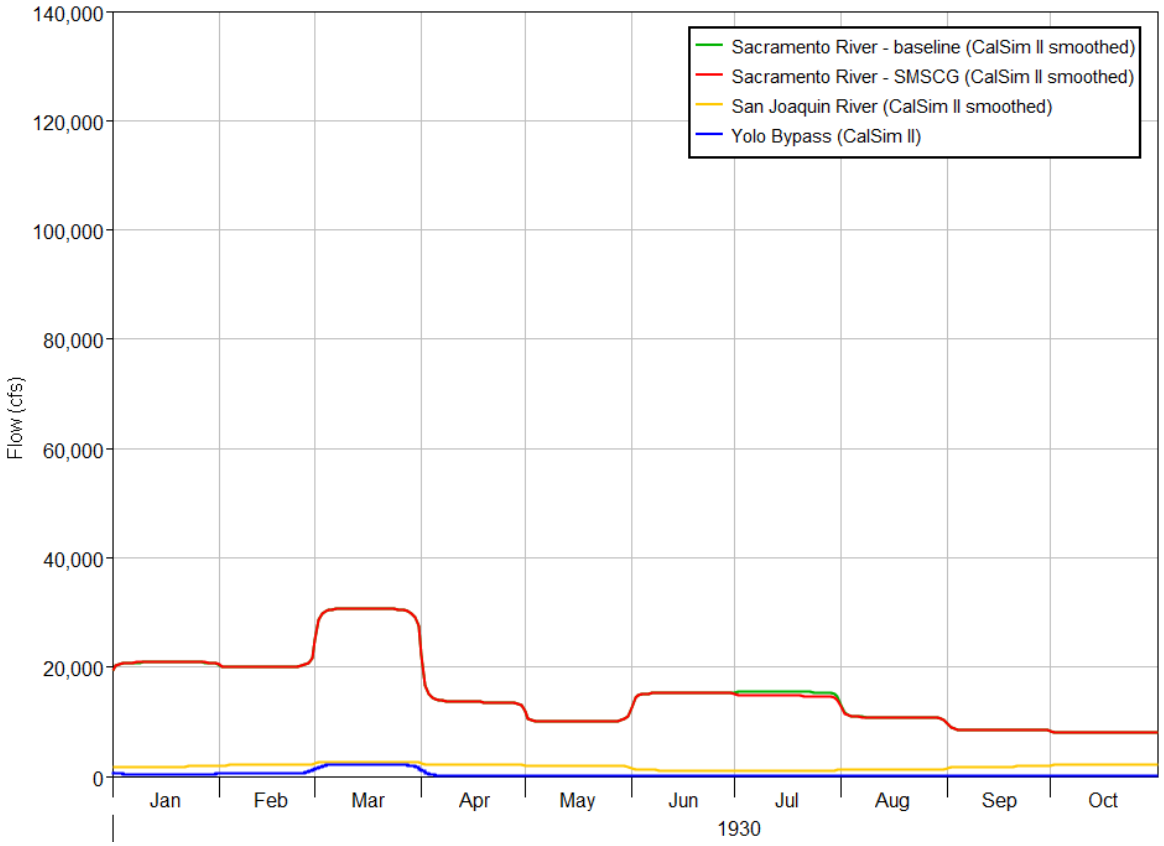

Figure 51 Major inflows for the Dry (1930 CS) scenario simulations

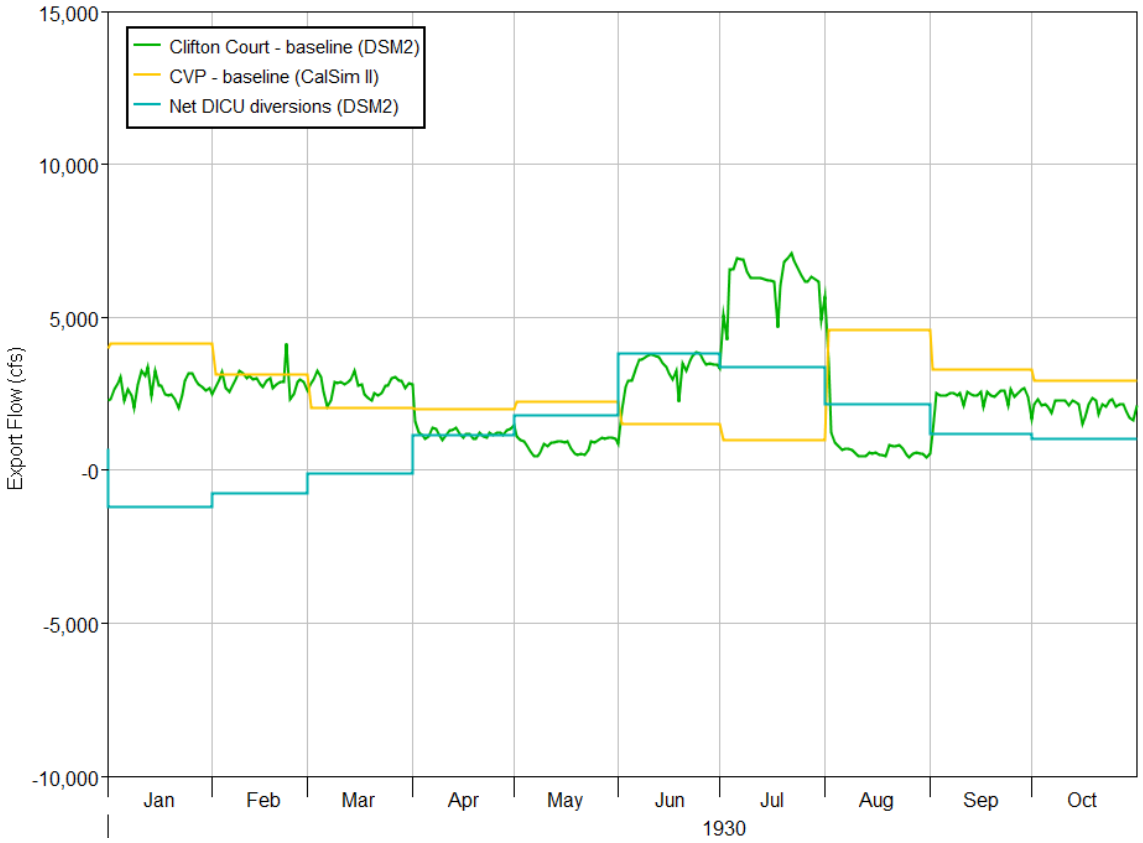

Figure 52 Major export flows for the Dry (1930 CS) scenario simulations

Above Normal Year (1940 CS)

Major inflows and exports for the Above Normal water year type (1940 CS) simulation period are plotted in Figure 53 and Figure 54, respectively.

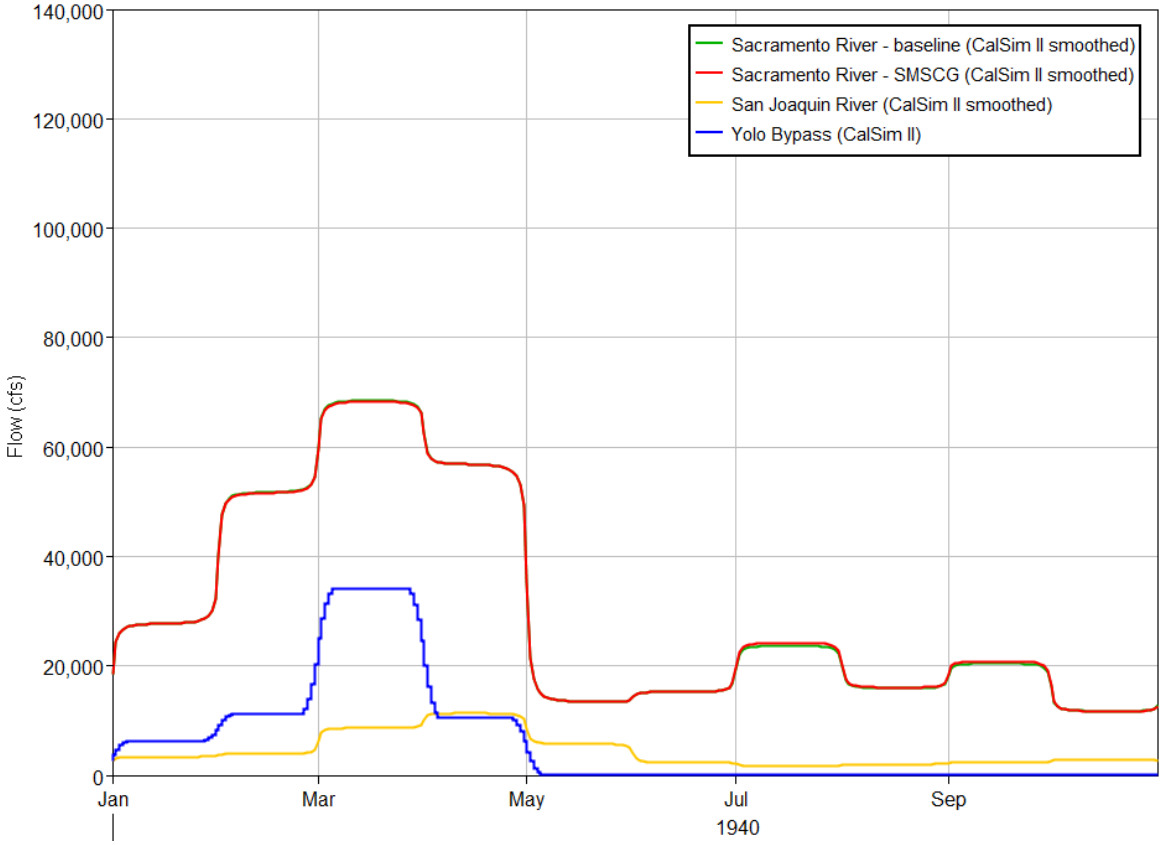

Figure 53 Major inflows for the Above Normal (1940 CS) scenario simulations. Sacramento River inflows differ slightly at times for SMSCG scenario simulations.

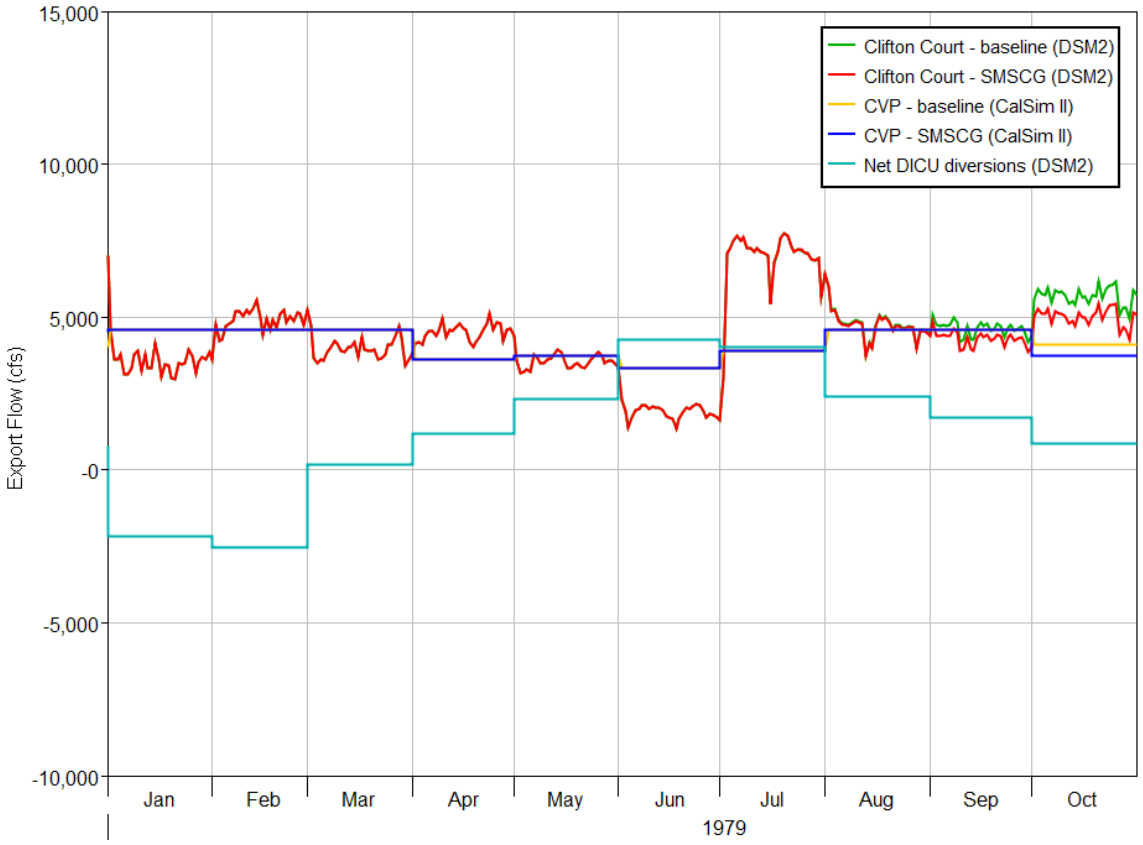

Figure 54 Major export flows for the Above Normal (1940 CS) scenario simulations

Below Normal Year (1979 CS)

Major inflows and exports for the Below Normal water year type (1979 CS) simulation period are plotted in Figure 55 and Figure 56, respectively.

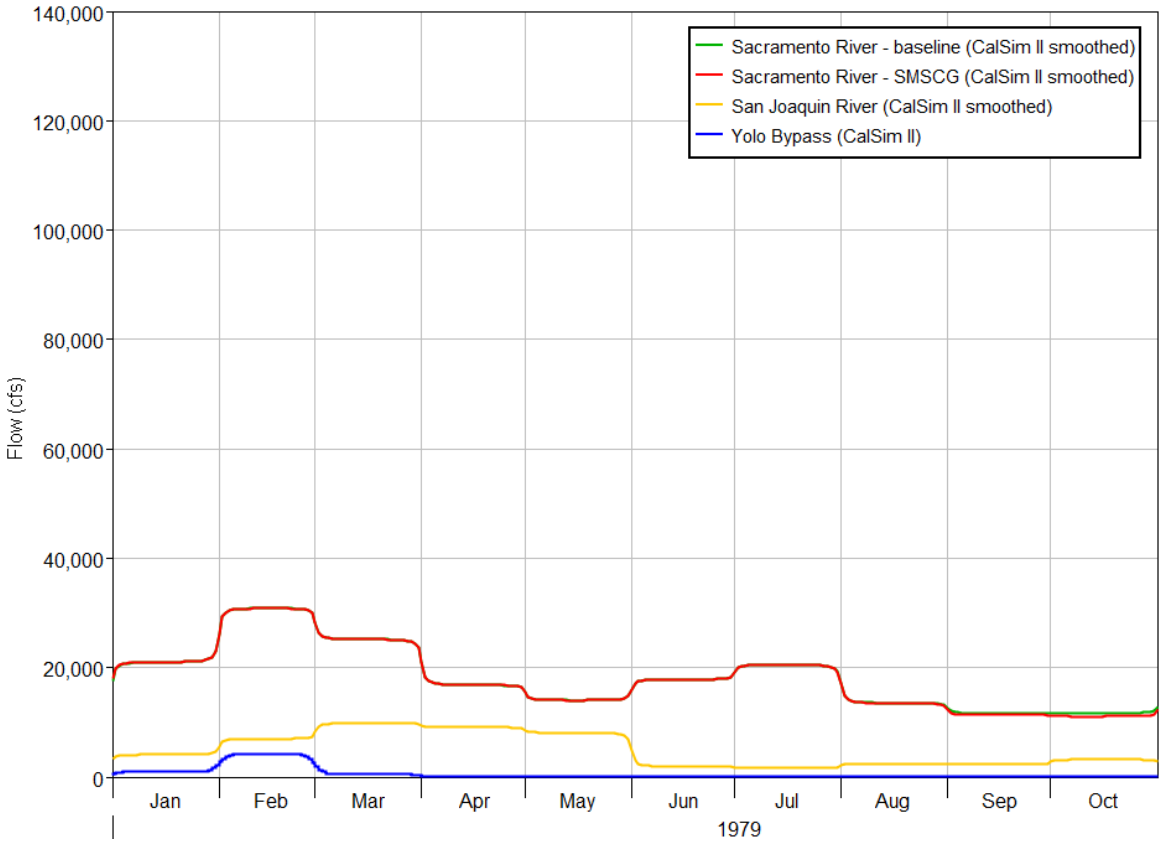

Figure 55 Major inflows for the Below Normal (1979 CS) No Action scenario simulations. Sacramento River inflows differ slightly at times for SMSCG scenario simulations.

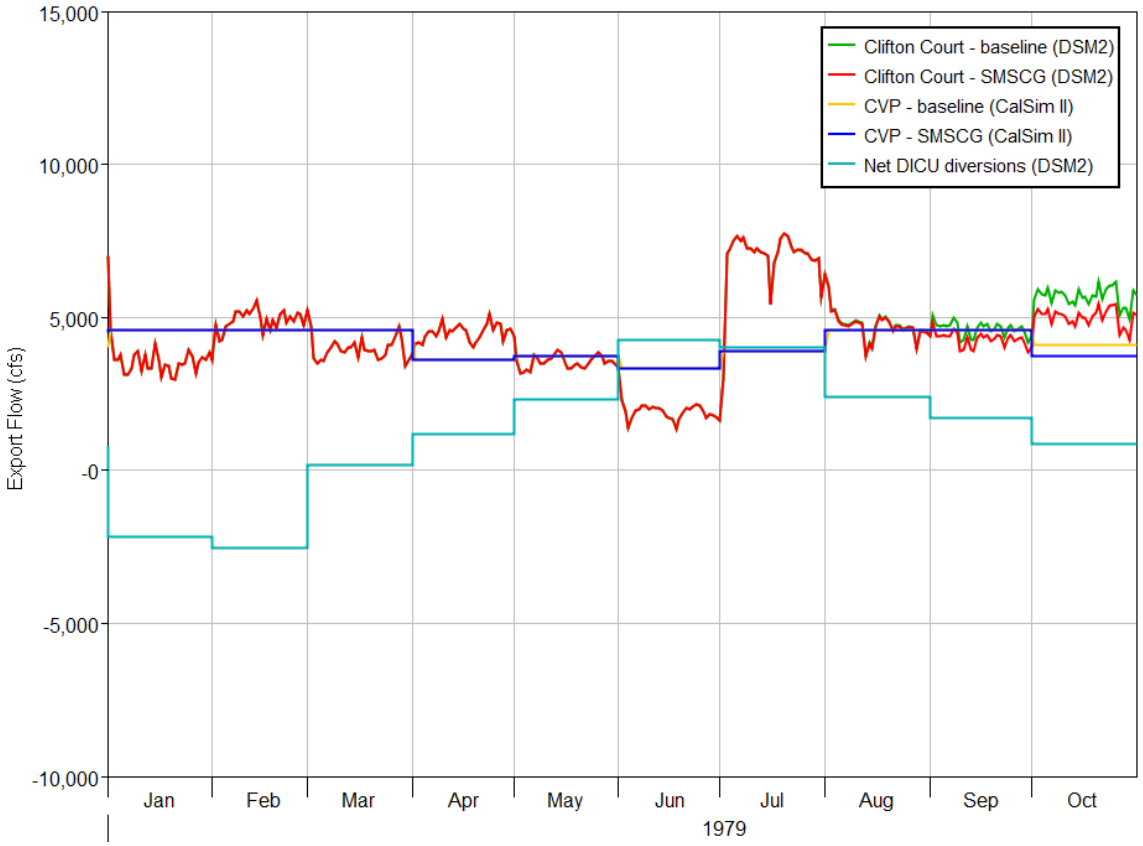

Figure 56 Major export flows for the Below Normal (1979 CS) scenario simulations

Wet Year (1986 CS)

Major inflows and exports for the Wet water year type (1986 CS) simulation period are plotted in Figure 57 and Figure 58, respectively. For this period, Yolo Bypass flows were smoothed using two passes of a 5-point moving average filter to ease the abrupt transitions between months for better model stability.

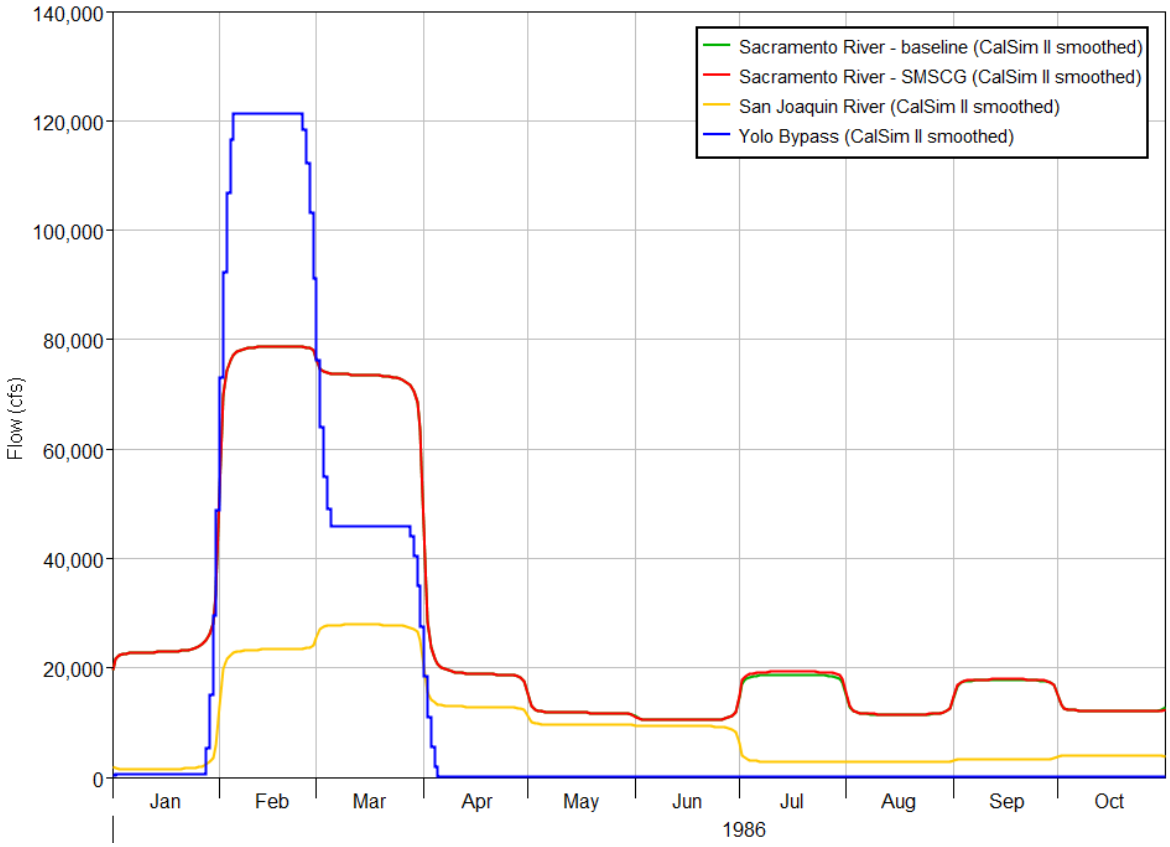

Figure 57 Major inflows for the Wet (1986 CS) scenario simulations. Sacramento River inflows differ slightly at times for SMSCG scenario simulations.

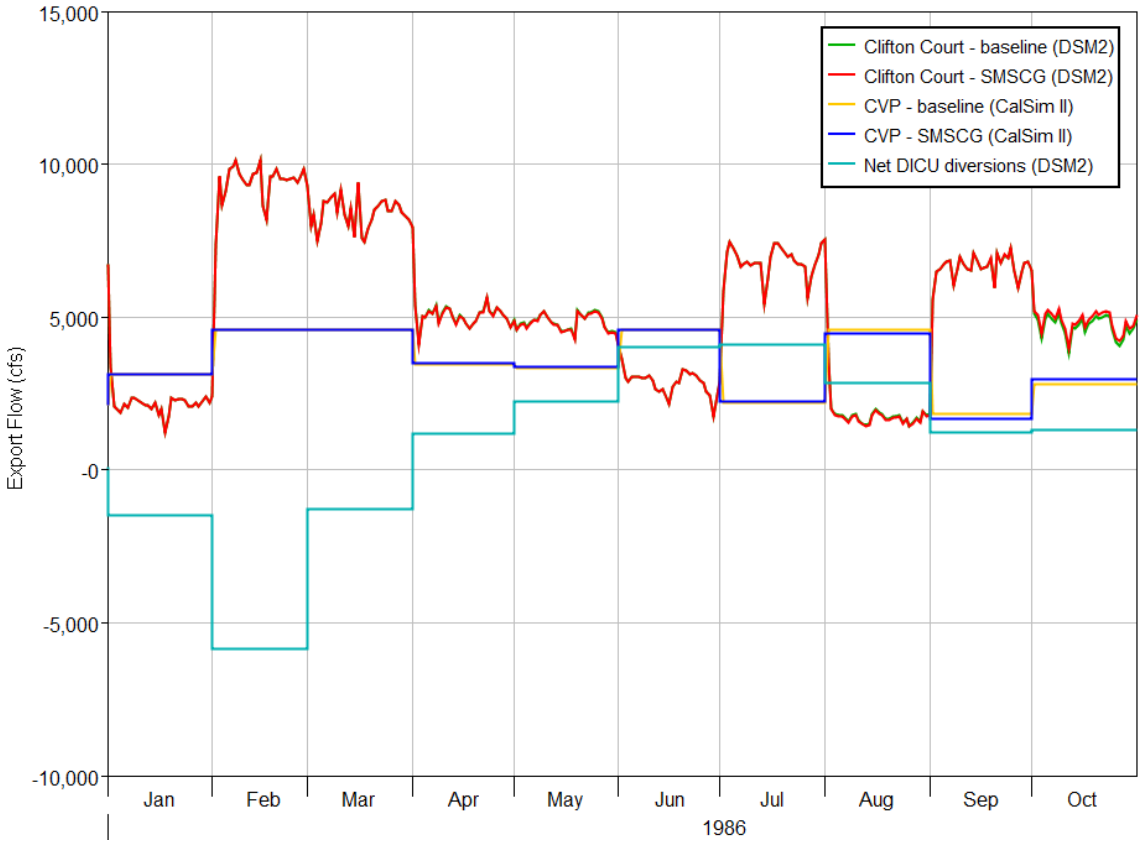

Figure 58 Major export flows for the Wet (1986 CS) scenario simulations

RESOURCE MANAGEMENT ASSOCIATES
WATER RESOURCES ENGINEERING

Numerical Modeling in Support of Reclamation Delta Smelt Summer/Fall Habitat Analysis

Calanoid Copepod Analysis Addendum

May 14, 2021

Prepared For:
United States Bureau of Reclamation

Prepared By:
Resource Management Associates
1756 Picasso Avenue, Suite G
Davis, CA 95618
Contact: Edward Gross
925-300-3387

INTRODUCTION

The primary goal of flow augmentation actions in the North Delta is to increase food resources for Delta Smelt and other species in the summer and fall. The two actions studied were the North Delta Flow Action (NDFA) in which flow into the Toe Drain is augmented in late August through late September, and the Deepwater Ship Channel (DWSC) Action in which flow from the Sacramento River into the DWSC is present in July. The North Delta Flow Action has occurred in several years and was accompanied by field studies that observed evidence of export of primary productivity and also high growth rate of *P. forbesi* in the productive water associated with the flow pulse in some years. The water associated with the initial flow pulse was found to have elevated calanoid copepod abundance and elevated chlorophyll in some years. The proposed DWSC flow augmentation has not happened historically but elevated calanoid copepod concentration has been observed in the DWSC. Effects of the SMSCG action on copepod distribution was not estimated because Sommer et al. (2020) did not note changes to observed copepod distribution from the SMSCG action in 2018.

The goal of this analysis is to provide a food web metric relevant to Delta Smelt. The analysis was limited to calanoid copepods which are a primary prey item of Delta Smelt in summer and fall (Slater and Baxter 2014). Estimates of biomass density were used by USBR in bioenergetic calculations and could perhaps be included as a component of a Habitat Suitability Index. To be consistent with the abiotic habitat suitability analysis, we report biomass density at a monthly time interval on a 10 m resolution raster. Since effects of the food subsidy actions are expected to be spatially limited, the results shown here are intended as potential upper bounds of management effects.

Our approach incorporated observed calanoid copepod catch per unit effort (CPUE) data, conservative tracer simulations and a simplified representation of copepod growth to estimate time and spatially variable calanoid copepod biomass per unit effort (BPUE) in the water volumes tagged with concentration of 1 in the tracer simulations. Because this water was associated with elevated biomass and was the water tracked by the tracer, it is referred to as "source water" here. The overall calanoid copepod BPUE was then estimated as a weighted average of the "source water" BPUE from the simulation and ambient (observed) BPUE based on observations. The weighting was based on the tracer concentration which represents the proportion of water present at a point in time and space that is "source water".

Observed Biomass Density

We estimated monthly calanoid copepod biomass density for June through October of 2018 and 2019 using monitoring data collected by the California Department of Fish and Wildlife, California Department of Water Resources and US Bureau of Reclamation using mesozooplankton nets. The specific data sources included the Environmental Monitoring Program (EMP) Zooplankton Study, the 20-mm Survey (20mm), the Fall Midwater Trawl (FMWT), the Summer Townet Survey (STN), the Fish Restoration Program (FRP) and Yolo Bypass monitoring (YOLO). The stations associated with these monitoring programs are shown in Figure 1. Additional information on these surveys and datasets is provided in Kayfetz et al. (2021). Data from these sources was accessed using the Zooplankton Data Synthesizer (https://deltascience.shinyapps.io/ZoopSynth/; Bashevkin et al. 2020). This tool

standardizes taxonomic names. However, the different programs do have differing taxonomic resolution with some identifying more individual species than others.

The catch per unit effort (CPUE) for taxa reported in the Zooplankton Data Synthesizer were converted to biomass per unit effort (BPUE) using dry carbon weights reported in Table 1. Only juvenile (copepodites) and adult life stages were included in this analysis because nauplii constitute a small portion of juvenile and adult delta smelt diet (Slater and Baxter 2014). A single carbon weight is used for each though it should be noted that actual carbon weight can vary greatly among different stages of juvenile copepods (Kimmerer et al. 2018).

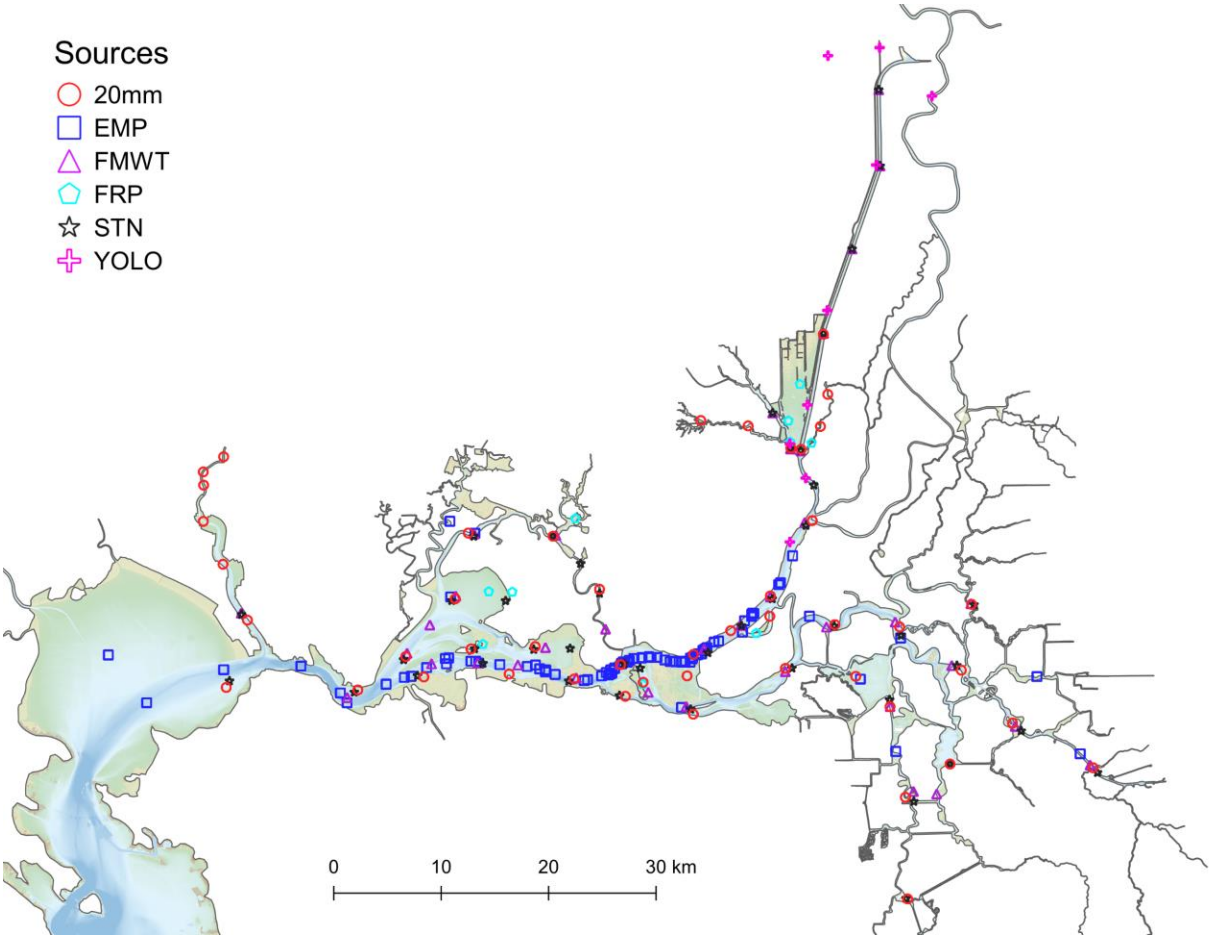

Figure 1 Stations associated with each source of data (survey program) used in calanoid copepod BPUE estimates

Table 1 Dry carbon weights of calanoid copepod taxa

Taxon Name	Life Stage	Carbon Weight (μg)
Acartiella sinensis	Adult	2.81
Acartia spp.	Adult	3.14
Diaptomidae	Adult	3.36
Eurytemora affinis	Adult	3.48
Other Calanoid adults	Adult	3
Pseudodiaptomus forbesi	Adult	3.265
Pseudodiaptomus marinus	Adult	4.9
Sinocalanus doerrii	Adult	3.413
Tortanus spp.	Adult	15.895
Acartiella sinensis	Juvenile	1.162
Acartia spp.	Juvenile	1.301
Diaptomidae	Juvenile	2
Eurytemora affinis	Juvenile	1.443
Other Calanoid juvenile	Juvenile	1.5
Pseudodiaptomus spp	Juvenile	1.246
Sinocalanus doerrii juvenile	Juvenile	1.811
Tortanus spp.	Juvenile	7.948

The spatial distribution of BPUE was estimated from values at individual stations. Prior to interpolation, the monthly BPUE estimate at each station was log transformed. It was then interpolated using a diffusion solution on the model grid and antilog transformed. The diffusion solution approach to interpolate and smooth the BPUE field accounted for hydraulic connectivity such that, for example, an estimated copepod BPUE in the Toe Drain had little influence on estimated BPUE in a geographically nearby point in the Deepwater Ship Channel because the diffusion approach interpolated and smoothed the BPUE field with distance along water, not distance across land. Regions further than approximately 10 km distance from any station were assigned a "no data" value for copepod density.

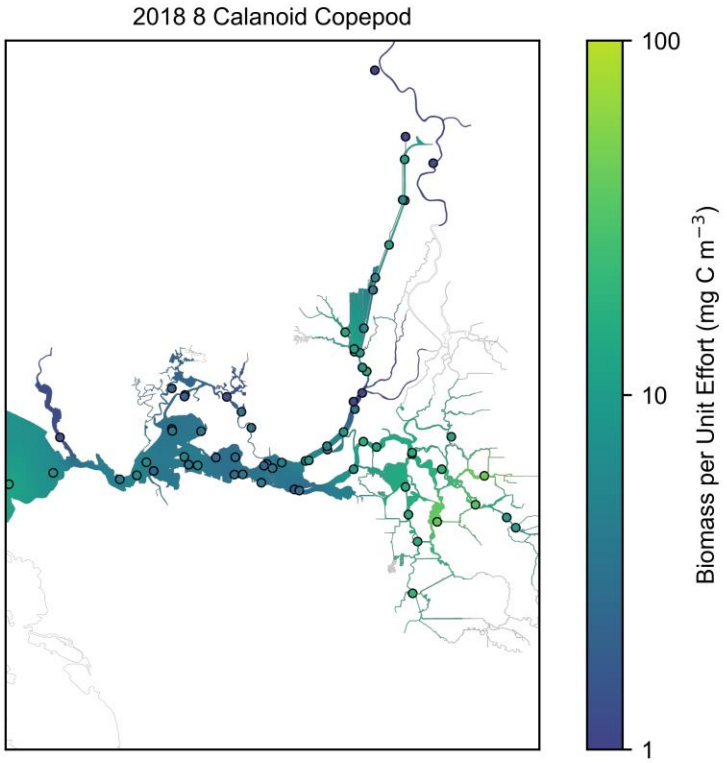

Figure 2. Observed calanoid copepod BPUE in August 2018. Circles indicate BPUE at individual stations and the continuous field is the interpolated BPUE distribution based upon the station data.

Calanoid copepod BPUE for historical conditions were estimated from CPUE observations for 2018 and 2019 (Figure 2), the two historical years used in our study with the most available zooplankton abundance data. Note that NDFA actions did occur in September of 2018 and 2019 and may have influenced the observed calanoid copepod distribution in those periods. However, we will use the term "Ambient" BPUE and "No Action" BPUE to refer to the observed conditions. During these periods there was no obvious indication of elevated observed calanoid copepod BPUE. Therefore, our NDFA alternatives are hypothetical cases in which incoming calanoid copepod BPUE associated with the NDFA was higher than during the historical conditions. The spatial coverage of zooplankton data in 2005 and 2009 was too limited to allow estimates of calanoid copepod distribution. The observed fields for 2018 and 2019 were used in the modeling approach described below with hydrodynamic results from each of 4 water year types (Wet, Above Normal, Below Normal, Dry) and 2 actions (NDFA and DWSC). Estimated BPUE from 2018 (Below Normal) was applied for both Dry and Below Normal water years and BPUE from 2019 (Wet) was applied for both Above Normal and Wet water year type simulations. The water year types and the years associated with different input data are provided in Table 2.

Table 2 Periods associated with calanoid copepod analysis inputs. Calanoid copepod BPUE was estimated both for the DWSC action and the NDFA action for each of the listed water year types. Model inputs for atmospheric forcing and other hydrodynamic model boundary conditions were applied from the Historical Year, boundary inflows were provided from CalSim II for the CalSim Year and copepod data was applied for the Copepod Data Year.

Water Year Type	*Historical Year*	*CalSim Year*	*Copepod Data Year*
Dry	2009	1930	2018
Above Normal	2005	1940	2019
Below Normal	2018	1979	2018
Wet	2019	1986	2019

Biomass Density Modeling Approach

Simulations which predict tracer concentration and associated age are useful to visualize the distribution of a tagged water volume through time as it is advected by net flows and mixed by dispersive processes. The "source water" was tagged with a concentration of one and age zero either as it enters the domain or in some region of the domain at a point in time. Predictions from the water age simulation approach were compared with field observation-based estimates of age in Gross et al. (2019).

In order to estimate copepod density for proposed flow actions, we applied a simple copepod model focused on transport of calanoid copepods from a source region through the model domain and uptake of phytoplankton by the calanoid copepods. The tracers used in the tracer concentration and age simulations represented the source of potentially elevated copepod abundance. For the NDFA, this "source water" was the water entering the model domain at the Toe Drain boundary near I80 because this water has been observed to have elevated copepod abundance in some years (Owens et al. 2019). For the DWSC action, the "source" was water initially present in the DWSC where elevated copepod abundance is sometimes observed. The tracer transport simulations estimated the spatial distribution of this source water though this model domain for the simulation period.

In addition to estimating the spatial distribution of the source water, we also estimated the age of that water using a constituent-based water age approach (Deleersnijder et al. 2001). For the NDFA, the predicted tracer age varied spatially because "new" (age 0) water entered at the boundary as long as flow in the Toe Drain was directed downstream (seaward). In contrast, the DWSC source water represented water initially in the DWSC, not water entering the DWSC. This was a deliberate choice because the observed copepod abundance in the Sacramento River adjacent to the upper part of the DWSC typically has lower copepod abundance than the DWSC. The source water age for the DWSC scenarios was spatially uniform because it was all initialized to zero at the beginning of the action and no "new" (age=0) tracer was introduced at any later point in time. Therefore, the

tracer age for the DWSC action at any point in time was the time elapsed since the beginning of the action.

As the source water containing elevated copepod and chlorophyll abundance was transported in the model domain, we allowed the predicted copepod BPUE associated with this water to change in time. The method for estimating the copepod density in the source water has been applied by Wang et al. (2019) to estimate evolving chlorophyll concentration in a source water as it is advected seaward. Following this approach, a simplified governing equation for the biomass density or BPUE is

$$\frac{\partial D_s}{\partial t} + \nabla \cdot (\boldsymbol{u} D_s) = \mu_{net} B \quad (1)$$

where D_s is biomass density (mg C m^{-3}) and μ_{net} (day^{-1}) is the net growth rate accounting for all growth and loss processes. An upper bound of μ_{net} of 0.4 day^{-1} from Owens et al. (2019) was used.

In a Lagrangian frame of reference this equation is equivalent to

$$\frac{dD_s}{da} = \mu_{net} D_s \quad (2)$$

where a (day) is the water age calculated by the constituent-based water age approach of Deleersnijder et al. (2001) to provide predictions of age throughout the model domain and simulation period. Given a known initial and boundary concentration, the biomass density inside source water present at all points in the model domain through time was estimated by the analytical equation

$$D_s(x,t) = \min\left(D_{s,max}, \quad D_s(x_{in}, t-a)\, e^{\mu_{net} a}\right) \quad (3)$$

where $D_s(x_{in}, t-a)$ is the concentration associated with incoming water. In the case of the NDFA, $D_s(x_{in}, t-a)$ was the calanoid copepod biomass density incoming to the Toe Drain during the flow pulse. Because unbounded growth could lead to unrealistic copepod biomass density estimates, we bounded the prediction of biomass density in the source water by $D_{s,max}$. $D_{s,max}$ was estimated by assuming that a portion of available phytoplankton biomass was converted to calanoid copepod biomass.

$$D_{s,max} = \quad D_s(x_{in}, t-a) + D_{s,uptake} \quad (4)$$

where $D_{s,uptake}$ is the maximum copepod biomass generated by uptake of phytoplankton biomass since entering the domain.

$$D_{s,uptake} = C_r C_g C_c Chla_s \quad (5)$$

where $Chla_s$ is chlorophyll concentration (mg m^{-3}) in the source water, C_r is the C/Chla ratio, C_g is the growth yield representing the portion of phytoplankton biomass that becomes zooplankton biomass, and C_c is a competition factor accounting for uptake of phytoplankton by species other than calanoid copepods or could also represent the portion of phytoplankton mass that is not available for uptake by calanoid copepods. C_r was set to 23 following Kimmerer and Thompson (2014). C_g was set to 0.35, roughly consistent with the 0.33 value used in Cloern (2007). C_c is uncertain and was set to 0.5 as a possible upper bound value. Note that part of the competition for phytoplankton would be exerted by clams in addition to other zooplankton species other than calanoid copepods.

A large advantage of this simple model was that it could be run offline efficiently after the tracer simulations were complete. Any elements of the formulation, including parameter values, could be readily changed and new predictions generated.

At each point in time (2-hour interval) and space (grid node) during the simulation, the concentration associated with the source water was calculated by Equation 3. However, because the source water made up only a portion, often a small portion, of the water present at a given location, the overall biomass density was estimated as a weighted average of the source water biomass density and the ambient (observed) biomass density

$$D(x,t) = C_s(x,t)D_s(x,t) + \big(1 - C_s(x,t)\big)D_{ambient}(x,t) \quad (6)$$

where $D(x,t)$ is the predicted calanoid copepod biomass density at a point in time and space, $C_s(x,t)$ is the tracer concentration indicating the proportion of water at (x,t) that is source water (e.g. from the NDFA flow pulse). $D_{ambient}(x,t)$ is the ambient biomass density estimated based on observations. Note that during September of 2018 and 2019 the ambient BPUE may have been influenced by the NDFA actions that occurred. However, since an observed effect was not apparent, we refer to the historical conditions as "No Action" estimates.

Biomass Density Estimates

Using the historical estimates of calanoid copepod BPUE and the simple model of copepod growth described above, we estimated calanoid copepod BPUE for flow action scenarios. Our intention was to estimate a likely upper bound of the management effect of the flow augmentations in the Toe Drain and the Sacramento DWSC on copepod abundance. We acknowledge that larger effects of flow actions could occur due to more complex food web dynamics than those considered here. For example, if the flow actions result in a large algal bloom in downstream regions, that could potentially lead to larger effects on calanoid copepod abundance than those estimated here.

The calanoid copepod BPUE associated with source water was specified based on observed data. For the NDFA all zooplankton data collected by DWR (Frantzich et al. 2018) in the Toe Drain from July through September was considered. This location and time period correspond to conditions that can be present at the time of a North Delta Flow Action. The stations in this region were RD22, I80, LIS, and STTD. The 75th percentile calanoid copepod BPUE at these stations in the July through September period for 2016 through 2019 was 5.4 mg C m^{-3}. A similar approach was applied to all stations in the DWSC for June and July, the period prior to and during an anticipated action, to estimate a 75th percentile BPUE of 19.5 mg C m^{-3}. A similar approach was applied to estimate the 75th percentile of chlorophyll for each scenario resulting in values of 23.0 mg m^{-3} for the NDFA and 2.1 mg m^{-3} for the DWSC action.

Several assumptions and approximations are inherent in our approach. Some are general to the approach and some are specific to the representation of the effects of individual actions.

- General
    - The observed calanoid copepod CPUE at stations was representative of actual calanoid copepod abundance
        - This may not be true if copepods had demersal behavior during the daytime (when sampling occurs) or tidal migration behavior

    - A single carbon weight was used for each gross life stage of calanoid copepods
        - This is particularly inaccurate for copepodites
    - Unidentified species had an assumed carbon weight in a representative range for calanoid copepods
        - This may introduce some sensitivity to the different taxonomic resolution of different surveys
    - Several model parameter values described above are approximate
        - In particular the competition parameter is unknown
    - Calanoid copepods are transported passively
        - Tidal migration and day-night patterns including demersal behavior during the day have been observed for calanoid copepods
    - The growth rate of calanoid copepods corresponded to roughly the highest observed rate for *P. forbesi* of 0.4 day-1 from Owens et al. (2019).
        - Actual growth could be particularly lower as chlorophyll levels drop
    - After the chlorophyll in the "source water" was taken up, growth and loss processes were in balance for calanoid copepods
        - Actual loss processes such as clam grazing can vary temporally and spatially
    - Observed ambient (No Action) BPUE is static during the month
        - We estimated a dynamic (2-hour interval) source water BPUE but only a monthly interval "ambient" BPUE because that is based upon observed data typically collected at a monthly interval
    - Historical calanoid copepod BPUE during September of 2018 and 2019 was not significantly influenced by historical NDFA actions
        - In contrast our scenarios estimate the effect of a high level of incoming calanoid copepod BPUE and chlorophyll during the NDFA actions
- North Delta Flow Action
    - Calanoid copepod BPUE and chlorophyll concentration incoming at I80 remain fixed during the flow action
        - Actual concentrations are observed to drop
    - The range of age of source water is simplified to the "mean age" estimated using the constituent-based age approach (Deleersnijder et al. 2001)
        - For a non-linear process such as copepod growth this introduces error
- DWSC
    - Uniform initial calanoid copepod BPUE and chlorophyll concentration in the DWSC

Several of these assumptions and approximations are known to be inaccurate but are retained for simplicity in some cases and to provide an upper bound estimate in other cases. For example, calanoid copepods are known to not be transported passively (Kimmerer et al. 2014) but since accounting for the effect of behavior on transport would require a more complex approach, this assumption is applied for simplicity. An inaccurate approximation used as an upper bound for the NDFA was that calanoid copepod BPUE and chlorophyll concentration incoming at I80 were constant in the simulation. Observations indicate that these concentrations actually dropped rapidly during historical North Delta Flow Actions (Owens et al. 2019; Frantzich et al. in progress).

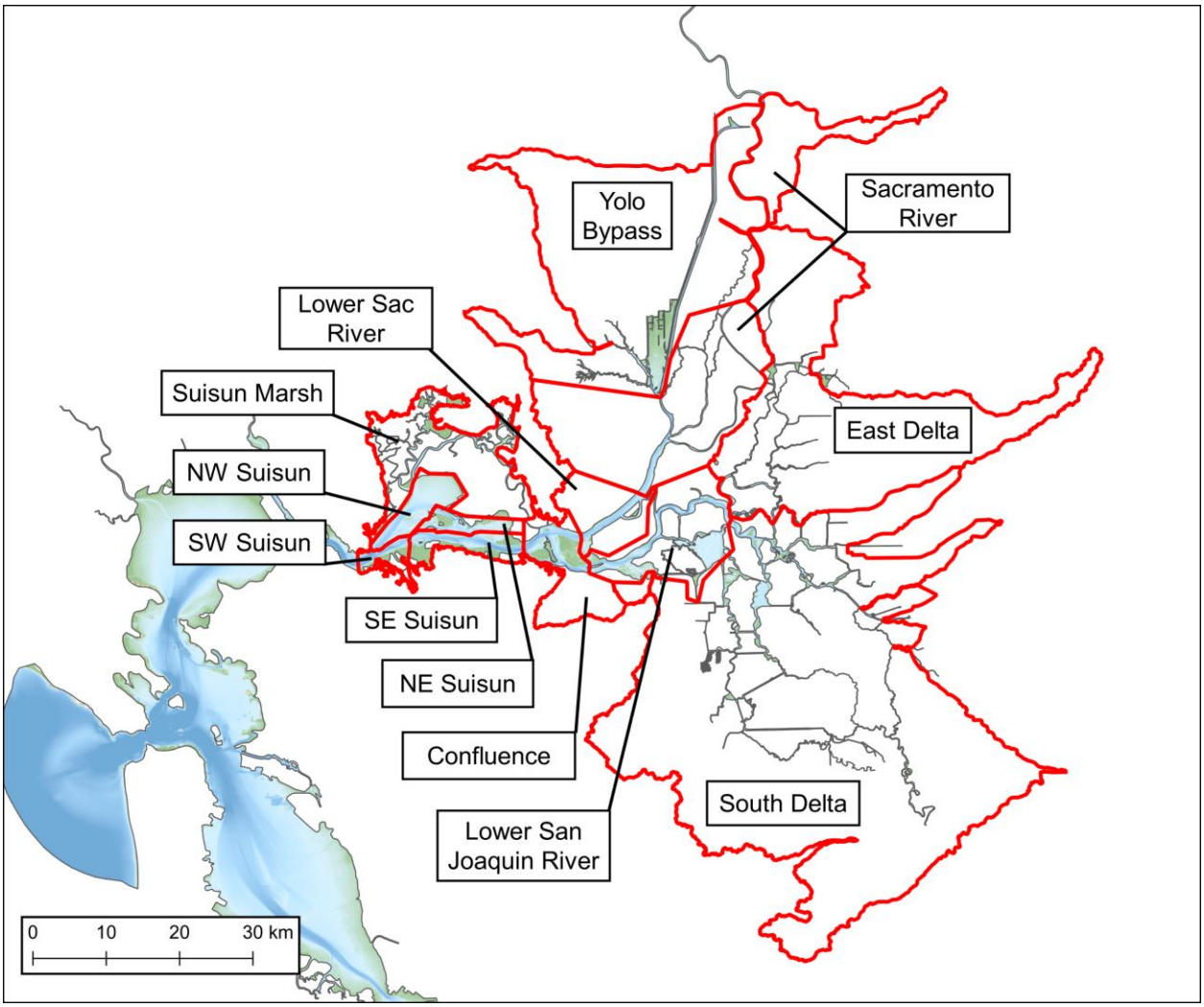

Figure 3 Regions used in the delta smelt IBM and for tabulation of calanoid copepod BPUE in this study.

The primary outputs of this analysis are 10-meter resolution maps of estimated monthly-averaged calanoid copepod BPUE and tabulated values for discrete regions. An example of these mapped model results is Figure 4, which shows the average predicted copepod abundance in October during the Wet water year type predicted for the NDFA flow action which extended from August 28 to September 23. The pattern of elevated biomass near to the confluence of Prosect Slough into the Liberty Island area is reflective of the NDFA action transporting copepods and their food resources into those areas.

The spatial difference between the ambient ("No Action") calanoid copepod distributions and the modeled distributions with the NDFA flow action can be seen in Figure 5. These predicted fields through time are available as animations. The snapshot in Figure 5, corresponding to 116 hours after the start of the NDFA flow action, shows that predicted BPUE increased relative to ambient BPUE, indicating that the copepod density in the source water is higher than the ambient (observed) copepod density. At this point in the simulation, the difference in BPUE in areas of concentrated NDFA action "source" water exceeded 10 mg C m^{-3}.

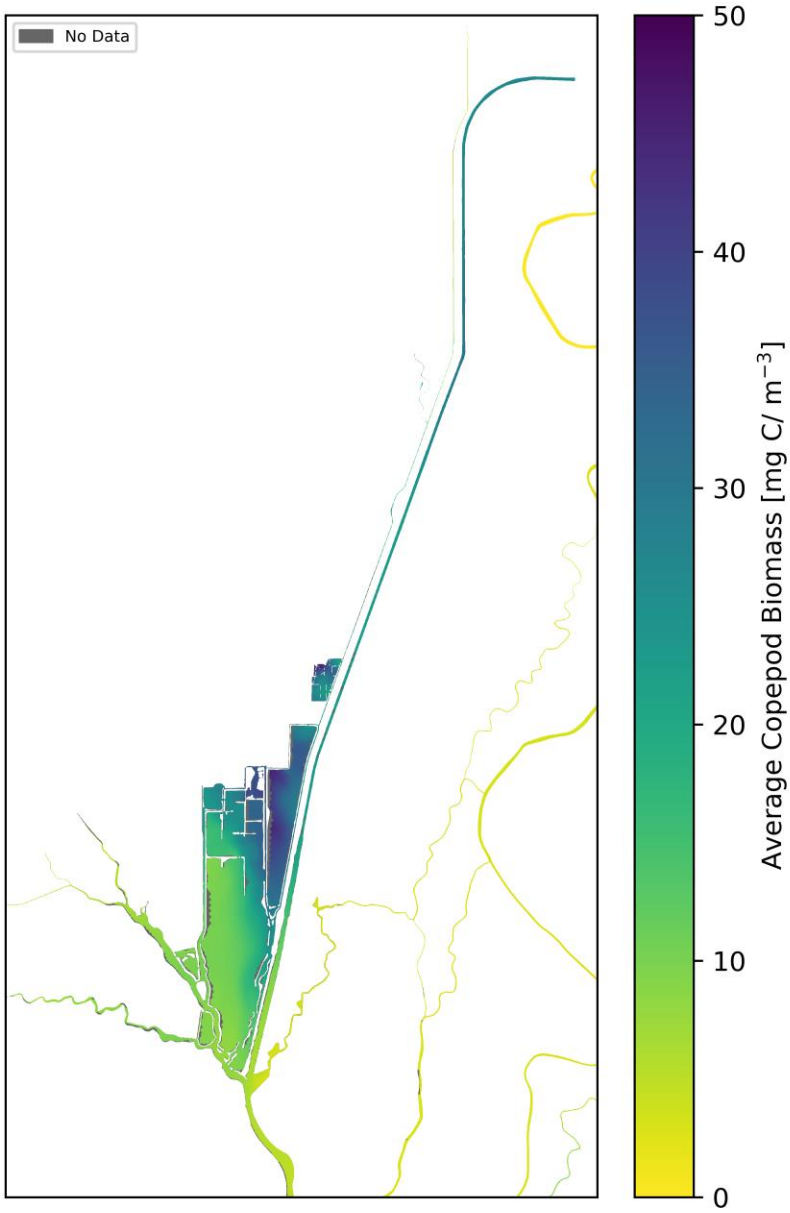

Figure 4 Predicted average monthly calanoid copepod biomass with NDFA action during Above Normal water year (1940 CalSim year).

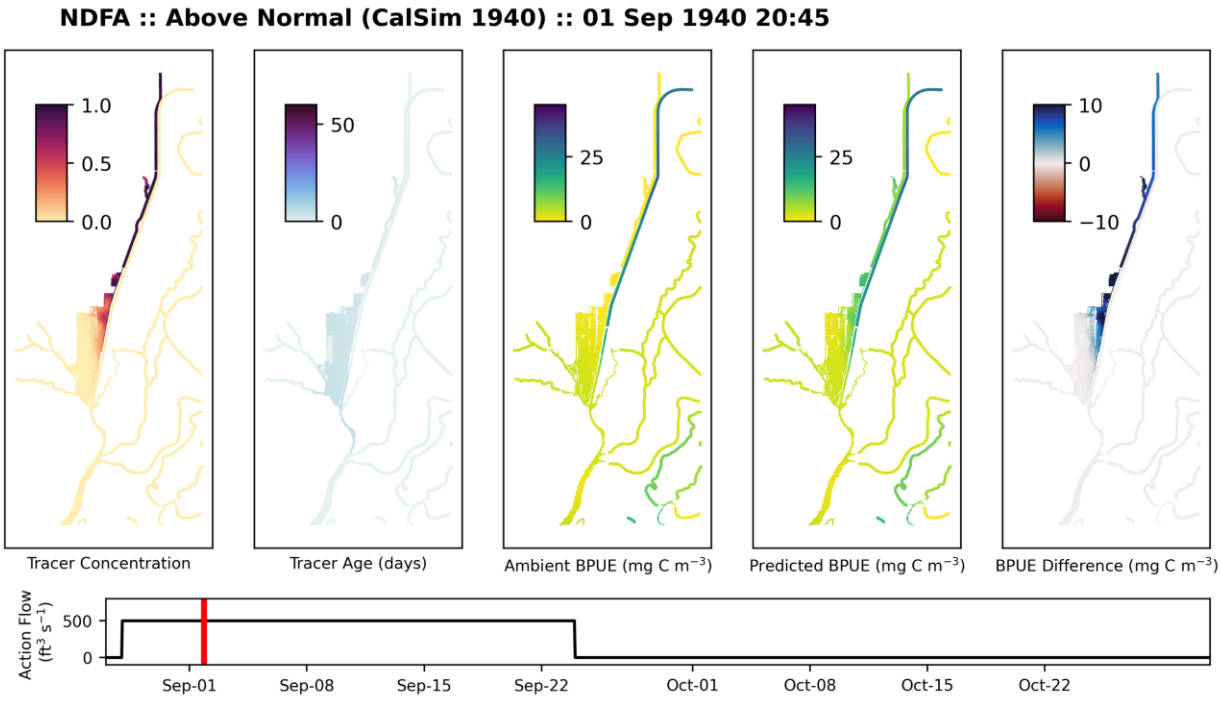

Figure 5 Snapshot of calanoid copepod and tracer results for the NDFA, during an Above Normal water year (CalSim year 1940). Predicted BPUE is a function of the concentration of the flow action water (tracer concentration), the age of this water (tracer age), and calculated initial calanoid copepod and food resource (chlorophyll) concentrations in the flow action source water. The difference between predicted and ambient (interpolated from observations) BPUE at this time in the simulation indicates greater calanoid copepod BPUE localized near to the flow action.

A similar snapshot demonstrates simulation progression for the DWSC flow action in Figure 6. 140 hours after the start of the flow action, much of the flow action source water was still in the Deepwater Ship Channel, due to its high volume relative to the action flow rate, and a high initial source water calanoid copepod BPUE. Some source water mixed into southern Liberty Island causing a slight increase in the predicted copepod BPUE there.

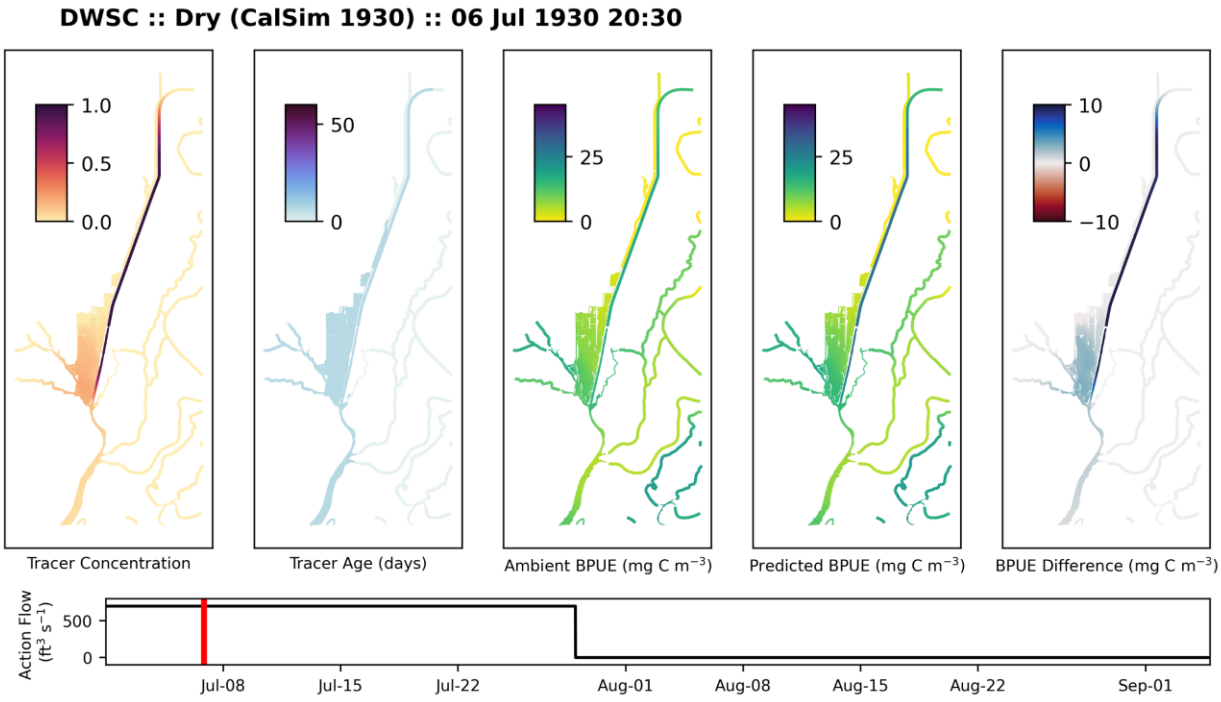

Figure 6 Snapshot of calanoid copepod and tracer results for the DWSC flow action, during a Dry water year (CalSim year 1930). Predicted BPUE is a function of the concentration of the "source" water (tracer concentration) corresponding to water initially in the DWSC, the age of this water (tracer age) since initiation of the flow action, and calculated initial calanoid copepod and food resource (chlorophyll) concentrations in the flow action source water. The difference between predicted and ambient (interpolated from observations) BPUE at this time in the simulation indicates greater calanoid copepod BPUE in and near the DWSC.

GeoTIFF data files indicating the spatially-variable difference between interpolated ambient and predicted monthly-averaged calanoid copepod BPUE are also available. These differences represent a likely upper bound of monthly-averaged changes in calanoid copepod biomass possible from flow actions. The NDFA action ended in September, and predicted calanoid copepod BPUE increased by 15 mg C m^{-3} above ambient over a large portion of Liberty Island (Figure 7 for Above Normal water year). This estimated effect persisted into October decreased as the NDFA water was diluted by mixing with ambient water.

Monthly-averaged BPUE difference plots show a smaller increase in copepod BPUE for the DWSC action during July, when the DWSC flow action took place (Figure 8) relative to the estimated NDFA flow action effect (Figure 7). The smaller estimated effect was partially due to hydrodynamics, with DWSC action source water (water in the DWSC at the beginning of the simulation) never reaching the high concentrations of NDFA source water in Liberty Island, but was mostly due to the specified calanoid copepod BPUE of the source water. Measured copepod concentrations were high in the DWSC, but food resources (chlorophyll) were low, therefore predicted copepod results are reflective of a generally poor growth environment. Therefore, DWSC action predicted BPUE were mostly a function of transport and dilution of initial DWSC BPUE rather than growth.

This pattern of greater increases in monthly-averaged predicted calanoid copepod BPUE from the NDFA flow action, compared to DWSC, held across the four different flow type years for the Yolo

Bypass region (Figure 9). The NDFA flow action differences are generally most visible in the Yolo Bypass, while the DWSC action produces very modest increases in calanoid copepod BPUE downstream into Eastern Suisun Bay and Suisun Marsh.

We stress that these are upper bound estimates of the potential flow action effect on calanoid copepod BPUE and are sensitive to the assumed calanoid copepod BPUE and chlorophyll in source water. Given the computational efficiency of the approach, a suite of such simulations could be performed to explore uncertainty related to these and other model inputs.

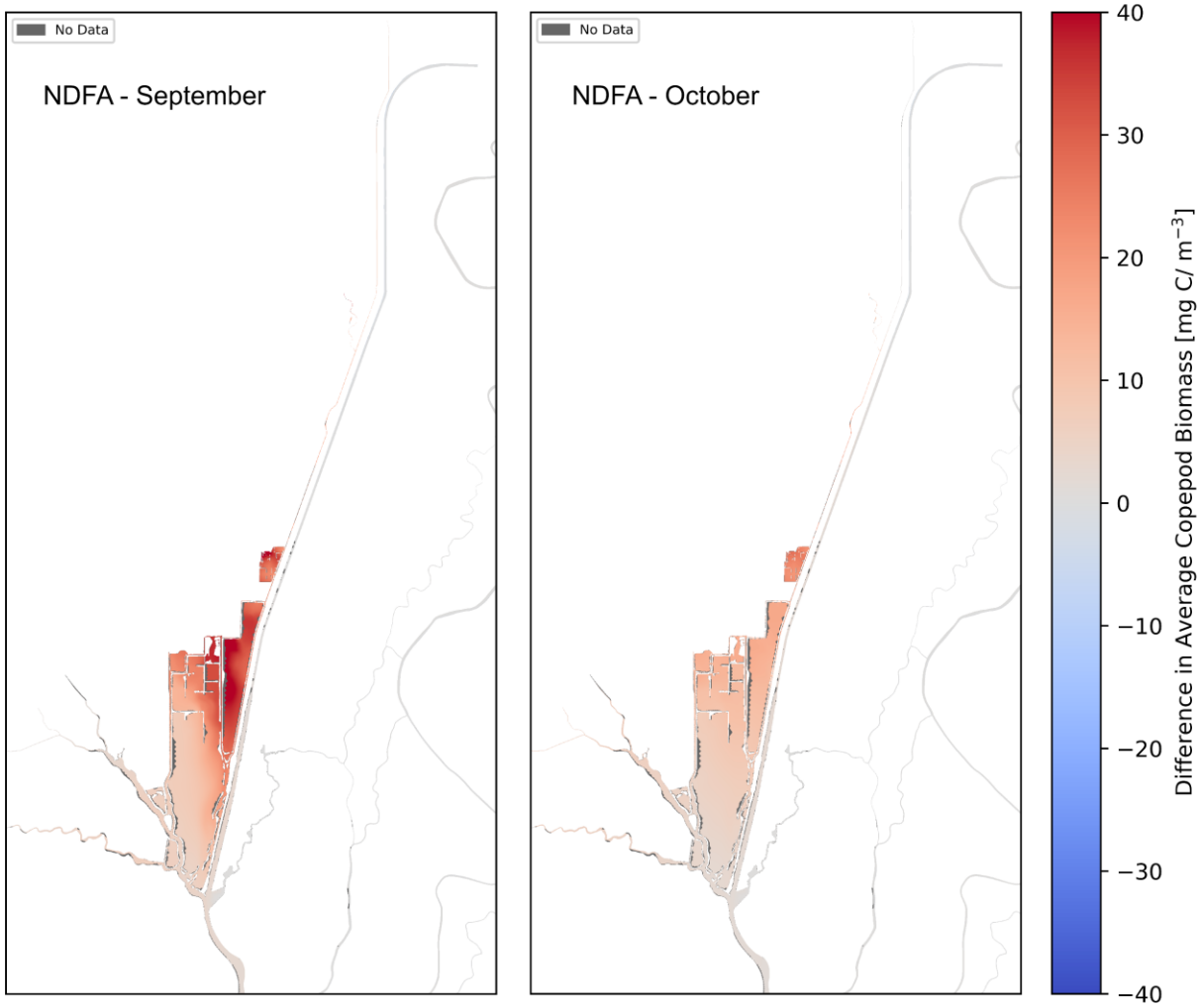

Figure 7 Difference between NDFA and No Action monthly-averaged calanoid copepod BPUE during September (left) and October (right) of the Above Normal water year (CalSim year 1940).

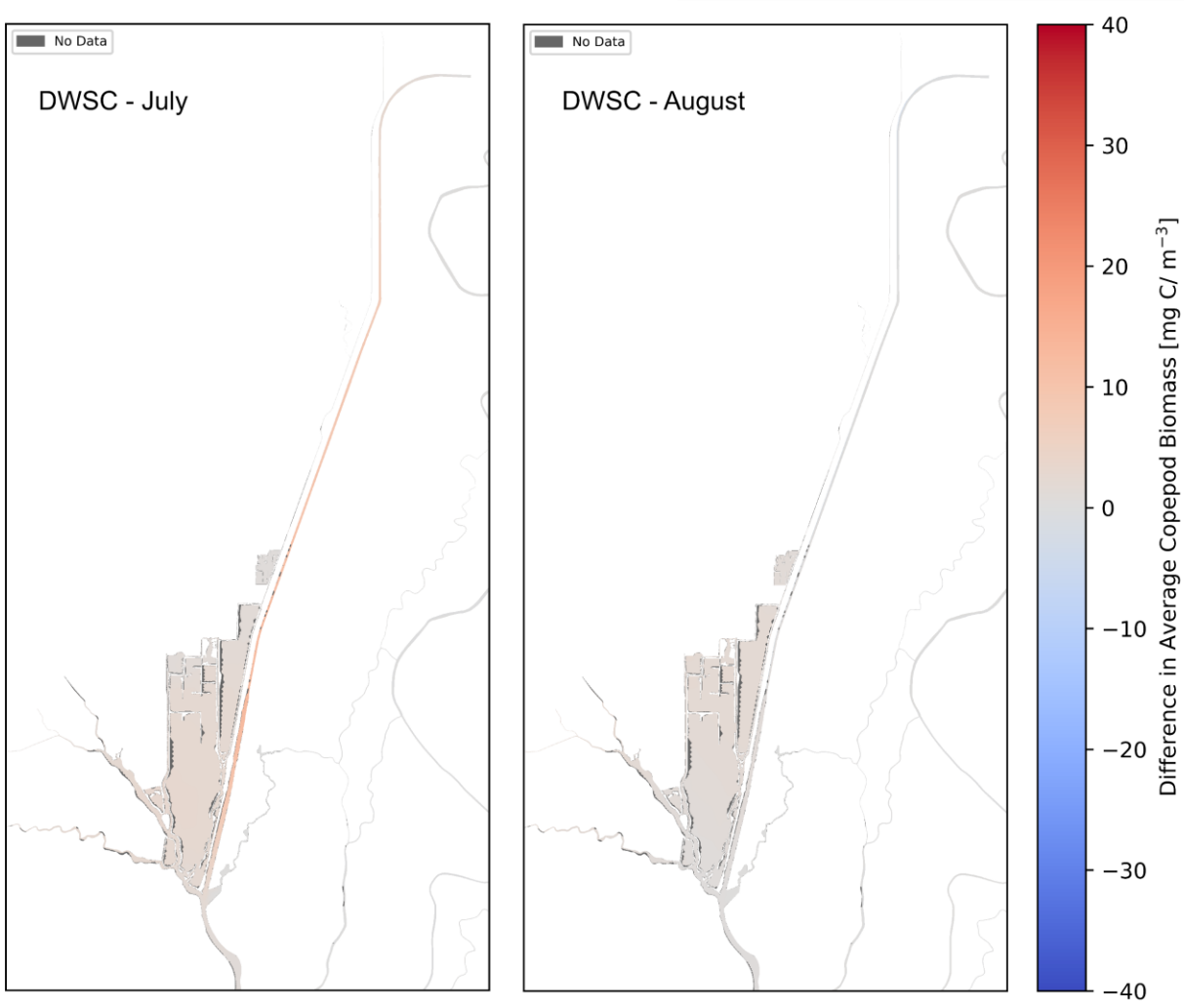

Figure 8 Spatial difference between precited and ambient monthly average calanoid copepod BPUE for the DWSC flow action, during July (left) and September (right), for Above Normal water year (CalSim year 1940).

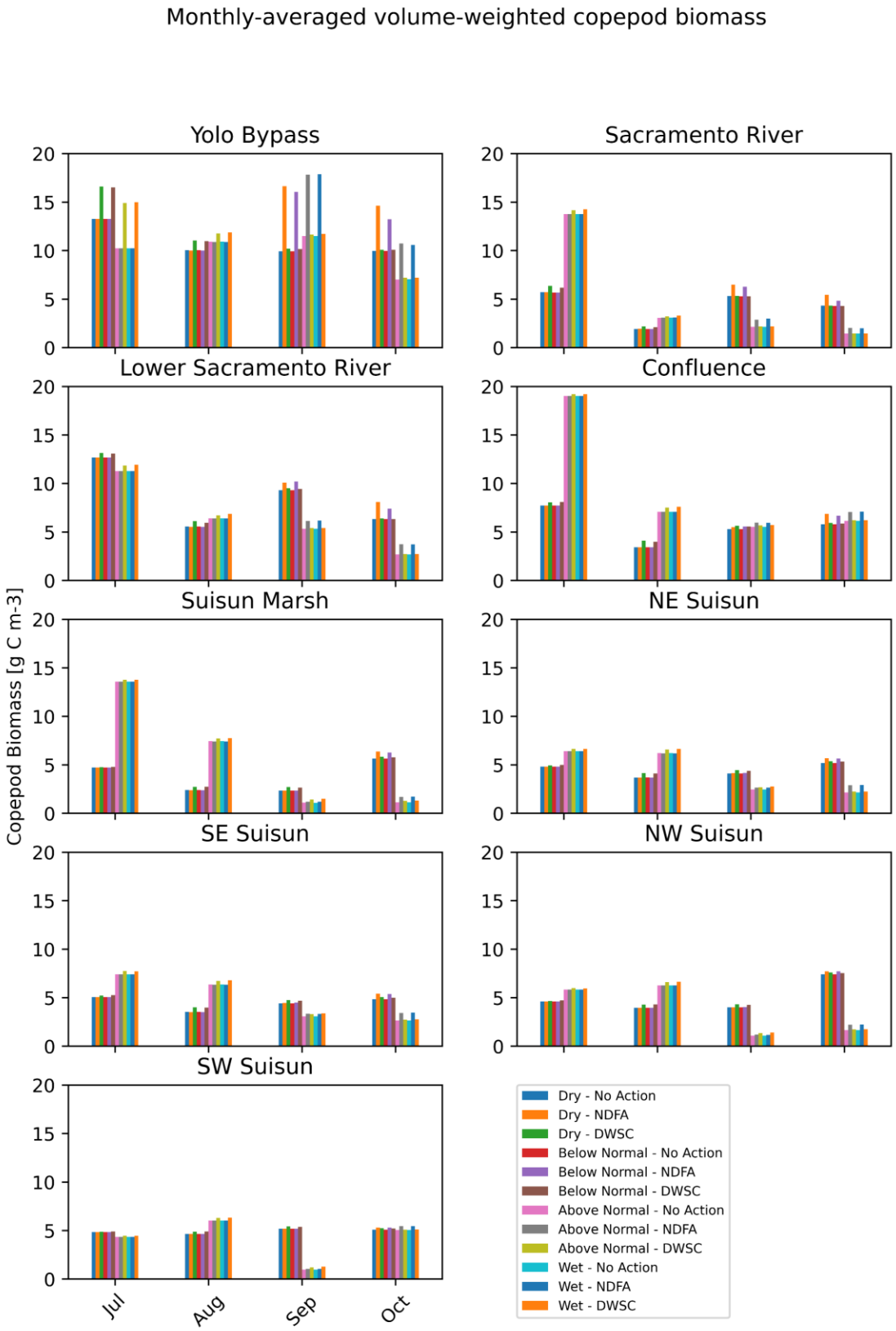

Figure 9 Regionally-averaged monthly calanoid copepod BPUE (Rose et al. 2013 IBM regions), for 4 water years types and 3 different management scenarios.

References

Bashevkin SM, Hartman R, Thomas M, Barros A, Burdi C, Hennessy A, Tempel T, Kayfetz K. 2020. Interagency Ecological Program: Zooplankton abundance in the Upper San Francisco Estuary from 1972-2018, an integration of 5 long-term monitoring programs. Environmental Data Initiative. doi:10.6073/PASTA/0C400C670830E4C8F7FD45C187EFDCB9. [accessed 2020 Jun 10]. https://portal.edirepository.org/nis/mapbrowse?packageid=edi.539.1.

Cloern, J.E. 2007. Habitat Connectivity and Ecosystem Productivity: Implications from a Simple Model. The American Naturalist. 169(1):21-33

Deleersnijder, E., J.M. Campin, and E.J.M. Delhez, 2001. The concept of age in marine modelling I. Theory and preliminary model results. J. Mar. Syst., 28, 229–267.

Frantzich, J., Sommer, T., and B. Schreier. 2018. Physical and biological responses to flow in a tidal freshwater slough complex. San Francisco Estuary and Watershed Science. 16(1):1-26.

Frantzich et al. DWR Report on NDFA studies in progress.

Gross, E., Andrews, S., Bergamaschi, B., Downing, B., Holleman, R., Burdick, S. and J. Durand. 2019. The use of stable isotope-based water age to evaluate a hydrodynamic model. Water 11:2207 https://doi.org/10.3390/w11112207

Kayfetz, K., S. M. Bashevkin, M. Thomas, R. Hartman, C. E. Burdi, A. Hennessy, T. Tempel, and A. Barros. 2021. Zooplankton Integrated Dataset Metadata Report. IEP Technical Report 93. California Department of Water Resources, Sacramento, California.

Kimmerer, W.J., Ignoffo, T.R., Kayfetz, K.R., Slaughter, A.M. 2018. Effects of freshwater flow and phytoplankton biomass on growth, reproduction, and spatial subsidies of the estuarine copepod Pseudodiaptomus forbesi. Hydrobiologia 807: 113-130.

Kimmerer, W.J., E.S. Gross, and M.L. MacWilliams. 2014. Tidal migration and retention of estuarine zooplankton investigated using a particle-tracking model. Limnology and Oceanography 59: 901–906.

Kimmerer, W. J. and A. Slaughter, 2016. Fine-scale distributions of zooplankton in the northern San Francisco Estuary. SFEWS., 14. https://escholarship.org/uc/item/96x1594c.

Kimmerer, W. J. and J.K. Thompson, 2014. Phytoplankton growth balanced by clam and zooplankton grazing and net transport into the low-salinity zone of the San Francisco Estuary. Estuaries Coasts., 37, 1202–1218.

Owens, S., T.R. Ignoffo, J. Frantzich, A. Slaughter, and W. Kimmerer, 2019. High growth rates of a dominant calanoid copepod in the northern San Francisco Estuary. Journal of Plankton Research. doi:10.1093/plankt/fbz064

Rose, K.A., Kimmerer, W.J., Edwards, K.P., and W.A. Bennett. 2013. Individual-based modeling of Delta Smelt population dynamics in the upper San Francisco Estuary: I. Model description and baseline results. Trans Am Fish Soc. 142:1238–1259. https://doi.org/10.1080/00028487.2013.799518

Slater, S. B.&R. D. Baxter, 2014. Diet, prey selection, and body condition of age-0 delta smelt, Hypomesus transpacificus, in the upper San Francisco Estuary San Francisco Estuary and Watershed Science 12: Article 1. Slaughter, A. M., T. R. Ignoffo & W. Kimmerer

Sommer T, Hartman R, Koller M, Koohafkan M, Conrad JL, MacWilliams M, et al., 2020. Evaluation of a large-scale flow manipulation to the upper San Francisco Estuary: Response of habitat conditions for an endangered native fish. PLoS ONE 15(10)

Wang, Z., H. Wang, J. Shen, F. Ye, Y. Zhang, F. Chai, Z. Liu, J. Du. 2019. An analytical phytoplankton model and its application in the tidal freshwater James River. Estuarine, Coastal and Shelf Science, 224(31)